FT-ICR Studies of the Structures, Energetics and Reaction Dynamics of Biological Molecules in the Gas Phase

Thesis by

Sherrie A. Campbell

In Partial Fulfillment of the Requirements

for the Degree of

Doctor of Philosophy

California Institute of Technology

Pasadena, California

1995

(Submitted September 23, 1994)

For my husband, Lance

and

my parents, Jerry and Bonnie

Acknowledgments

There are many people whom I wish to thank for their contributions to the research presented in this thesis and for their support during my graduate stay at Caltech. I am greatly indebted to my research advisor, Jack Beauchamp, for all the support he provided through his motivation, friendship, financial backing, and never-ending flow of clever research ideas. He has helped me grow as a scientist, and as a person. I would like to thank my committee members, Peter Dervan, Ahmed Zewail, and Erick Carreira, for their insightful conversations over the years and their words of encouragement. Additionally, Bob McIver and Rick Hunter of IonSpec Corporation deserve a special thanks for their guidance and ingenuity in getting the new spectrometer operating properly.

The Beauchamp Group has been an interesting mix of characters, and each has played a special role during my graduate stay. I would like to thank Karl Irikura for taking the time to teach me the secrets of ICR while he was writing his thesis. I can only now appreciate what a burden that must have been! Seung Koo Shin, Shu Li, Andy Sikes, Srihari Murthy, Elaine Marzluff, Jim Smith, Kevin Crellin, Hakno Lee, and Marcel Widmer deserve thanks for all of the discussions dealing with chemistry, computers, or life in general. I also thank Mary Rodgers for her friendship and commiseration during the past two years. Her candid discussions, experimental insight, campus connections, and Land's End catalogues are well missed.

Several members of the Caltech community warrant mentioning for their invaluable assistance. I can always rely on Dian Buchness for a friendly smile, a good lunch, and answers to all the bureaucratic questions I might have. Thanks to Tom Dunn, Tony Stark, and Jess Miller for their timeless help in making this project a reality. A special thanks to Guy Duremberg for his assistance and unending patience in the machining shops. It is amazing what can get done for a woman bearing a smile and a loaf of zucchini bread.

The list of Caltech thank yous would not be complete without mentioning the numerous friends I have made through the chemistry department and recreational facilities. Most notably, I would like to thank Roxanne Male-Brune for her friendship and occasional words of wisdom. I've enjoyed the times we've had immensely. Thanks to Christine Nelson, Teri Longin, and Sakae Suzuki for letting me live through their adventures. Bob Blake deserves a special thanks for keeping me supplied with homemade brownies at high stress times. A very special thanks to Steve Fryer and the Monday/Friday/Saturday step aerobics class for reducing the stress (and the effects of the brownies).

I thank my parents and the rest of my family for their love and tolerance the past five years while my life was on hold. Your care and concern was deeply appreciated. Lastly, I thank my husband for all the love, patience, encouragement and support given to me throughout the years. He has earned this degree along with me, and I look forward to starting the next chapter of our lives together!

Abstract

Fourier transform ion cyclotron resonance (FT-ICR) mass spectroscopy has been used to investigate the energetics and reaction dynamics of biological molecules in the gas phase. Experimental results aid in predicting gas phase protonation sites and molecular conformations of peptides and amino acids. Correlations of proton affinities with adiabatic lone-pair ionization energies indicate that amino acids lacking basic side chains protonate on the amine nitrogen, while more basic amino acids protonate on their side chain. These results have been similarly applied to small peptides, with protonation predicted on the N-terminus for peptides lacking basic amino acid residues.

Two novel experimental methods have been developed for measuring gas phase proton affinities, which utilize infrared multiphoton dissociation and collision induced dissociation techniques to cleave proton-bound dimers of reagent gases. The dimers fragment into two products with the more basic reagent retaining the proton. A simplified RRKM analysis is used to determine proton affinities from product ion abundances.

Isotopic hydrogen exchange reactions of protonated glycine oligomers with a series of reagent bases have been performed, and the exchange mechanisms and energetics identified. Although it is not the sole determining factor, the extent and rates of H/D exchange increase with reagent basicity, with ND_3 being the most efficient exchange gas studied. Exchange of the N-terminus hydrogens occurs via an onium ion mechanism in which an endothermic proton transfer is rendered energetically favorable

by simultaneous solvation of the ammonium ion. Exchange of the C-terminus occurs via a salt bridge intermediate, in which the carboxylate and ammonium ion is stabilized by interactions with the nearby protonated N-terminus.

Finally, the H/D exchange reactions of several peptides possessing basic residues with ND_3 have been investigated. The results indicate that basic amino acids hinder exchange processes as protonation energetics and molecular folding become more important. Calculations using semiempirical AM1 and PM3 methods were performed to identify the gas phase configurations of the protonated peptides and determine if stable salt bridge structures are possible. Potential energy surfaces were also calculated for all exchange processes.

Table of Contents

INTRODUCTION

> "Mass spectrometry is one of the most important experimental tools currently available to the chemistry and biochemistry communities. It cannot be said to be a scientific end in itself. The lasting scientific value of efforts in development of novel instrumentation and techniques must ultimately be decided in terms not of the ingenuity, imagination, and persistence which have been devoted to them, but of the useful information they provide."[1]

A virtual revolution in the application of mass spectrometry to problems in molecular biology has occurred in recent years. This results from the development of "soft ionization" techniques which make it possible to transfer fragile biomolecules into the gas phase and from the refinements made to mass analyzers for studying high molecular weight species. Desorption of amino acids or larger biological samples from a matrix using laser desorption (MALDI),[2] plasma desorption,[3] or fast atom bombardment[4] (FAB) is an efficient method for producing singly charged species. In fact, MALDI-time of flight mass spectrometry is routinely employed for analyzing singly charged proteins with masses in excess of 100,000 Dalton.[5] Electrospray[6] and thermospray[7] ionization techniques produce multiply charged gas phase ions, and are widely used for characterizing large proteins and other biological molecules.

The most common applications of mass spectrometry for biological molecules have been for identifying compounds in a complex mixture and determining amino acid or nucleotide sequence in an oligomer. In the first application, the mass spectrometer is used simply as a sample detector. In the second application (applying the techniques

of collision induced dissociation or metastable decay[8]), the mass spectrometer is an invaluable tool for obtaining sequence information of modified species which cannot be evaluated by standard solution techniques.[9,10] In many instances, though, mass spectrometry has not substantially surpassed the capabilities of solution methods for obtaining sequence information of simple, unmodified biomolecules. In fact, the most successful attempts at sequencing biopolymers via mass spectrometry utilize solution chemistry to cleave the molecule, then rapidly analyze the products in a spectrometer.[11,12,13]

It is increasingly evident that for further advancements to be made in gas phase sequencing techniques, a knowledge of the fundamental gas phase properties of the biomolecules (such as functional group basicities and reactivities) will be required. Unfortunately, in much of the reported research on biomolecules, mass spectrometers have been used merely as detection devices and the capabilities of these instruments to provide a breadth of kinetic and thermodynamic information have not been explored. The lack of quantitative studies of the energetics of ion formation, determination of specific functional group properties and reactivity, and analysis of uni- and bimolecular reaction rates in biopolymers led us to vigorously pursue these topics. An additional interest in developing sequencing methods to *selectively* cleave biomolecule linkages in the gas phase directed our research into the fields of infrared multiphoton dissociation, collision induced dissociation and isotopic hydrogen exchange reactions.

The experiments described in this thesis (except where noted) were performed in an external ion source Fourier transform ion cyclotron resonance mass spectrometer

(FT-ICR) which is specifically designed for investigating the reaction kinetics and dynamics of large molecules in the gas phase. FT-ICR is one of the most versatile techniques available for studying gas phase ion-molecule reactions. The ability to trap and store ions allows gas phase reactions to be observed and characterized for several minutes to hours. This feature makes the FT-ICR a more desirable spectrometer for investigating reaction kinetics than a time of flight or sector instrument. Additionally, since biological molecules typically have high masses, FT-ICR is preferred over quadrupole spectrometers which exhibit upper mass to charge (m/z) limits of 3000-4000 Dalton. Detection of higher masses requires the ions be multiply charged, which can complicate the interpretation of results. The design, construction, and implementation of an external ion source FT-ICR mass spectrometer is the subject of chapter 1.

To understand the reaction kinetics and dissociation dynamics of peptides and proteins in the gas phase, we found it instructive to first investigate several thermodynamic properties of their fundamental components, i.e., the amino acids. Correlations of proton affinities with adiabatic lone-pair ionization energies are useful for assessing the site of protonation in molecules.[14] Results of correlations of this type for the amino acids indicate that those species which lack highly basic side chains protonate on the amine nitrogen, while other amino acids (such as lysine, histidine, and arginine) preferentially protonate on their side chain. The results of these studies are reported in chapter 2. From these results, it is reasonable to make predictions as to the

site of protonation in peptide and protein biopolymers, knowing the arrangement of the amino acids.

When measuring the gas phase proton affinity of a molecule, a proton transfer equilibrium reaction is typically established between two species of similar basicity. At equilibrium conditions, the species of higher basicity will exhibit a larger abundance of the protonated ion in the mass spectrum than the species of lower basicity. The ratio of these ion abundances can be used to estimate the relative differences in proton affinities between the two species. In our proton affinity studies of biomolecules, we commonly observe adduct formation of the two species at the collision rate, making it difficult to establish a proton transfer equilibrium or identify exothermic proton transfers.

Chapter 3 describes a novel method for determining relative proton affinities using infrared multiphoton dissociation (IRMPD) techniques[15] to fragment adducts of protonated reagent gases. Proton-bound adducts or clusters of the reagents are slowly energized by infrared radiation until the lowest energy pathway for dissociation is accessed and hydrogen bond cleavage occurs. This process merely dissociates the cluster into two intact products, with the reagent of higher basicity preferentially retaining the proton. A method for extracting dissociation thresholds and activation energies from product ion distributions using RRKM theory[16] is presented.

Chapter 4 introduces a second, and more general, technique for measuring gas phase proton affinities which utilizes collisional dissociation of the proton-bound clusters by off-resonance translational excitation.[17] In these experiments, rf excitation is applied at a frequency slightly different from the cyclotron frequency of the cluster

ion to be translationally excited. This causes the cluster ion energy to oscillate with time. Collisional activation is achieved by multiple collisions at elevated translational energies, with sequential encounters resulting in accumulation of sufficient internal excitation to produce dissociation. A simplified RRKM analysis is used to determine proton affinities from product ion abundances. The methodology is similar to that introduced by Cooks and co-workers[18] for the extraction of thermochemical data from competitive dissociation processes of metastable ions, but varies in the interpretation of the results.

These fundamental studies of amino acid protonation energetics set the ground work to proceed with investigations into larger biomolecules. Knowing the site of protonation in simple amino acids aides in predicting the site of protonation in larger molecules. Gas phase structures of biomolecules are not well characterized, though, since there are relatively few experiments which extract this information. Several research groups have used collision induced dissociation (CID) as a tool for identifying the amino acid composition of gas phase peptides and proteins.[19,20,21] Dissociation processes yield fragments which are specific for certain amino acids and can be used to reconstruct the primary sequence of the molecule. Unfortunately, these experiments have been less useful in elucidating secondary structure information for the molecules.

In contrast to CID techniques, distinctive chemical reactivity remains the principle experimental method for probing the structures of complex ions in the gas phase. Other than adduct formation and the simple process of proton transfer, there is little known about the gas phase ion chemistry of biological molecules. Isotopic

hydrogen exchange reactions are the only notable exception. Winger et al.[22] reported perhaps the first gas phase H/D exchange results for protein ions. Multiply protonated bovine proinsulin and α-lactalbumin were reacted with D_2O prior to detection. The native and disulfide bond reduced forms of the proteins displayed different reactivities in the gas phase with the D_2O exchange reagent, allowing the different conformations to be distinguished according to their reactivity. Suckau et al.[23] probed the gas phase reactivity of multiply protonated cytochrome *c* with D_2O. Their exchange results were interpreted to indicate that more than one molecular conformation can exist for a specific mass to charge species in a spectrum, and that gas phase species with distinctive exchange reactivity could be correlated with known solution phase structures. With the limited range of studies that have been performed to date, very little is known about the mechanism and energetics of H/D exchange processes for biological molecules.

A systematic study of isotopic hydrogen exchange is described in chapter 5, in which the attention is focused on the mechanisms and energetics of H/D exchange of simple glycine oligomers reacting with a series of reagent gases. The glycine oligomers are ideal model systems for understanding the mechanisms of H/D exchange. There are no basic side chains present, hence the site of protonation in all the oligomers studied is the N-terminus nitrogen. The simplicity of these oligomers allows us to model our results using semiempirical AM1 and PM3 calculations to quantify potential energy surfaces for selected systems and to predict stable conformations of the peptides in the gas phase.

Several unique mechanisms for the exchange of the labile hydrogens of the glycine oligomers are proposed. An onium ion mechanism is invoked for the facile exchange of the oligomers with ammonia, ND_3. Semiempirical calculations predict that exchange occurs when a nominally endothermic proton transfer from the N-terminus is accompanied by simultaneous solvation of the resultant ammonium ion by the peptide. Exchange of the amide hydrogens by ND_3 occurs via a tautomer mechanism, in which a proton is transferred from the N-terminus to an amide carbonyl in concert with transfer of the amide hydrogen to the ammonia base. In this process, the ammonium ion is solvated by a peptide tautomerized at the amide linkage. Most notable is the prediction of the exchange of the C-terminus via a salt bridged intermediate, in which the hydroxyl proton is transferred to the exchange gas creating an ion pair which is stabilized by the nearby protonated N-terminus. There is considerable interest in the structural and functional roles of salt bridges in proteins, and the prediction of salt bridged intermediates in the exchange of these relatively simple glycine oligomers led us to investigate more interesting peptides.

The presence of basic residues may allow the formation of intramolecular gas phase salt bridges in peptides with appropriate arrangements of amino acids. We examined the isotopic hydrogen exchange of several peptides with strongly basic side chains in an attempt to understand the structural and energetic constraints on H/D exchange imposed by these groups. The results of these investigations are the topic of chapter 6. Peptides which lack basic residues, such as the glycine oligomers and leucine enkephalin, exchange *all* labile hydrogens with the ND_3 reagent. Introduction

of basic residues into the peptide, such as arginine, has a significant impact on exchange. Leucine enkephalin arginine exchanges only 6 of 14 labile hydrogens, while bradykinin (with two arginine groups) exchanges none of its 18 sites with ND_3. Semiempirical calculations predict that bradykinin exists in a salt bridge configuration in the gas phase with two protonated arginines interacting with a deprotonated C-terminus, but also identify a non-salt bridge structure of similar energy. In both structures, the charge sites are completely encapsulated and not readily accessible to an approaching ND_3 exchange reagent.

For all peptides studied, the charge site seems to be intimately involved in H/D exchange and the presence of basic residues or rigid secondary structures inhibits facile exchange processes. Gas phase structures of small peptides can be conjectured from their H/D exchange results, but attempts to assign structures to large biomolecules with diverse amino acid composition should probably be approached with caution.

References

1. Burlingame, A. L.; Boyd, R. K.; Gaskell, S. J. *Anal. Chem.* **1994**, *66*, 634R.

2. Karas, M.; Hillenkamp, F. *Anal. Chem.* **1988**, *60*, 2299.

3. Torgerson, D. F.; Skowronski, R. P.; Macfarlane, R. D. *Biochem. Biophys. Res. Commun.* **1974**, *60*, 616.

4. Barber, M.; Bordoli, R. S.; Sedgewick, R. S.; Tyler, A. N. *J. Chem. Soc., Chem. Commun.* **1981**, 325.

5. Hillenkamp, F.; Karas, M.; Beavis, R. C.; Chait, B. T. *Anal. Chem.* **1991**, *63*, 1193A.

6. (a) Meng, C. K.; Mann, M.; Fenn, J. B. *Z. Phys. D.* **1988**, *10*, 361. (b) Fenn, J. B.; Mann, M.; Meng, C. K.; Wong, S. F.; Whitehouse, C. M. *Science* **1989**, *246*, 64.

7. (a) Blakely, C. R.; Vestal, M. L. *Anal. Chem.* **1983**, *55*, 750. (b) Vestal, M. L.; Fergusson, G. J. *Anal. Chem.* **1985**, *57*, 2373.

8. Biemann, K. *Methods in Enzymology*, Vol. 193; McCloskey, J., Ed.; Academic Press; San Diego, California, **1990**, p. 351.

9. Jensen, M. S.; Hojrup, P.; Rasmussen, J. T.; Knudsen, J. *Biochem. J.* **1992**, *284*, 809.

10. Dizhoor, A. M.; Ericsson, L. H.; Johnson, R. S.; Kumar, S.; Olshevskaya, E.; Zozulya, S.; Neubert, T. A.; Stryer, L.; Hurley, H. B.; Walsh, K. A. *J. Biol. Chem.* **1992**, *267*, 16033.

11. Chait, B. T.; Kent, S. B. *Science* **1992**, *257*, 1885.

12. Schar, M.; Bornsen, K. O.; Gassmann, E. *Rapid Commun. Mass Spectrom.* **1991**, *5*, 319.

13. Pieles, U.; Zurcher, W.; Schar, M.; Moser, H. E. *Nucl. Acid R.* **1993**, *21*, 3191.

14. Staley, R. H.; Kleckner, J. E.; Beauchamp, J. L. *J. Am. Chem. Soc.* **1976**, *98*, 2081.

15. For a review of this field, see: Thorne, L. R.; Beauchamp, J. L. *Gas Phase Ion Chemistry,* Vol. 3; Bowers, M. T., Ed.; Academic Press, New York, **1983**.

16. (a) Marcus, R. A.; Rice, O. K. *J. Phys. Colloid Chem.* **1951**, *55*, 894. (b) Marcus, R. A. *J. Chem. Phys.* **1952**, *20*, 359.

17. Gauthier, J. W.; Trautman, T. R.; Jacobsen, D. B. *Anal. Chim. Acta* **1991**, *246*, 211.

18. McLuckey, S. A.; Cameron, D.; Cooks, R. G. *J. Am. Chem. Soc.* **1981**, *103*, 1313.

19. Johnson, R. S.; Martin, S. A.; Biemann, K. *Int. J. Mass Spectrom. Ion Processes* **1988**, *86*, 137.

20. Hunt, D. F.; Yates, J. R., III; Shabanowitz, J.; Winston, S.; Hauer, C. R. *Proc. Natl. Acad. Sci, U.S.A.* **1986**, *83*, 6233.

21. Schwartz, B. L.; Bursey, M. M. *Biol. Mass Spectrom.* **1991**, *21*, 92.

22. Winger, B. E.; Light-Wahl, K. J.; Rockwood, A. L.; Smith, R. D. *J. Am. Chem. Soc.* **1992**, *114*, 5897.

23. Suckau, D.; Shi, Y.; Beu, S. C.; Senko, M. W.; Quinn, J. P.; Wampler, F. M.; McLafferty, F. W. *Proc. Natl. Acad. Sci.* **1993**, *90*, 790.

CHAPTER 1

Design, Construction, and Implementation of an External Ion Source Fourier Transform Ion Cyclotron Resonance Mass Spectrometer.

Instrumental Design and Construction

The experiments described in this thesis (except where noted) were performed in an external ion source Fourier transform ion cyclotron resonance mass spectrometer (FT-ICR) which is specifically designed for investigating the reaction kinetics and dynamics of biological molecules in the gas phase. The FT-ICR has been built to our specifications by IonSpec Corporation (Irvine, CA) and is similar in design to the instrument described by McIver and co-workers.[1] Several novel features make this instrument ideal for studying ion-molecule reactions of large non-volatile molecules. These include an external source for desorbing and ionizing biological samples, a guide for transporting ions to the detection cell against a magnetic field gradient, a high field 7 Tesla superconducting magnet for increased trapping and mass resolution of heavy ions, and an ionization gauge mounted atop the detection cell for directly measuring reagent gas pressures.

A schematic diagram of the instrument is shown in Figure 1. This apparatus has three differentially pumped regions, separated by conductance limiting apertures. The first region houses the ion source, the second, an octopole ion guide and the third, the ICR detection cell. These regions are pumped by 3 APD-6 cyrogenic pumps (APD Cryogenics Inc.), rated at a speed of 1000 L/sec. In this configuration, typical operating pressures above the third pump are $5x10^{-10}$ Torr, as measured by an internal Granville-Phillips ionization gauge.

Ion Source Region. The ion source region consists of an external sample probe and a high vacuum ionization chamber. The sample probe is a linear motion

Figure 1. Schematic diagram of the external ion source FT-ICR spectrometer. Ions are transferred from the source region to the ICR detection cell which is housed in the homogeneous region of a 7 Tesla superconducting magnet using an octopole ion guide.

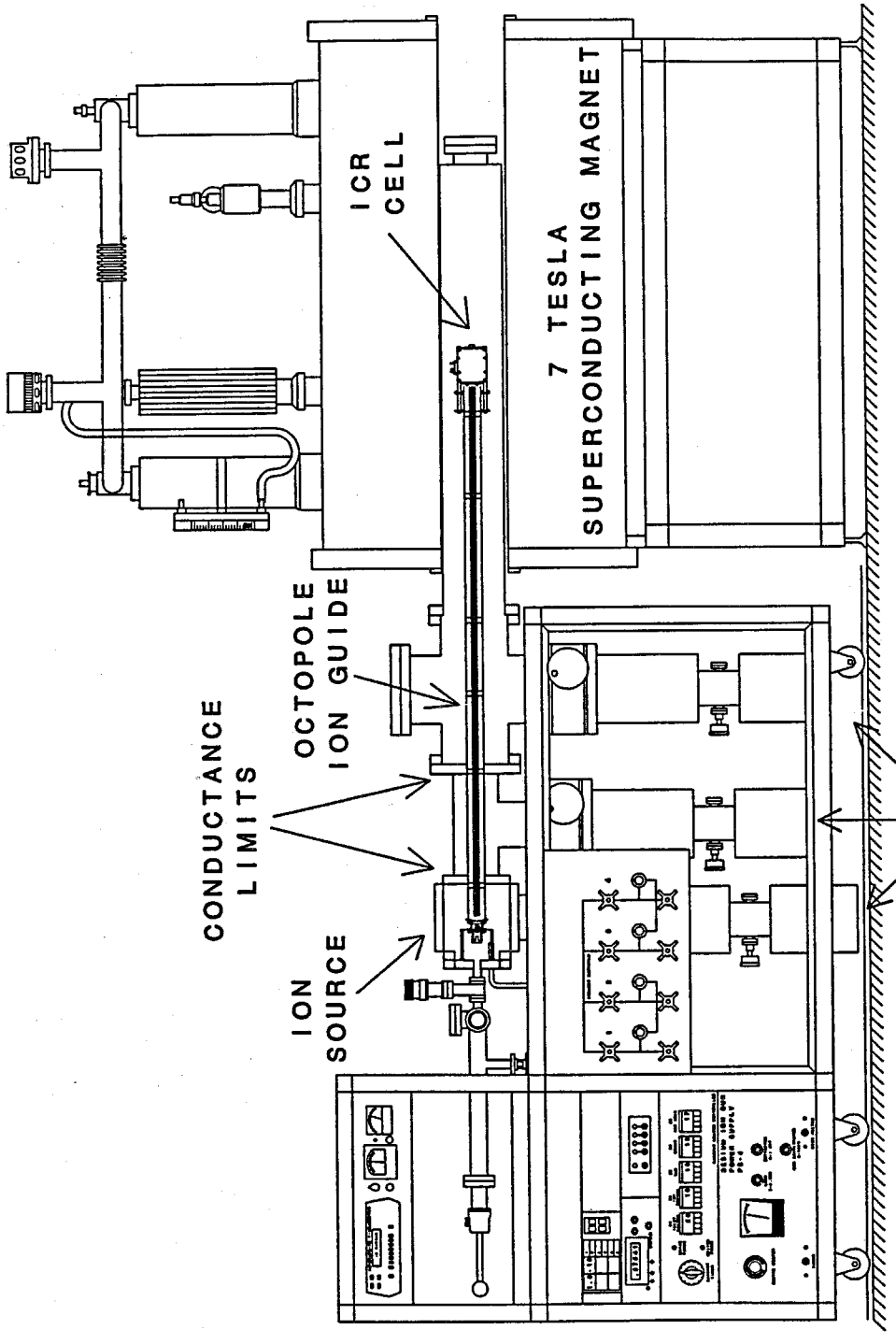
ICR
CELL
7 TESLA
SUPERCONDUCTING MAGNET
OCTOPOLE
ION GUIDE
CONDUCTANCE
LIMITS
ION
SOURCE
DIFFERENTIAL
PUMPING

Figure 1

feedthrough assembly (MDC Vacuum Products Corp.) that is electrically grounded to the instrument. A copper tip, on which a sample is applied, is secured to the end of the feedthrough assembly using an 0-80 set screw. The copper tip is machined with a 45 degree angled face, which is the optimum geometry for sample desorption in our apparatus. An Alcatel two stage, direct drive mechanical pump (UM-2004A) is used to evacuate the probe region from atmospheric pressure to 10 mTorr. At this pressure, the MDC 1-1/2 inch gate valve which separates the external probe region from the ionization source can be opened and the sample probe can be slid into the high vacuum chamber.

The ionization source is housed inside a 6 inch stainless steel cube with a 4 inch Pyrex view port on one face. Source pressures are maintained between 10^{-6} and 10^{-8} Torr, depending on the volatility of the sample, using an APD-6 cryogenic pump. The fast ion bombardment source, supplied with the mass spectrometer by IonSpec Corporation, consists of an ion gun and six steering lenses which are assembled as a cube. Cesium ions are generated using an Antek 160-250B ion gun, accelerated to 4-6 keV, and directed at the sample probe tip for a duration of 100 ms. The probe tip is positioned inside the cube of steering lenses, and the sample ions (which are desorbed by Cs^+ bombardment) are extracted towards the octopole ion guide. Typical extraction voltages range from -350 to -450 volts for singly charged positive ions.

Octopole Ion Guide. The octopole ion guide efficiently transports ions from the source region to the ICR detection cell in the high magnetic field. It spans two regions of differential pumping and can be accessed through the 6 inch stainless steel

"T," the 6 inch 6-way cross, and the 41 inch long detection arm. The octopole is constructed from eight 1/8" stainless steel rods that are 47" long, and is assembled with ceramic supports at six locations along its length. The rods are positioned with 0.170" between the center of the ion guide and the inner rod surface. The octopole is powered by an ENI power amplifier (Model 2100L), driven by a Wavetek function generator (Model 190). Typical rf voltages range from 50-1000 $V_{peak\text{-}peak}$ for transporting ions to the ICR detection cell. The high voltages required for the octopole are derived from an air coil transformer with the secondary coil forming a tuned LC circuit with the octopole rods. The circuit resonates at approximately 1.2 MHz.

ICR Detection Cell. The ICR detection cell is constructed from six stainless steel plates and has dimensions of 2"x2"x3". It is located at the end of the octopole ion guide, inside the 41 inch long detection arm. Ion transfer from the octopole into the ICR detection cell has been enhanced through the incorporation of a split injection electrode mounted at the entrance of the ICR detection cell.[2] The electrode aides in converting ion translational motion along the z-axis into cyclotron motion in the xy plane. The homogeneous magnetic field, which is required for detection, is supplied by an Oxford Instruments Mk.II 7 Tesla superconducting magnet with a 6 inch warm bore. Reaction and collision gases are delivered directly into the ICR detection cell through an inlet manifold equipped with two Varian leak valves (Model 951-5106) and two General Valve pulsed valves (Series 9). The pulsed valves can be operated manually or controlled by electronic TTL pulses. Pressures in the detection region are measured using an ionization gauge in the Schulz-Phelps geometry mounted atop the

cell.[3] This ionization gauge is calibrated against an MKS pressure transducer (Model 390) which has been modified to perform in a high magnetic field.

An OMEGA data system manufactured by IonSpec Corporation is used to provide control pulses for the cesium ion gun, pulsed valves, rf octopole ion guide, split injection electrodes and the ICR detection cell. A Pentek direct digital frequency synthesizer (Model 3100, 8 MHz) is used for the swept rf excitation and ion ejection pulses. The OMEGA data system additionally digitizes and processes the time domain spectra accumulated in each experiment. Transients of up to 256 kilobytes can be recorded. A 486 computer with an array processor is employed for experiment control and data storage and manipulation.

Implementation

We initially investigated the controlled dissociation of protonated peptide ions in an attempt to improve gas phase sequencing techniques. Peptide fragmentation is standardly promoted by colliding an ion with elevated translational energy against a high static pressure of background gas. Translational energy is efficiently converted to vibrational energy, and bond cleavage occurs.[4] Collisional excitation is accomplished in an FT-ICR using off-resonance translational excitation techniques.[5] In these experiments, rf excitation is applied at a frequency slightly different from the cyclotron frequency of the ion to be translationally excited. This causes the ion energy to oscillate with time, with an average given by Equation 1, where q is the charge of the

ion, E_o is the amplitude of the applied electric field, and $(\omega-\omega_c)$ is the difference between the applied excitation frequency and natural cyclotron frequency of the ion. A

$$\langle E_{ion,cm} \rangle = \frac{m_{gas}}{m_{gas} + m_{ion}} \left[\frac{q^2 E_o^{\,2}}{4 m_{ion} (\omega - \omega_c)^2} \right] \qquad (1)$$

typical excitation experiment of this type consists of several steps, including preparation of the peptide sample, production of an ion population, transfer to and trapping of the ions in the ICR detection cell, isolation of the peptide ion of interest, collisional activation of the peptide ion and finally detection of the dissociation products.

Samples are prepared by applying a thin layer of matrix (4:1 mixture of glycerol:trifluoroacetic acid) to a copper probe tip and then dissolving the peptide directly into the matrix. An ion population is generated and transferred to the ICR detection cell by simultaneously applying a 100 ms pulse of 6 keV cesium ions to the probe tip, a 50-250 V, 1.2 MHz sine wave having a dc offset to the octopole rods, and an 18 V differential to the split injection electrode. The ions are trapped with a 1.85 to 2.20 V trapping potential and the transmitter and receiver plates are held at ground potential. The peptide ions are isolated by applying a series of radio frequency pulses to eject unwanted matrix, fragment and cluster ions that are generated in the desorption process. Nitrogen is used as the collision gas at static pressures in the range of 1-2 $x10^{-7}$ Torr. The peptide ions are excited at a frequency which is typically 1000 to 2000 Hz lower than the resonant frequency of the ion for 1 second. Under these conditions,

the ions undergo roughly 3 to 5 collisions during the excitation period. Dissociation energies are varied to generate a complete family of fragment ions for the peptides.

The low-energy collision induced dissociation spectra of protonated leucine enkephalin (YGGFL), a pentapeptide lacking basic side chains, is shown in Figure 2. At a center of mass collision energy of 1.5 eV, the peptide dissociates into numerous fragments of varying intensities. Each fragment represents cleavage of the peptide at a distinct location, and the resulting set of fragment ions allows for the reconstruction of the amino acid sequence of the peptide. The most intense peak (b_4) results from cleavage of the peptide bond between phenylalanine and leucine, with charge retention towards the N-terminus of the peptide. The a_4 ion is generated by the direct fragmentation of the protonated parent ion and also by the sequential decomposition of the b_4 ion.

Unfortunately, not all protonated peptides that were studied dissociated as thoroughly as leucine enkephalin. In fact, peptides which possess basic amino acid residues, such as arginine and lysine, exhibit some side chain cleavage and very little backbone cleavage. This is attributed to the proton being preferentially located on the side chain of these peptides, instead of the N-terminus or peptide backbone. As a result, these peptides do not produce ions which are useful for determining the amino acid sequence. The incorporation of a single arginine amino acid into leucine enkephalin, yielding leucine enkephalin arginine (YGGFLR), makes the peptide nearly resistant to low energy cleavage. The low-energy collision induced dissociation spectra for this peptide is shown in Figure 3. With the collision gas pressure held constant and

Figure 2. Isolation and collision-induced dissociation spectra of protonated leucine enkephalin at m/z=556. The major product observed is the b_4 ion, resulting from cleavage of the peptide bond between phenylalanine and leucine. Off-resonance excitation was performed for 1 second using N_2 as the collision gas at approximately $1x10^{-7}$ Torr. The center of mass collision energies used were a) isolation only, no excitation and b) 1.5 eV.

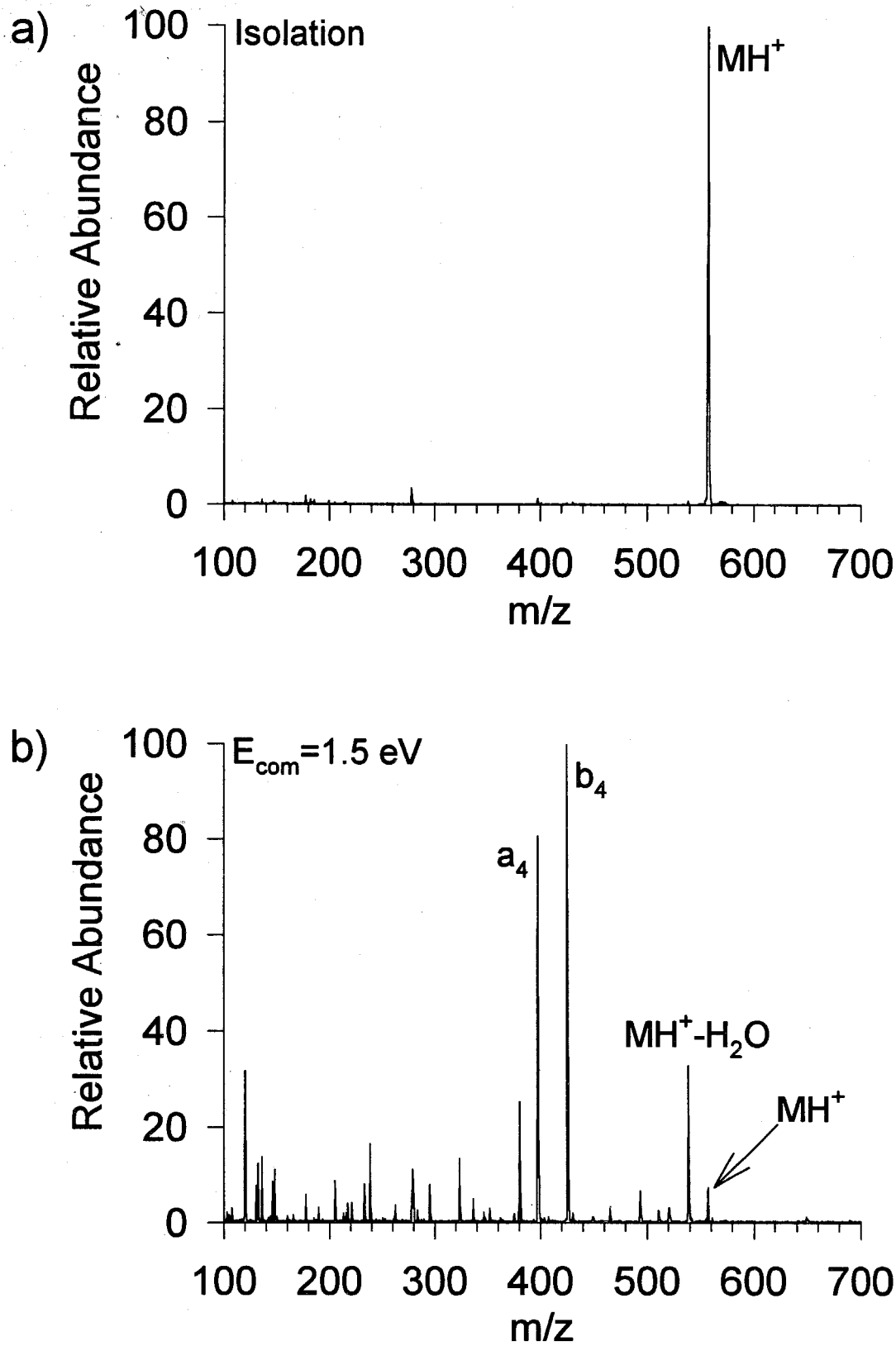
a)
Isolation
MH+
Relative Abundance
100
80
60
40
20
0
100 200 300 400 500 600 700
m/z
b)
Ecom=1.5 eV
b4
a4
MH+-H2O
MH+
Relative Abundance
100
80
60
40
20
0
100 200 300 400 500 600 700
m/z

Figure 2

Figure 3. Isolation and collision-induced dissociation mass spectra of protonated leucine enkephalin arginine at m/z=712. The y_1 dissociation fragment (m/z=175), resulting from cleavage of the arginine amino acid, is observed in small amounts. Off-resonance excitation was performed for 1 second using N_2 as the collision gas at approximately $1x10^{-7}$ Torr. The center of mass collision energies used were a) isolation only, no excitation, and b) 3.1 eV.

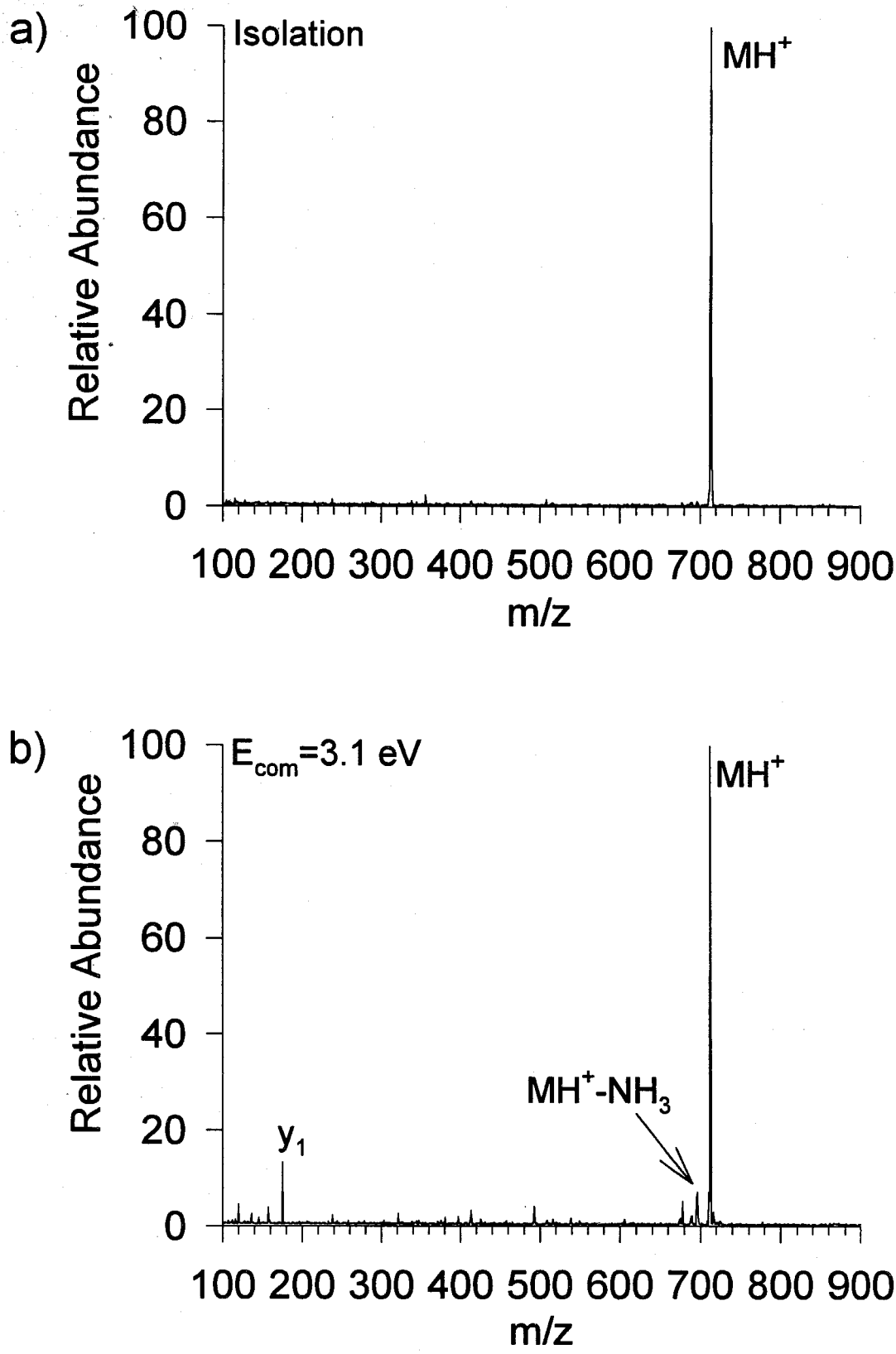
a)
Isolation
MH+
Relative Abundance
100
80
60
40
20
0
100 200 300 400 500 600 700 800 900
m/z
b)
Ecom=3.1 eV
MH+
MH+-NH3
y1
Relative Abundance
100
80
60
40
20
0
100 200 300 400 500 600 700 800 900
m/z

Figure 3

the center of mass energy more than doubled (3.1 eV), leucine enkephalin arginine displays very little fragmentation as compared with leucine enkephalin.

These two examples demonstrate the difficulty in applying low-energy collision induced dissociation techniques as a general method for peptide sequencing in an FT-ICR mass spectrometer. Most interesting peptides found in nature and those produced from enzymatic digestion of proteins possess at least one basic amino acid in their sequence. Although low-energy collision induced dissociation is a successful technique for sequencing many of the simple peptides studied in this thesis, the inability to produce useful fragments from more complex peptides with basic amino acid residues prevents its general application.

References

1. Lebrilla, C. B.; Amster, I. J.; McIver, R. T. *Int. J. Mass Spectrom. Ion Processes* **1989**, *87*, R7.

2. Caravatti, P. United States Patent No. 4,924,089, Issued May 8, 1990, "Method and Apparatus for the Accumulation of Ions in a Trap of the Ion Cyclotron Resonance Spectrometer, by Transferring the Kinetic Energy of the Motion Parallel to the Magnetic Field into Directions Perpendicular to the Magnetic Field."

3. Schulz, G. J.; Phelps, A. V. *Rev. Sci. Instrum.* **1957**, *28*, 1051.

4. Marzluff, E. M.; Campbell, S.; Rodgers, M. T.; Beauchamp, J. L. *J. Am. Chem. Soc.* **1994**, *116*, 6947.

5. Gauthier, J. W.; Trautman, T. R.; Jacobsen, D. B. *Anal. Chim. Acta* **1991**, *246*, 211.

CHAPTER 2

Correlations of Lone Pair Ionization Energies with Proton Affinities of Amino Acids and Related Compounds. Site Specificity of Protonation.

International Journal of Mass Spectrometry and Ion Processes, 117 (1992) 83–99
Elsevier Science Publishers B.V., Amsterdam

Correlations of lone pair ionization energies with proton affinities of amino acids and related compounds. Site specificity of protonation*,**

Sherrie Campbell[a], J.L. Beauchamp[a], Mara Rempe[b] and D.L. Lichtenberger[b]
[a]*Arthur Amos Noyes Laboratory of Chemical Physics, California Institute of Technology, Pasadena CA 91125 (USA)*
[b]*Department of Chemistry, University of Arizona, Tucson AZ 85721 (USA)*

(First received 13 December 1991; in final form 25 March 1992)

ABSTRACT

The gas phase proton affinities of amino acids are compared with their adiabatic ionization energies obtained from photoelectron spectra. Using primary aliphatic amines as reference species, a linear correlation is found between the proton affinities and the adiabatic nitrogen lone pair ionization energies for those amino acids which protonate on the amine group, even in cases where the nitrogen lone pair is not the highest occupied molecular orbital. Many of the amino acids fit the correlation well, which confirms the prediction of amine protonation from earlier studies and also corroborates the assignment of the bands in the complex photoelectron spectra of these species. Proline and sarcosine, amino acids with a secondary nitrogen, deviate from this correlation and instead fit a correlation using secondary aliphatic amines as reference species. Deviations from the correlation exist for molecules, such as lysine, methionine and tryptophan, which contain an intramolecular hydrogen bond between the basic side-chain and the amine site. The gas phase proton affinities of these species are larger than predicted by the correlation. Deviations from the correlation are also predicted for very basic amino acids, such as histidine and arginine, which protonate preferentially on the side-chain instead of the amine group.

Keywords: amino acids; proton affinities; lone pair ionization energies; protonation sites.

INTRODUCTION

It is well known that amino acids form zwitterions in solution. However, studies have established that amino acids possess a non-ionic form as the dominant species in the gas phase. Simple gas phase thermochemical calculations [1] estimate that the transfer of a proton from the carboxyl group in glycine to the amine terminus is nominally endothermic by 33 kcal mol^{-1}. This is substantiated by electronic structure calculations [2] which predict that the

Correspondence to: J.L. Beauchamp, Noyes Laboratory 127-72, California Institute of Technology, Pasadena CA 91125, USA.
* Dedicated to Professor Charles H. DePuy on the occasion of his 65th birthday.
** Contribution No. 8548 from the Arthur Amos Noyes Laboratory of Chemical Physics.

0168-1176/92/$05.00

zwitterion is less stable than the non-ionic form of glycine in the gas phase by 20 kcal mol^{-1}. Protonation or cationization of the neutral amino acid in the gas phase can be accomplished by a variety of techniques. Desorption of an amino acid or larger biological sample from an acidic matrix via laser desorption [3], plasma desorption [4], or fast atom bombardment (FAB) [5] has become an efficient method for producing charged species. Electrospray [6] and thermospray [7] ionization techniques are also used to produce multiply charged gas phase biological species. Unfortunately, covalent attachment of an ionized functional group (such as a quaternary nitrogen) is the only method currently available where one can select the specific site of ionization [8].

The addition of a proton or cation to a large biological molecule, such as a peptide, may occur at a number of sites owing to the many basic functional groups within the molecule. Ionization of these multifunctional species is a complex process, accompanied by folding of the molecule to allow several basic sites to simultaneously interact with and solvate the charge center [9,10]. We have undertaken a systematic study aimed at better understanding the site specificity and energetics of peptide protonation, as well as the gas phase structures of these species, beginning in the present paper with an examination of the amino acids themselves.

In assessing the protonation energetics of molecules, it has proven fruitful to examine correlations of proton affinities with adiabatic lone pair ionization energies of basic sites [11]. Such correlations are observed even when the site of protonation is not associated with the highest occupied molecular orbital (lowest ionization energy). These correlations have several applications. If the lone pair ionization potential of a basic site in a molecule can be determined using photoelectron spectroscopy, then such correlations can be used to predict the intrinsic base strength of that site, even when the molecule may possess another basic site. Similarly, if the site of protonation can be determined, the correlation can be used to estimate the orbital ionization energy of the site, which is useful in assigning bands in complex photoelectron spectra [11]. Deviations from the correlations indicate unusual interactions which lead to differential stabilization of either the radical ions or conjugate acids of n-donor bases [12]. Intramolecular hydrogen bonding interactions can also lead to deviations from a correlation of proton affinities with orbital ionization energies, since these correlations generally consider isolated functional groups.

The present study examines the correlation of adiabatic lone pair ionization energies with proton affinities of amino acids. The following two sections of the paper assess the available data for protonation energetics of amino acids and ionization energetics as derived by photoelectron spectroscopy (PES). The final section presents the correlation of these data and discusses implica-

tions which it has for the site specificity of protonation and structures of this important class of molecules.

PROTON AFFINITIES OF AMINO ACIDS

Studies of gas phase proton transfer equilibria, generalized in reaction (1), have provided a wealth of data for the base strengths of organic molecules.

$$B_1H^+ + B_2 \rightleftharpoons B_1 + B_2H^+ \quad (1)$$

Equilibrium constants measured for proton transfer reactions yield values for the relative free energies of protonation ($\Delta G°$). These values can be converted to relative enthalpies of protonation ($\Delta H°$) if the entropy change can be estimated or determined by measuring the equilibrium constant at several temperatures. The proton affinity (PA) of a species is defined as the enthalpy change for reaction (2).

$$BH^+ \rightarrow B + H^+ \quad (2)$$

Locke and McIver [1,13] report the gas phase basicities for 19 of the 20 common amino acids using the technique of ion cyclotron resonance (ICR) spectroscopy. Of the 20 commonly occurring amino acids, only arginine could not be evaporated off a heated probe tip into vacuum without substantial decomposition. The basicity of sarcosine (*N*-methyl glycine) was also recorded using this technique. Although sarcosine is not one of the common amino acids, it is a methyl derivative of glycine possessing a secondary nitrogen center. The gas phase basicity values of the stable species were obtained by bracketing the amino acid between bases of known strength. An increasing ladder of experimental basicities was generated and the values were reported with an uncertainty of $\pm 0.2\,\mathrm{kcal\,mol^{-1}}$.

The proton transfer reactions studied by Locke and McIver were performed at different temperatures, depending on the volatility of the amino acid. These experiments establish accurate $\Delta G°$ values at a particular temperature. PAs refer to the enthalpy of protonation, and are usually reported at 298 K. In the absence of detailed studies over a wide range of temperature, the usual procedure used to relate differences in free energies and enthalpies of protonation is to estimate the entropy changes, considering mainly changes in rotational symmetry numbers for the neutral bases and their conjugate acids. This procedure does not yield the correct values or even order of PAs when a phenomenon such as internal hydrogen bonding contributes unusually large entropy changes. The results of Locke and McIver for amino acid PAs are listed in Table 1, derived from the free energy differences, assuming that the proton was attached only to the amine group in order to estimate entropy changes and that no cyclization occurred. As recognized by Locke and McIver

TABLE 1

PAs of the amino acids obtained from metastable decomposition, ICR proton transfer and HPMS proton transfer reactions

Metastable decomposition of $[B_1B_2H]^+$ [a]	ICR proton transfer reactions [b,c]	HPMS proton transfer reactions [d]
PA order	PA (kcal mol^{-1}) [e]	PA (kcal mol^{-1}) [e]
Gly	212.0	209.9
Ala	214.8	213.9
Cys	214.7	
Ser	217.2	
Val	217.4	215.6
Asp	217.1	
Leu	218.5	216.2
Thr	218.8	
Ile	219.3	
Phe	220.5	216.8
Met	221.8	
Tyr	222.7	
Asn	220.2	
Pro	223.1	220.1
Glu	216.9	
Trp	225.8	
Gln	218.8	
Lys	230.7	
His	232.3	
Arg		

[a] Reference 15.
[b] References 1 and 13.
[c] Entropy values estimated at 0.6 cal mol^{-1} K^{-1}.
[d] Reference 14.
[e] PAs relative to PA(NH_3) = 204.0 kcal mol^{-1}.

this does not yield correct values for species where protonation leads to formation of an intramolecular hydrogen bond and cyclization.

Meot-Ner et al. [14] also report gas phase basicities for six amino acids using the technique of high pressure mass spectroscopy (HPMS) (Table 1). The six species studied could not form intramolecular hydrogen bonds, and the entropy differences in the proton exchange reaction determined by van't Hoff plots were determined to be negligible. Thus, as an approximation, it was assumed that for proton transfer reactions between amino acids and reference bases, basicity differences were equivalent to PA differences ($\delta\Delta G° = \delta\Delta H°$). The relative order of the six amino acid PAs determined by Meot-Ner et al.

agrees with the order reported by Locke [13], although the absolute PA values for these species differ by up to 3.7 kcal mol^{-1}. Locke suggests that the disagreement in PA values may in part be attributed to the difficulties associated with accurately measuring the partial pressures of the amino acids in proton transfer equilibrium reactions. The pressure of the reacting amino acid base is difficult to measure since most amino acids are involatile and decompose upon heating. Some of the more volatile decomposition products have relatively high base strengths and interfere with the studies of proton transfer equilibrium. In the studies of Meot-Ner et al. the partial pressures of the amino acids could not be measured directly, but were estimated based on measured ion/molecule reaction rates. These estimated values were used in the basicity and PA calculations.

Bojesen [15] reports for 20 amino acids (Table 1) the relative order of PAs obtained from metastable yields measured in the competitive dissociation of proton bound dimers in the second field-free region of a reverse geometry sector mass spectrometer. The intermediate indicated in reactions (3) and (4) was directly generated by FAB of an acidic matrix containing the bases B_1 and B_2 [16]. The metastable yields of the protonated bases B_1H^+ and B_2H^+ were measured and assumed to be proportional to the dissociation rates. Bojesen assumed that the order of the dissociation rates for processes (3) and (4) was equal to the order of the PAs of B_1 and B_2 if the reverse activation energies and entropy effects of the two reactions could be ignored [15].

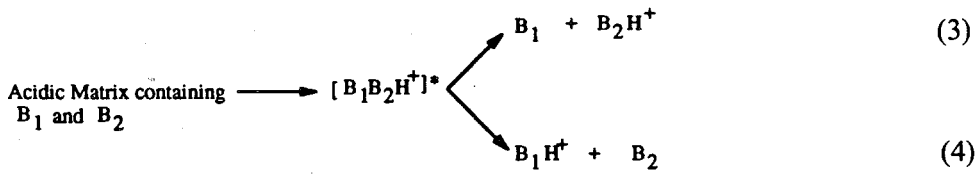

(3)

(4)

Hence, when the B_1H^+ ion was more abundant than the B_2H^+ ion after decomposition, the PA of B_1 was greater than the PA of B_2. While this bracketing method did not provide quantitative data, it did provide reasonable estimates for the order of gas phase PAs. Other investigators have used this methodology to derive thermochemical data and attempted to be more quantitative in the analysis of metastable yields [17].

With the exception of four amino acids, the relative order of PAs reported by Bojesen [15] agrees with the order reported by Locke [13]. Aspartic acid appears too high in Bojesen's order of PAs, but is within the experimental uncertainty of the ICR values. Bojesen's data yield PAs of asparagine, glutamic acid and glutamine which appear higher than those predicted by the ICR bracketing technique by approximately 2.5, 6.2 and 7.0 kcal mol^{-1} respectively. The reason for this discrepancy is not obvious. The importance of cyclic intramolecular hydrogen bonded structures in the metastable

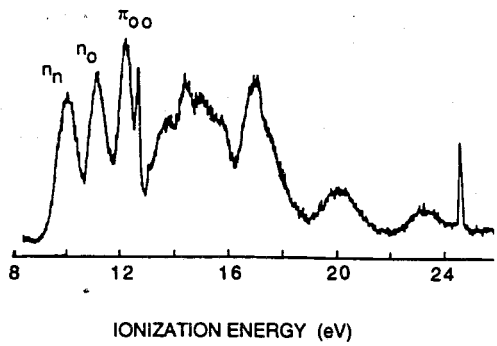

Fig. 1. HeII photoelectron spectrum of glycine, recorded by Cannington and Ham [18]. Nitrogen lone pair, carbonyl oxygen lone pair, and oxygen π orbitals appear as distinct peaks.

experiments is difficult to assess, since the reactants and products are characterized by broad, ill-defined internal energy distributions. It is interesting to note that the largest deviations involve amino acids with the ability to cyclize in acidic media and lose water (Scheme 1).

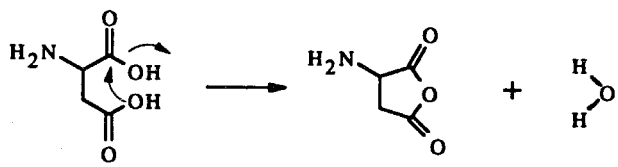

Scheme 1.

Perhaps a proton bound dimer of a cyclized amino acid and a water molecule is detected in the metastable decomposition experiment. This species would possess the same mass as the protonated amino acid and would have enhanced PA owing to multiple hydrogen bonds.

PHOTOELECTRON SPECTRA OF AMINO ACIDS AND RELATED COMPOUNDS

Since most of the common amino acids can be regarded as derivatized glycine molecules, the photoelectron spectrum of glycine ($H_2NRCHCO_2H$, R = H) [18] serves as a standard for comparison with the more complex species (Fig. 1). The HeI and HeII photoelectron spectra for a number of amino acids have been recorded and include the assignments for the nitrogen lone pair (n_N), carbonyl oxygen lone pair (n_O), and oxygen π (π_{OO}) orbitals [18–22]. These orbitals are most affected in the photoelectron spectrum when substitution on the α-carbon occurs. Typically, the lowest ionization energy is attributed to the nitrogen lone pair orbital, n_N, and is spectrally isolated in a distinct band from the n_O and π_{OO} peaks. The oxygen lone pair (n_O) ionization potential is found approximately 1 eV higher in energy than the n_N orbital.

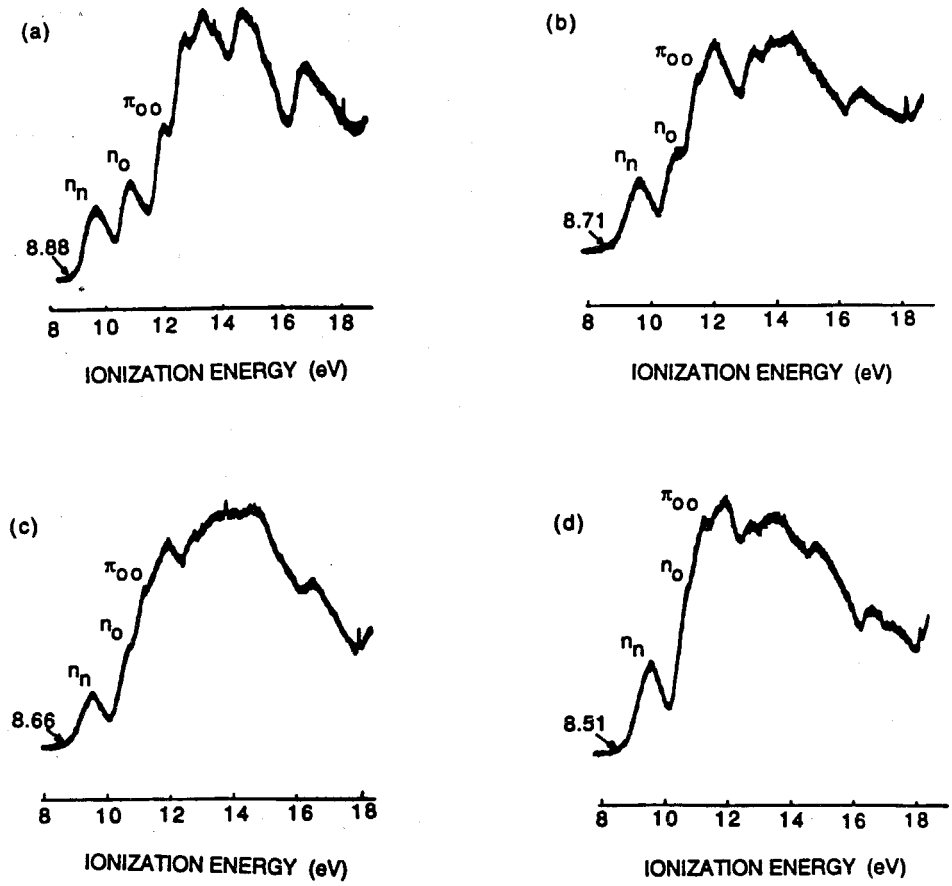

Fig. 2. The highest occupied molecular orbital (lowest ionization energy) in most of the amino acids is the nitrogen lone pair orbital of the amine. The substitution of an alkyl group on the side-chain of an amino acid lowers the ionization energy of the nitrogen lone pair orbital. The spectra of the alkyl amino acids recorded by Klasnic [19] clearly displays this trend. The adiabatic ionization energy decreases from 8.88 eV for alanine (a), to 8.71 eV for valine (b), 8.66 eV for isoleucine (c), and finally 8.51 eV for leucine (d).

The π_{OO} ionization occurs at even higher energy, and is not as clearly resolved as the other two bands. Except where noted, all displayed photoelectron spectra are obtained with a HeI light source.

The adiabatic ionization potential (IP) of the nitrogen lone pair (n_N) orbital changes as the amino acid side-chain varies. As the electron donating ability of the side-chain increases, the n_N IP shifts to lower energy since the lone pair orbital destabilizes. This trend is clearly demonstrated in the photoelectron spectra of amino acids with alkyl side-chains (Fig. 2). The destabilization of

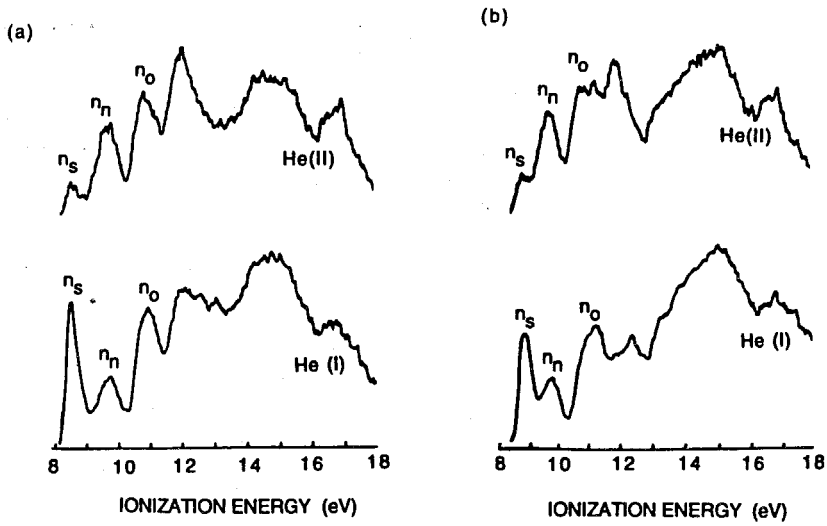

Fig. 3. Molecules such as (a) methylcysteine and (b) methionine have ionizable functional groups in the side-chain which provide the highest occupied molecular orbital. The HeI and HeII spectra of these compounds recorded by Cannington and Ham [18] identify the sulfur lone pair at lower ionization energy than the nitrogen lone pair.

the lone pair orbital increases the electron donor ability of the site and leads to enhanced basicity. As a result, PAs increase as IPs decrease.

The highest occupied molecular orbital (lowest IP) of some amino acids is not the nitrogen lone pair (n_N) orbital, but is an orbital associated with a functional group of the side-chain. Amino acids such as methionine and cysteine have the sulfur lone pair orbital (n_S) of the side-chain at the lowest ionization energy (Fig. 3). The aromatic phenyl π orbitals in the side-chains of phenylalanine and tyrosine also have low ionization energies which makes distinguishing between the π and n_N orbitals difficult (Fig. 4). Although the π_3, π_2, and n_N bands in the phenylalanine spectrum appear to overlap, each orbital can be assigned by comparing the peaks to similar known spectra [23]. In contrast, the tyrosine spectrum clearly shows the π_3 spectral peak at the lowest energy. The electron donating hydroxyl substituent attached at the para position of the aromatic ring destabilizes the π_3 orbital and decreases its IP [24]. Since the π_3 IP shifts to lower energy, the peaks in the tyrosine spectrum are better resolved and are easily identified.

The amino acid tryptophan has the most difficult photoelectron spectrum to interpret and was recorded for this study (Fig. 5)[a]. Seki and Inokuchi [22]

[a] Photoelectron spectra were recorded on an instrument featuring a 36 cm radius hemispherical analyzer (10 cm gap) with customized sample cell, excitation sources, and detection and control electronics. See e.g. ref. 25.

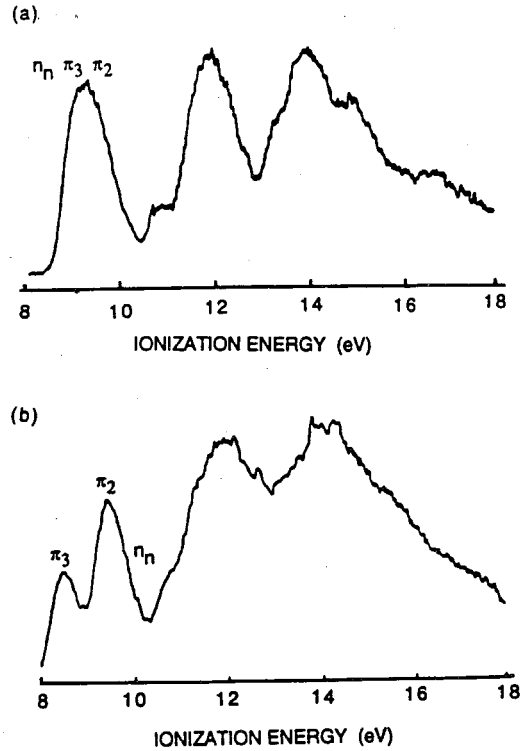

Fig. 4. Photoelectron spectra of (a) phenylalanine and (b) tyrosine, recorded by Cannington and Ham [18], in which the aromatic π and n_N orbitals have very similar energies. Only by comparison with model compounds can the overlapping peaks in the phenylalanine spectrum (a) be identified. The tyrosine spectrum (b) is more easily resolved since the π_3 orbital is destabilized by the substitution of the hydroxyl group on the para position of the side-chain ring.

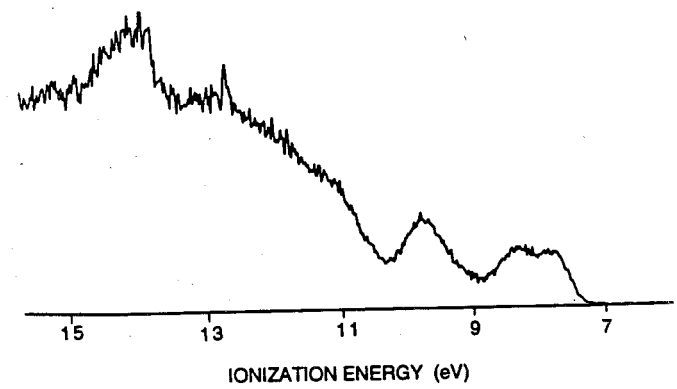

Fig. 5. Photoelectron spectrum of tryptophan (full spectrum).

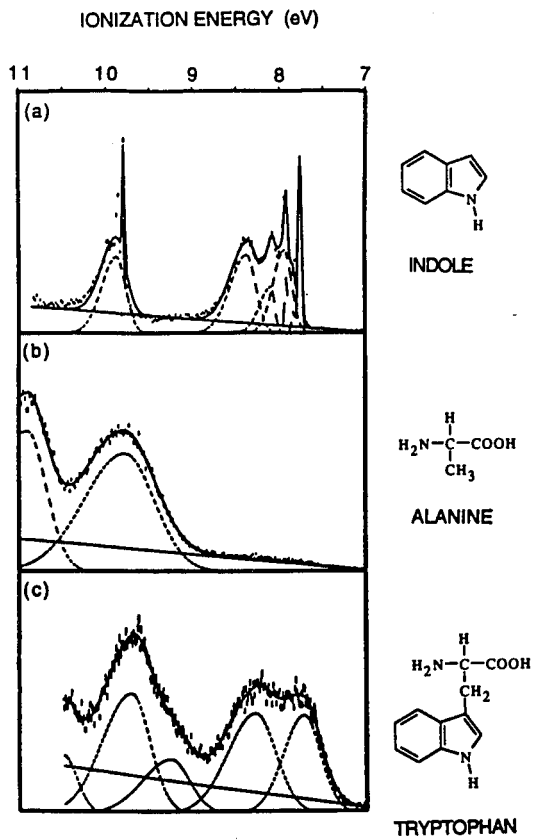

Fig. 6. The tryptophan molecule can be broken into two pieces: an indole moiety and an alanine moiety. The photoelectron spectrum of indole (a) displays distinct ionization bands for the low energy aromatic π and higher energy n_N orbitals. The photoelectron spectrum of alanine (b) clearly shows the n_N orbital of the amine as the lowest ionization energy, but the value is similar to that of the n_N orbital in the indole. The tryptophan spectrum (c) appears to be a summation of the indole and alanine spectra. Since the n_N peaks from the indole and alanine overlap, it is difficult to identify the IP of the amine.

recognized that the molecular structure of tryptophan could be separated into two distinct subunits: an alanine moiety and an indole moiety. Comparing ionization energies of distinct bands in the low energy region of these molecules, Seki and Inokuchi predicted the molecular orbital characteristics of each band of tryptophan. Figure 6 shows spectra for indole, alanine, and tryptophan with the low energy ionization region enlarged. The spectrum of indole has six overlapping π orbital peaks in a band between 7.5 and 9.0 eV, and two peaks between 9.5 and 10.5 eV. The spectrum of alanine has only one peak for the n_N orbital at 9.0–11.0 eV. The spectrum of tryptophan appears to be a combination of the indole and alanine spectra. Deconvolution of the

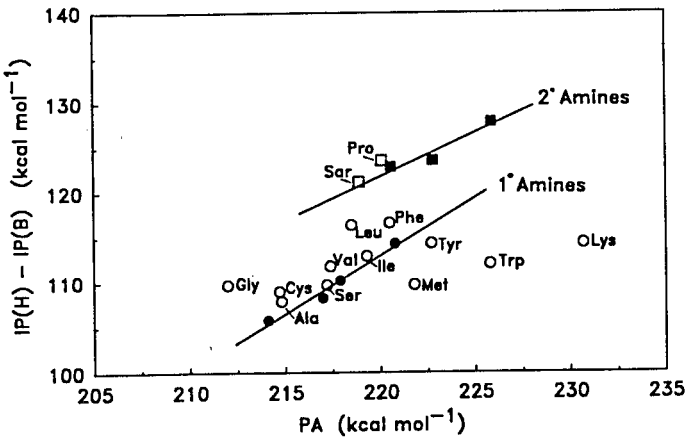

Fig. 7. The correlation of the nitrogen lone pair ionization energy of the amine group with the PA of numerous amino acids is shown (open circles). Most of the amino acids fit the correlation with the primary amine data (filled circles), which is consistent with the amine group being the preferred site of protonation. As expected, proline and sarcosine fail to fit the correlation for the primary amines and instead fit the correlation for the secondary amines (filled squares). Data for all the amines are listed in Table 2. Deviations from the correlation are explained in the text. The lines through the points are least-squares fits to the reference aliphatic amine data for primary and secondary amines.

broad spectral bands of tryptophan using gaussian peak fitting programs [26] can separate many of the expected peaks. From inspection, the lower energy band contains the IPs from the aromatic rings of the indole subunit. The second band (roughly between 8.7 and 10.5 eV) contains the nitrogen lone pair IPs for the amine and indole groups. The comparison of adiabatic IPs suggests that the first (lower energy) peak in the second band of tryptophan belongs to the nitrogen lone pair of the amine. However, the assignment of the peak is somewhat uncertain since substitution onto the indole ring could shift the energy of the aromatic orbitals, or possibly the nitrogen orbital of the indole.

Because of geometry changes which accompany ionization, the nitrogen lone pair IP of the amine is usually a broad band in the photoelectron spectrum, making assignment of the adiabatic IP difficult. Estimates of the adiabatic IPs, which are summarized in Table 2, may be in error by as much as ± 0.2 eV, especially in cases where the nitrogen lone pair is not the highest occupied molecular orbital. The absence of entries in Table 2 indicates that photoelectron spectra for these species were not available. For the amino acids listed in Table 2, the difference in vertical and adiabatic nitrogen lone pair ionization energies is a constant 1.0 ± 0.1 eV, with only glycine and serine being slightly larger with differences of 1.2 eV. For this ionization process, the Franck–Condon envelope does not in any case suggest unusual interactions

TABLE 2

PAs and ionization energies for the amino acids and reference bases used in the correlation diagram of Fig. 7

Species (B)	PA (B)[a]	PES[b]	1st IP[c]	N IP[d]	D[B^+–H][e]
Amino acids					
Gly	212.0	18	8.8	8.8	101.3
Ala	214.8	19	8.88	8.88	106.0
Cys	214.7	18	8.0	8.83	104.7
Ser	217.2	18	8.8	8.8	107.4
Val	217.4	19	8.71	8.71	104.6
Asp	217.1	–[f]	–	–	–
Leu	218.5	19	8.51	8.51	101.2
Thr	218.8	–	–	–	–
Sar	218.9	18	8.3	8.3	97.6
Ile	219.3	19	8.66	8.66	105.4
Phe	220.5	20	8.5	8.5	103.8
Met	221.8	18	8.0	8.8	111.1
Tyr	222.7	18	8.0	8.6	107.4
Asn	220.2	–	–	–	–
Pro	220.1	18	8.2	8.2	96.5
Glu	216.9	–	–	–	–
Trp	225.8	22	7.2	8.7	112.8
Gln	218.8	–	–	–	–
Lys	230.7	18	8.6	8.6	115.4
His	232.3	–	–	–	–
Arg	> 232.0	–	–	–	–
Reference bases					
$MeNH_2$	214.1	33	8.97	8.97	107.3
$EtNH_2$	217.0	33	8.86	8.86	107.7
$PrNH_2$	217.9	33	8.78	8.78	106.8
tBuNH$_2$	220.8	34	8.60	8.60	105.5
$(Me)_2NH$	220.6	33	8.23	8.23	96.8
(Me)EtNH	222.8	30	8.20	8.20	98.3
$(Et)_2NH$	225.9	34	8.01	8.01	97.0

[a] PAs in kilocalories per mole, see text for refs.
[b] References for photoelectron data.
[c] Lowest adiabatic IP in electronvolts.
[d] Nitrogen lone pair IP in electronvolts.
[e] Homolytic bond dissociation energy in kilocalories per mole.
[f] Indicates that no data are available for these species.

in the molecular ion or different conformations with unusually different ionization energies.

The adiabatic ionization energy for the n_N orbital of threonine is not included in Table 2. The photoelectron spectrum of threonine has been recorded, but the ionization energies are reported only in tabular form [18]. Unfortunately, the data presented do not agree with earlier published results [20]. The ionization energy of the n_N orbital is reported as 0.2 eV higher than the n_N ionization energy for serine. The addition of a methyl substituent to the side-chain of an amino acid should not increase the adiabatic n_N ionization energy, and the result reported for threonine is contrary to theoretical predictions and chemical intuition.

CORRELATION OF LONE PAIR IONIZATION ENERGIES WITH PA OF AMINO ACIDS

The PA of a molecule is related to the homolytic bond energy in the conjugate acid [$D(B^+-H)$] by the thermochemical cycle of Scheme 2. If the homolytic bond dissociation energy is constant for a particular functional group, the PA will exhibit a linear correlation with the quantity IP(H) − IP(B), eqn. 5[b]:

$$PA = IP(H) - IP(B) + [D(B^+ - H)] \quad (5)$$

The correlation of the nitrogen lone pair ionization energy of the amine group with the PA of numerous amino acids is shown in Fig. 7. Included in the figure for comparison is the correlation observed for several simple primary and secondary amines (data in Table 2). A least-squares fit of the primary amine data yields a line of slope 1.29 and correlation coefficient (R^2) of 0.98. Many of the amino acids fit the primary amine correlation reasonably well, which is consistent with the amine group being the preferred site of

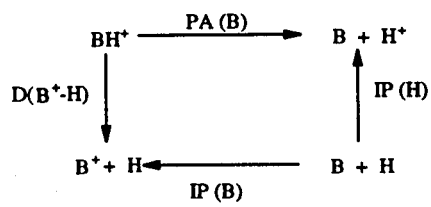

Scheme 2.

[b]The range in PAs for a specific functional group may be ascribed to inductive and polarization stabilizing effects on the cation BH^+ compared with the neutral B. For the species where amino group protonation is indicated, inductive and polarization effects probably make only minor contributions to relative homolytic bond energies, since BH^+ and B^+ are of the same charge type and the charge is localized mainly at the nitrogen center for both species. Hence, homolytic bond energies can be considered constant for a particular functional group. See e.g. ref. 27.

protonation [1,14]. A least-squares fit of the amino acid data (excluding glycine, tryptophan, methionine and lysine) yields a line of slope 0.97 and correlation coefficient (R^2) of 0.63. Failure to observe an exact correlation can be attributed to several factors. There are orbital interactions in the more complex amino acids which are not operative in the simple aliphatic amines. Such interactions tend to increase orbital energies of the highest occupied molecular orbitals, which include the nitrogen lone pair. This increase corresponds to a decrease in the ionization energy [28] which might explain the observation that the majority of the points in Fig. 7 for the amino acids are slightly above the correlation line for aliphatic amines. Such speculation may be unwarranted, however, since the scatter of the points for the amino acids around the primary amine correlation line may reflect the difficulty of accurately assigning adiabatic IPs from the photoelectron spectra, as previously discussed. We have chosen to display the photoelectron spectra in part to make this problem clear.

Proline and sarcosine fail to fit the correlation for primary amines, as expected, and instead fit the correlation for secondary amines. The two different correlations shown correspond to homolytic bond dissociation energies of 107 and 97 kcal mol^{-1} for primary and secondary amines respectively. This decrease in homolytic bond dissociation energies on going from primary to secondary amines is analogous to the decrease in primary and secondary C–H bond energies in isoelectronic hydrocarbons.

Interestingly, for the primary amines, glycine exhibits a noticeable deviation from the correlation. As noted above, glycine has one of the largest differences between vertical and adiabatic ionization energies (1.2 eV compared with 1.0 eV for most of the amino acids). A difference of 1.0 eV would bring glycine into closer agreement with the correlation. However, the deviation may be real and could signal the importance of a stable conformation of the molecular ion which can be accessed in the photoionization process.

The point for lysine in Fig. 7 does not fit the correlation. As noted above, the PA value for this species was derived with no attempt to consider the effects which intramolecular hydrogen bond formation has on the differences between $\delta\Delta H°$ and $\delta\Delta G°$ values for proton transfer equilibrium. The deviation of lysine from the correlation represents the strength (enthalpy) of the intramolecular hydrogen bond, less the free energy change which results from cyclization. Meot-Ner [9] calculated the net stabilization (or deviation) to be approximately 7 kcal mol^{-1} for each additional bond formed in amine complexes. If we estimate the entropy of cyclization (ΔS_{cycl}) to be approximately -20 eu, then this indicates an internal hydrogen bond strength of about 18 kcal mol^{-1} for the eight-membered ring: 10 kcal mol^{-1} is attributed to the deviation of lysine from the correlation in Fig. 7, plus approximately

8 kcal mol^{-1} for the free energy of cyclization ($-T\Delta S$) at the experimental temperature of 415 K. This bond strength is somewhat less than the unstrained intermolecular hydrogen bond strengths between primary amines (roughly 23 kcal mol^{-1} for ethylamine) [29] and comparable with the intramolecular hydrogen bond strengths in diaminoalkanes (18.5 kcal mol^{-1} for 1,4-diaminobutane) [30].

The point for methionine in Fig. 7 is also displaced from the correlation in a direction which suggests the possibility of intramolecular hydrogen bond formation (six-membered ring). The 4 kcal mol^{-1} deviation is significantly less than the 10 kcal mol^{-1} deviation noted for lysine and corresponds to a hydrogen bond strength of approximately 12 kcal mol^{-1}. This result is consistent with hydrogen bond strengths to sulfur being typically less than to nitrogen centers.

Another amino acid included in Fig. 7 for which a major deviation from the correlation is observed is tryptophan. As previously shown, the photoelectron spectrum of tryptophan is complex, and the adiabatic nitrogen lone pair ionization energy is roughly estimated to be 8.7 eV. Plotting the nitrogen lone pair ionization energy as this value displays behavior similar to lysine in which the PA is larger than expected by approximately 7 kcal mol^{-1}, corresponding to a 15 kcal mol^{-1} hydrogen bond strength (again assuming ΔS_{cycl} to be -20 eu for cyclization and using an experimental temperature of 420 K) [13]. This suggests that a somewhat weaker hydrogen bond compared with lysine results from the constrained ring geometry of the indole substituent.

As mentioned earlier, the correlation can be used to estimate the orbital ionization energy of the site of protonation if the PA of the molecule can be determined. Although the PA for histidine is known, it is difficult to predict the nitrogen lone pair ionization energy of the species from the correlation. Histidine, and similarly arginine, is anticipated to deviate from the correlation. These two species are among the most basic amino acids, and protonate on the side-chain.

CONCLUSIONS

A linear correlation exists between the PAs and nitrogen lone pair ionization energies of the amino acids which protonate on the amine group. The correlation is even observed for those species such as tyrosine and cysteine, where the nitrogen lone pair is not the highest occupied molecular orbital. Although the majority of the amino acids fit the correlation well, a few species deviate. Lysine, methionine and tryptophan, which form intramolecular hydrogen bonds when protonated have enhanced PAs over the values predicted from the correlation. This is easily explained since the free energy

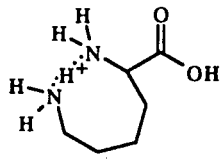

[LYSINE]H^+

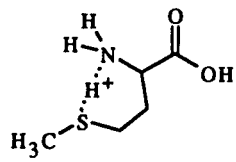

[METHIONINE]H^+

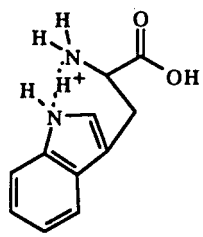

[TRYPTOPHAN]H^+

change associated with the entropy lost in cyclization is more than compensated for by stabilization gained by forming hydrogen bonds.

It is of interest to speculate about the possibility of extending correlations of the type presented here for the simple amino acids to more complex multifunctional molecules, such as peptides. In addition to the amine terminus and the more basic side groups, it becomes necessary to consider the amide linkage as a potential site of protonation. Accurate determination of PAs in equilibrium studies for species beyond methylated dipeptides will probably be difficult because of low volatility of the neutral species. In addition, intramolecular hydrogen bond formation will be more prevalent and this usually results in high PAs (where reference species may be lacking) and low rates for proton transfer reactions. Metastable studies of the type performed by Bojesen may be more fruitful, but the origin of the substantial quantitative differences from equilibrium studies noted above for selected compounds needs to be identified before the results can be regarded without suspicion. A similar technique, developed in our laboratory [31], involves forming an adduct of the protonated biomolecule with a reference base and determining the preferred dissociation pathway when the hydrogen bond is broken using cw infrared laser multiphoton activation [32]. With respect to the other variables in the correlation discussed in the present work, the complexity and poor resolution of photoelectron spectra of small peptides will make it difficult to assign specific ionizations with any certainty. With some hope of further progress, we are currently examining acylated amino acids as models for the amide group in peptides, and N-alkylated amino acids to determine the possibility that the base strength of the amine terminus can be substantially increased.

ACKNOWLEDGMENTS

We gratefully acknowledge the financial support of S.C. from a NIH-NRSA traineeship in Biotechnology, and are indebted to the Beckman Foundation and Institute for the continuing support of the research facilities. This work was supported in part by the National Science Foundation under Grant CHE-9108318.

REFERENCES

1 M.J. Locke and R.T. McIver, J. Am. Chem. Soc., 105 (1983) 4226.
2 L.R. Wright and R.F. Borkman, J. Am. Chem. Soc., 102 (1980) 6207; J. Phys. Chem., 86 (1982) 3956.
3 M. Karas and F. Hillenkamp, Anal. Chem., 60 (1988) 2299.
J. Grotemeyer and E.W. Schlag, Acc. Chem. Res., 22 (1989) 399.
4 D.F. Torgerson, R.P. Skowronski and R.D. Macfarlane, Biochem. Biophys. Res. Commun., 60 (1974) 616.
P. Roepstorff, Acc. Chem. Res., 22 (1989) 421.
5 M. Barber, R.S. Bordoli, R.S. Sedgewick and A.N. Tyler, J. Chem. Soc., Chem. Commun., (1981) 325.
6 C.K. Meng, M. Mann and J.B. Fenn, Z. Phys. D, 10 (1988) 361.
J.B. Fenn, M. Mann, C.K. Meng, S.F. Wong and C.M. Whitehouse, Science, 246 (1989) 64.
7 C.R. Blakely and M.L. Vestal, Anal. Chem., 55 (1983) 750.
M.L. Vestal and G.J. Fergusson, Anal. Chem., 57 (1985) 2373.
8 J.E. Vath and K. Biemann, Int. J. Mass Spectrom. Ion Processes, 100 (1990) 287.
9 M. Meot-Ner, J. Am. Chem. Soc., 106 (1984) 278.
10 R. Grese, R. Cerny and M. Gross, J. Am. Chem. Soc., 111 (1989) 2835.
11 R.H. Staley, J.E. Kleckner and J.L. Beauchamp, J. Am. Chem. Soc., 98 (1976) 2081.
12 R.H. Staley and J.L. Beauchamp, J. Am. Chem. Soc., 96 (1974) 1604.
13 M. Locke, Ph.D. Thesis, University of California, 1983 (unpublished).
14 M. Meot-Ner, E.P. Hunter and F.H. Field, J. Am. Chem. Soc., 101 (1979) 686.
15 G. Bojesen, J. Am. Chem. Soc., 109 (1987) 5557.
16 G. Bojesen, J. Chem. Soc., Chem. Commun., (1986) 244.
17 S.A. McLuckey, D. Cameron and R.G. Cooks, J. Am. Chem. Soc., 103 (1981) 1313.
18 P. Cannington and N. Ham, J. Electron Spectrosc. Relat. Phenom., 32 (1983) 139.
19 L. Klasnic, J. Electron Spectrosc. Relat. Phenom., 8 (1976) 161.
20 P. Cannington and N. Ham, J. Electron Spectrosc. Relat. Phenom., 15 (1979) 79.
21 T. Debies and J.W. Rabalais, J. Electron Spectrosc. Relat. Phenom., 3 (1974) 315.
22 K. Seki and H. Inokuchi, Chem. Phys. Lett., 65 (1979) 158.
23 S. Campbell, J.L. Beauchamp, M. Rempe and D.L. Lichtenberger, to be published.
24 D. Turner, C. Baker, A. Baker and C. Brundle, Molecular Photoelectron Spectroscopy, Wiley–Interscience, New York, 1970.
25 D.L. Lichtenberger, G.E. Kellogg, J.G. Kristofzski, D. Page, S. Turner, G. Klinger and J. Lorenzen, Rev. Sci. Instrum., 57 (1986) 2366.
26 D.L. Lichtenberger and R.F. Fenske, J. Am. Chem. Soc., 98 (1976) 50.
27 W.G. Henderson, M. Taagepera, D. Holtz, R.T. McIver, Jr., J.L. Beauchamp and R.W. Taft, J. Am. Chem. Soc., 94 (1972) 4728.
28 R. Hoffman, Acc. Chem. Res., 4 (1971) 1.
29 M. Meot-Ner, Molecular Structure and Energetics, Vol. 4, VCH, New York, 1987, p. 74.
30 D. Aue and M. Bowers, Gas Phase Ion Chemistry, Vol. 2, Academic Press, New York, 1979.
31 S. Campbell and J.L. Beauchamp, to be published.
32 L.R. Thorne and J.L. Beauchamp, Gas Phase Ion Chemistry, Vol. 3, Academic Press, New York, 1984, p. 41.
33 K. Kimura and S. Katsuma, Handbook of He(I) Photoelectron Spectra of Fundamental Organic Molecules, Halsted Press, New York, 1981.
34 H. Rosenstock, J. Phys. Chem. Ref. Data, 6 (1977).

CHAPTER 3

Infrared Laser Multiphoton Dissociation of Proton Bound Dimers of Biomolecules: A New Method to Probe the Acid Base Properties of Local Sites in Complex Molecules.

Infrared Laser Multiphoton Dissociation of Proton Bound Dimers of Biomolecules: A New Method to Probe the Acid Base Properties of Local Sites in Complex Molecules.

Sherrie Campbell and J.L. Beauchamp

Contribution No. 8598 from the Arthur Amos Noyes Laboratory of Chemical Physics

California Institute of Technology, Pasadena, California 91125

Abstract

New techniques such as matrix assisted laser desorption, electrospray ionization, and fast atom or ion bombardment make it possible to obtain quasimolecular (e.g., protonated) ions of thermally fragile biomolecules without significant decomposition or fragmentation. These ions can be studied using a variety of mass spectrometric techniques, most powerful among which is Fourier transform ion cyclotron resonance spectroscopy (FT-ICR). One of the important advantages of FT-ICR is the ability to store ions for long periods of time, facilitating studies of processes such as bimolecular reactions and laser photodissociation. One significant application of FT-ICR has been to study the acid-base properties of molecules in the gas phase. In

this article we demonstrate a new method to probe the acid-base properties of local sites in biomolecules using a novel application of infrared multiphoton dissociation. The usual method of studying proton transfer reactions with appropriate reference bases does not work well with large molecules due to their propensity for radiative bimolecular cluster formation. The difficulty which this introduces can be circumvented by dissociating the proton bound dimer by infrared multiphoton excitation with a cw CO_2 laser. Infrared heating assists dissociation along the lowest energy pathway and fragments the dimer to leave the proton preferentially on the more basic site. We illustrate this technique by demonstrating that the proton affinity of N-acetyl glycine is intermediate between glycine and alanine.

Introduction

Identification of large involatile biological molecules by mass spectrometry has become a routine task as a result of improved experimental methodology for the formation of quasimolecular ions in which the species of interest is typically ionized by protonation, deprotonation or cationization (e.g., alkali ion attachment). Volatilization of a biomolecule from an appropriate matrix via laser desorption,[1] plasma desorption,[2] or fast atom or ion bombardment[3] has become an efficient method for producing charged species. Electrospray and thermospray ionization[4] are also useful methods for biomolecule analysis, often producing multiply charged quasimolecular ions. The addition of a proton or cation to a biological molecule may occur at a number of sites due to the many basic functional groups within the molecule. If the species is not too

complex, it has proven useful in assessing protonation energetics of molecules to examine correlations of proton affinities with adiabatic lone-pair ionization energies of basic sites.[5] Such correlations can be used to predict the intrinsic base strengths of the sites and ascertain the site of protonation in simple molecules. It is difficult, however, to predict the site of protonation in complex molecules, such as proteins and peptides, since folding of the molecule can allow several basic sites to simultaneously interact with and solvate the charge center. In addition, the more usual methods for determining experimental proton or cation binding energies do not work well for large molecules as a result of the tendency to form adducts rather than undergo even exothermic proton or cation transfer reactions with reference bases. In this study we present a new technique which was developed to determine the acid-base properties of local sites in complex molecules.

Most methods which can be successfully employed to generate quasimolecular ions of biological molecules can be regarded as "soft" ionization, since the ions have low internal energies and little tendency to fragment. In fast atom bombardment (FAB), for example, some fragmentation occurs spontaneously upon ionization, but the abundance of these ions is relatively low. While this is useful in the analysis of complex mixtures and the accurate determination of biomolecule molecular weights, it is often useful to have internal energies sufficiently high to promote fragmentation processes. For example, if sequencing of a peptide is desired, fragment ions are necessary to determine the amino acid composition. This cleavage is most often accomplished in mass spectrometers by collision induced dissociation (CID) where fragmentation results

from energetic collisions with neutral atoms and molecules. Multiphoton excitation of molecules by continuous wave (cw) infrared radiation offers an alternative form of controlled molecular activation which has not been widely explored in applications to biomolecule mass spectrometry.[6,7]

The requirements to observe multiphoton dissociation with a cw infrared laser can be summarized as follows. The molecules must absorb in the region of accessible intense laser lines (9-11 microns for a CO_2 laser). The density of states in the molecule must be sufficiently high to efficiently couple energy out of the pumped mode(s) and into other vibrational degrees of freedom where it becomes randomized, in competition with processes such as spontaneous and stimulated emission and collisional deactivation. This generally requires that the density of states exceeds $10^3/cm^{-1}$, which is the inverse bandwidth of a flowing gas CO_2 longitudinal discharge laser. This can generally be satisfied at room temperature with molecules having more than ten heavy atoms and a thermal internal energy distribution. As shown in Figure 1, the molecule continues to absorb energy through the pumped mode(s) until sufficient internal energy is accumulated to effect dissociation.

Infrared radiative cooling of large vibrationally excited molecules is significant on a 1 second time scale.[6] As a result, laser intensities must be sufficient to pump a significant fraction of the molecular population to levels of internal excitation where dissociation occurs on this time scale. The competing processes of excitation and deactivation are depicted in Figure 2. Finally, it is important to recognize that the energy in excess of the activation energy required to produce dissociation at a

Figure 1. Infrared multiphoton dissociation processes observed with cw lasers typically involve a pumped mode or modes which are strongly coupled to other vibrational modes in the molecule. Energy transfer out of the pumped mode is rapid, and energy continues to accumulate until the dissociation limit is passed.

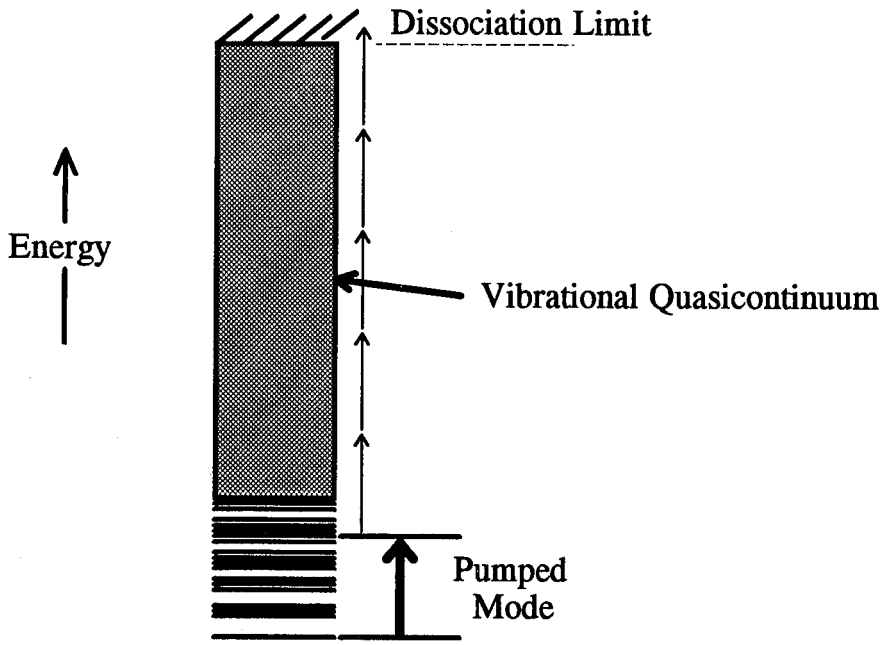
Dissociation Limit
Energy
Vibrational Quasicontinuum
Pumped
Mode

Figure 1

Figure 2. Schematic illustration of molecular vibrational energy distribution during infrared laser multiphoton dissociation processes. IR pumping competes with IR emission and collisional deactivation. With large molecules the energy distribution may have to significantly exceed the activation energy before dissociation can compete with IR emission.

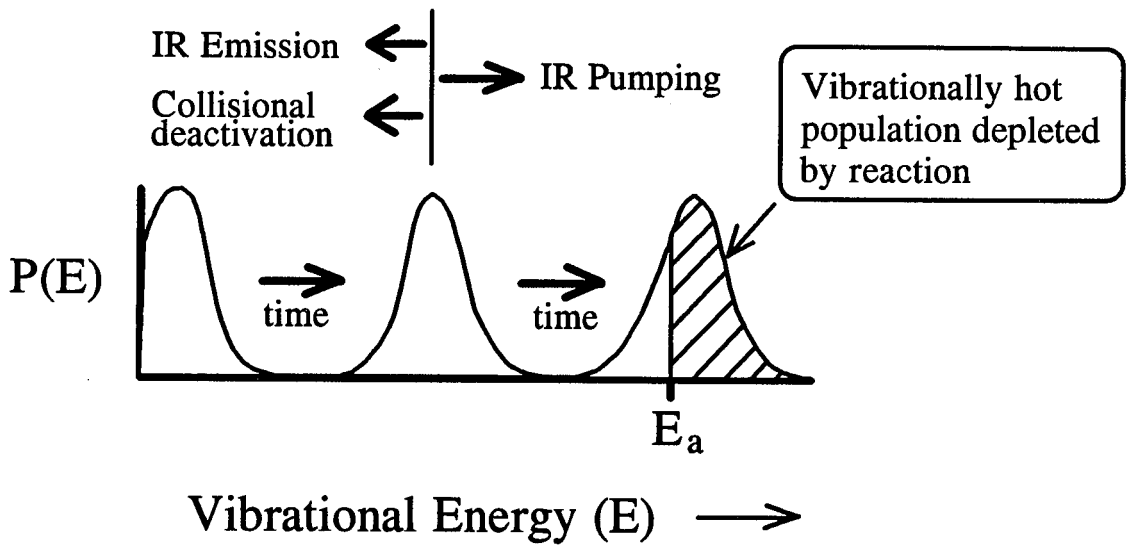
IR Emission
Collisional deactivation
IR Pumping
Vibrationally hot population depleted by reaction
P(E)
time
time
E_a
Vibrational Energy (E)

Figure 2

particular rate increases rapidly with increasing molecular size. These requirements can be quantified using RRKM calculations to describe the unimolecular reaction dynamics.[8] It may be necessary to pump the internal energy distribution shown in Figure 2 to many times the activation energy to achieve dissociation rates which can compete with radiative cooling or meet even more restrictive temporal constraints imposed by the mass spectrometric technique being used to examine the dissociation process. In time of flight and sector instruments, dissociation rates in excess of 10^4-10^5 sec^{-1} are required to effect fragmentation prior to detection. The time scale of trapped ion FT-ICR experiments is much longer, and dissociation rates of 1 sec^{-1} can be accommodated.

The techniques of FT-ICR are uniquely suited for studying slow multiphoton dissociation of gas phase ions.[9] In FT-ICR experiments ions may be trapped and irradiated under nearly collisionless conditions for times up to several seconds. The ability to detect and mass analyze reactants and products at any instant of time during the trapping and irradiation cycle provides direct information regarding reaction pathways and the kinetics of dissociation processes. Furthermore, both reactive and non-reactive (buffer) gases can be added to allow for the effects of collisions during the storage period to be observed. We believe the cw infrared laser multiphoton activation of gas phase biological ions holds great promise as a means of controlled molecular activation to be used in conjunction with experiments designed to probe the properties and structures of complex biological molecules.

In this paper, we demonstrate the application of cw infrared laser multiphoton dissociation (IRMPD) of model biological systems to determine the acid-base properties of local sites in complex molecules, by examining the preferred direction of dissociation of proton bound dimers of the molecule of interest with appropriate reference bases. The gas phase proton affinity of a base, B_1, is defined as the negative of the enthalpy change for Reaction 1. The usual method employed to determine

$$B_1 + H^+ \rightarrow B_1H^+ \qquad (1)$$

proton affinities of molecules in the gas phase involves observation of proton transfer equilibria such as shown in Reaction 2, where B_2 is a reference species with known

$$B_1H^+ + B_2 \rightarrow B_2H^+ + B_1 \qquad (2)$$

proton affinity.[10] With sufficiently large molecules the clustering process (Reaction 3) can become important, and can even occur as a bimolecular process if the initially formed proton bound dimer is radiatively stabilized by infrared emission before it can dissociate.[11]

$$B_1H^+ + B_2 \rightarrow B_1B_2H^+ \qquad (3)$$

The present study starts with stable proton bound dimers and examines the kinetics of the competitive dissociation processes (Reaction 4) and (Reaction 5), using infrared laser multiphoton excitation to activate the proton bound dimer. Our results exemplify the temporal constraints associated with this experimental methodology and serve as an example for future quantitative studies involving IRMPD.

$$B_1B_2H^+ + nh\nu \rightarrow B_1H^+ + B_2 \quad (4)$$

$$\rightarrow B_2H^+ + B_1 \quad (5)$$

Experimental

Experimental techniques associated with ion cyclotron resonance spectroscopy (ICR) and in particular FT-ICR, have been previously described in detail.[9] Experiments were performed using an IonSpec FT-ICR data system in conjunction with a 1-inch cubic trapping cell modified for infrared photochemistry.[12] Experiments were carried out at 2 Tesla using a Varian 15-inch electromagnet.

Appreciable vapor pressure of the amino acids was generated by heating a quartz tube of solid sample in vacuum directly under the trapping cell. Because of this arrangement, neutral pressures could not be accurately determined. Based on the observed reaction kinetics and assuming typical ion-molecule reaction rates, we estimate that sample pressures were in the range 10^{-7}-10^{-8} Torr. A typical experimental pulse sequence is shown in Figure 3. Positive ions were generated by electron impact ionization, using a nominal electron beam energy of 15 to 20 volts. Ions were stored in

Figure 3. Trapped ion timing sequence for studies of infrared laser multiphoton dissociation processes. The quench pulse removes residual ions from the FT-ICR cell. Ion formation involves pulsing the electron beam to form ions from the gaseous sample. After a suitable reaction delay, the desired ion is isolated and subjected to laser irradiation.

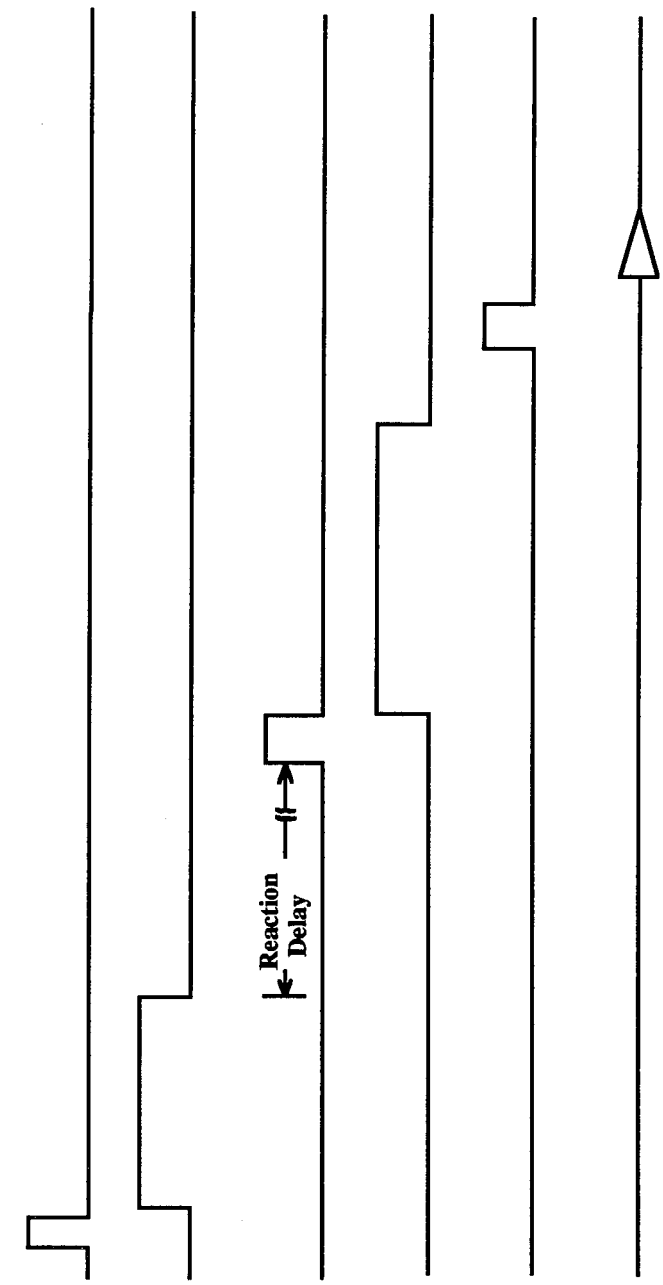
Quench Pulse
Ion Formation
Ion Selection
Reaction Delay
Laser Irradiation
Detect Pulse
Signal
Time

Figure 3

the trapping cell and mass-selected by a series of ion ejection pulses. The unfocused infrared beam from a grating tuned Apollo 550A cw CO_2 laser enters the vacuum system through a NaCl window (25.4 mm diameter x 3.5 mm thick) and passes through a 92% transmittance mesh to irradiate trapped ions. The transmitter plate reflects the beam for a second pass through the ion-trapping region and out of the apparatus. The CO_2 laser beam is externally triggered by a control pulse from the IonSpec data system. Several infrared multiphoton dissociation spectra of mass-selected proton bound dimer ions considered in this study were obtained at a constant laser intensity, but showed no dependence on wavelength. Dissociation rates were measured for a range of laser powers, determined using a Scientech surface absorbing disc calorimeter.

Results and Discussion

Reactions of N-acetyl glycine with alanine. Meot-Ner measured the gas phase proton affinity of N-acetyl glycine methyl ester and found it slightly larger than the proton affinity of alanine.[13] It was predicted from those results that the acid, N-acetyl glycine, would have a proton affinity similar to or slightly smaller than that of alanine. Since proton affinities can be extracted from proton transfer reaction data, experiments were initially attempted which would establish gas phase proton transfer equilibria in mixtures of N-acetyl glycine with alanine (PA = 214.8 kcal/mol) and glycine (PA = 212.0 kcal/mol).[5]

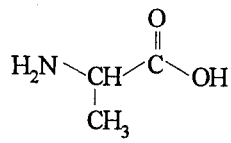

Alanine

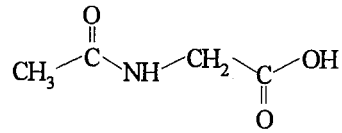

N-acetyl Glycine

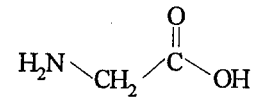

Glycine

Proton exchange equilibrium between N-acetyl glycine and alanine could not be established due to radiative bimolecular cluster formation. Protonated molecules clustered with the neutral background gas in the vacuum chamber and created primarily heterodimers of N-acetyl glycine and alanine (Figure 4). It is of particular interest that only the heterodimer is observed in abundance, suggesting that it is inherently more stable than the two homodimers which can be formed in this mixture. This suggests that some type of synergistic hydrogen bonding gives this species special stability. The proton bound heterodimer was isolated by ejecting all remaining lower and higher mass ions from the FT-ICR cell and dissociated by infrared multiphoton excitation with a cw CO_2 laser (Figure 5). The dissociation products detected were the intact protonated alanine and N-acetyl glycine ions. Only the weaker hydrogen bonds which hold the complex together are broken. More complex processes involving extensive rearrangement were not observed. The relative abundances of the two product ions were not equivalent but were in a ratio of approximately 4:1 alanine:N-acetyl glycine. To the extent that it could be accurately determined, this ratio did not vary significantly with either laser wavelength or power. Originally it was naively hoped that at low laser intensities only a single product would be observed. The quantitative analysis of

Figure 4. Variation of ion abundance with time following ionization of a mixture of N-acetyl glycine and alanine by electron impact (15 eV). A variety of different ions (not shown) are formed which react to give the two protonated molecules. The heterodimer is the major ion observed at long times.

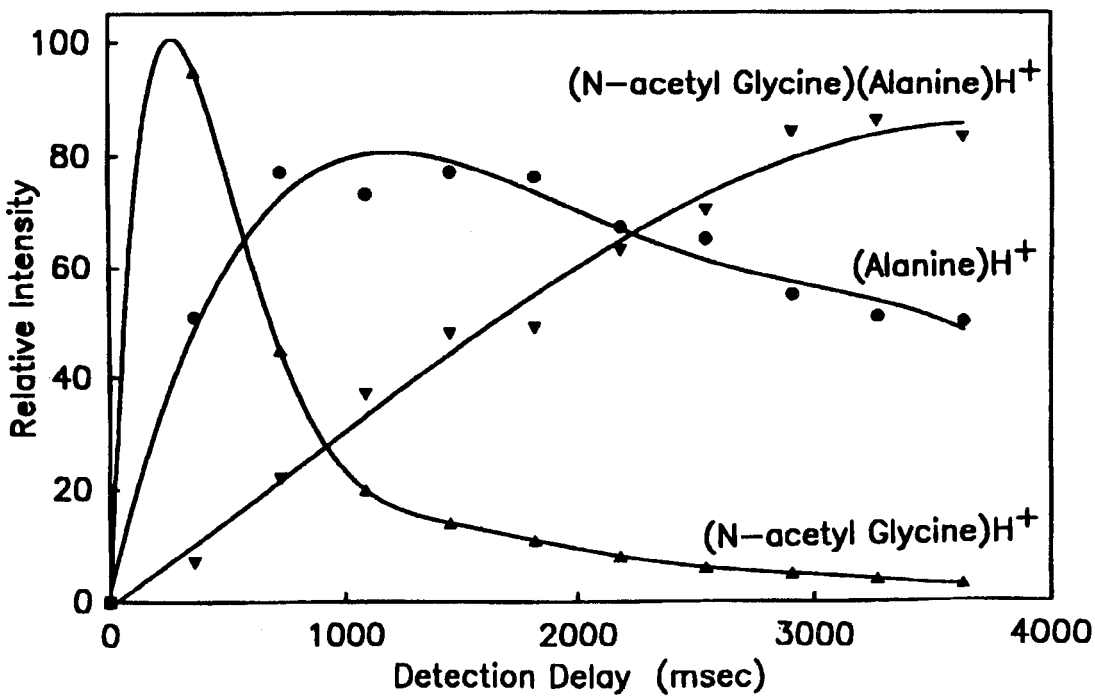
100
80
60
40
20
0
Relative Intensity
0
1000
2000
3000
4000
Detection Delay (msec)
(N–acetyl Glycine)(Alanine)H+
(Alanine)H+
(N–acetyl Glycine)H+

Figure 4

Figure 5. Intensity of proton bound dimer of N-acetyl glycine and alanine as a function of time. The laser (15 W cm^{-2}) is switched on at 4 seconds and the dimer intensity decreases with time as a result of multiphoton dissociation.

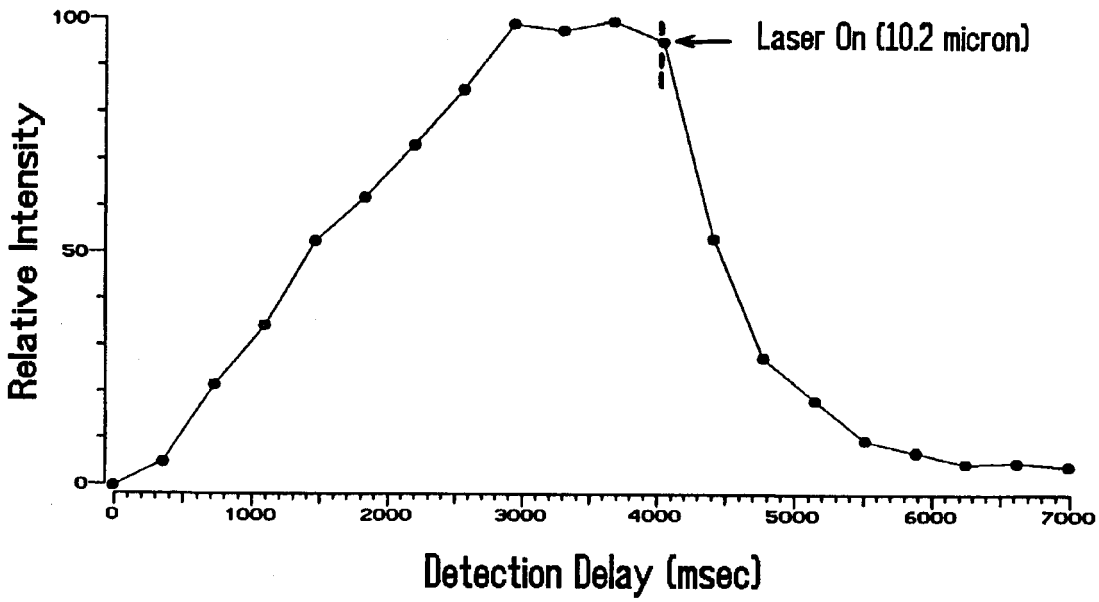
Relative Intensity
100
50
0
0
1000
2000
3000
4000
5000
6000
7000
Laser On (10.2 micron)
Detection Delay (msec)

Figure 5

the dissociation kinetics presented below makes it clear why this does not happen and might not be expected even if the proton affinity differences were large compared to the energy of a single infrared photon (2.7 kcal/mol).

Reactions of N-acetyl glycine with glycine. The gas phase proton affinity of N-acetyl glycine was predicted to be slightly higher than the proton affinity of glycine, due to the ability of the acetylated molecule to solvate the charge with an intramolecular hydrogen bond. Proton transfer equilibrium studies to determine the more basic of the two species produced results similar to those described above, with formation of a proton bound heterodimer as the primary product. Infrared multiphoton dissociation of the cluster produced protonated ions of intact N-acetyl glycine and glycine molecules with no additional fragmentation. Product ion abundances of 2.5:1 N-acetyl glycine:glycine were observed and both protonated species were detected at the lowest laser intensities. These experiments suggest that the proton affinity of N-acetyl glycine is intermediate between glycine and alanine.

Photodissociation kinetics and the temporal constraints for cw laser infrared multiphoton dissociation. As shown in Figure 5, the proton bound dimer of N-acetyl glycine and alanine readily undergoes IRMPD with modest laser intensities. This is not surprising since a molecule of this complexity should easily be in the vibrational quasicontinuum at room temperature. Evaluation of the photodissociation kinetics is straightforward using data such as shown in Figure 5 for the disappearance of the proton bound dimer after the laser is switched on. Results are shown in Figure 6 for several laser intensities, and the rates taken from the slopes are shown plotted in

Figure 6. Semilog plot showing the decay of the proton bound dimer of N-acetyl glycine and alanine after the infrared laser is turned on. The resulting rate (taken from the slope) increases with increasing laser intensity. Other conditions are as shown in Figure 5.

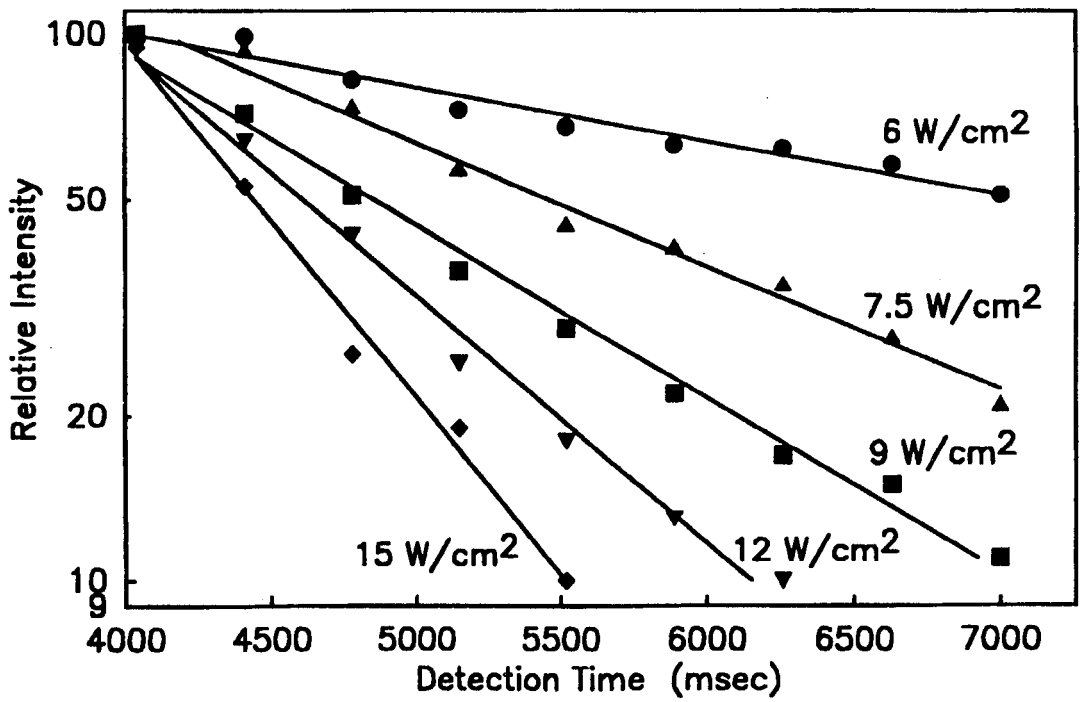
100
50
20
10
Relative Intensity
4000
4500
5000
5500
6000
6500
7000
Detection Time (msec)
6 W/cm2
7.5 W/cm2
9 W/cm2
12 W/cm2
15 W/cm2

Figure 6

Figure 7 as a function of laser irradiance (expressed in W cm^{-2}). The data in Figure 7 show that the dissociation rate approaches zero with irradiances below 5 W cm^{-2}. Note that this corresponds to photodissociation rates which drop below 1 sec^{-1}. As noted in the introduction, unless the dissociation rates exceed this value, infrared emission will lead to significant relaxation of the vibrationally excited molecules in competition with laser pumping.

The dissociation kinetics can be further quantified using RRKM calculations to model this process. The hydrogen bond strength between a protonated oxygen (the carbonyl of the amide linkage in N-acetyl glycine) and a basic site on alanine (either the nitrogen or the carbonyl oxygen) is approximately 30 kcal/mol, which is taken to be the activation energy for the process leaving the proton on the more basic site (alanine). We take 31.7 kcal/mol as the activation energy for the higher energy process in which the proton is retained on N-acetyl glycine. Using the Whitten-Rabinovitch approximation to evaluate state densities for both the energized molecule and the activated complex gives the predicted rates as a function of excess energy shown in Figure 8.

The model calculations shown in Figure 8 illustrate several points. First, in agreement with our experimental observations, the ratio of the two products varies only minimally with excess energy, from 4.0 at 10 kcal/mol to 3.5 at 15 kcal/mol, which encompasses the range of dissociation rates considered in our experiments (Figure 7). To produce dissociation at a rate which can compete with radiative cooling, the energy in excess of the activation energy must be approximately 10 kcal/mol, which is large in

Figure 7. Variation of infrared laser multiphoton dissociation rate of the proton bound dimer of N-acetyl glycine and alanine with laser irradiance. The rate approaches zero with irradiance levels below 5 W cm^{-2} due to cooling of the proton bound dimer by infrared emission.

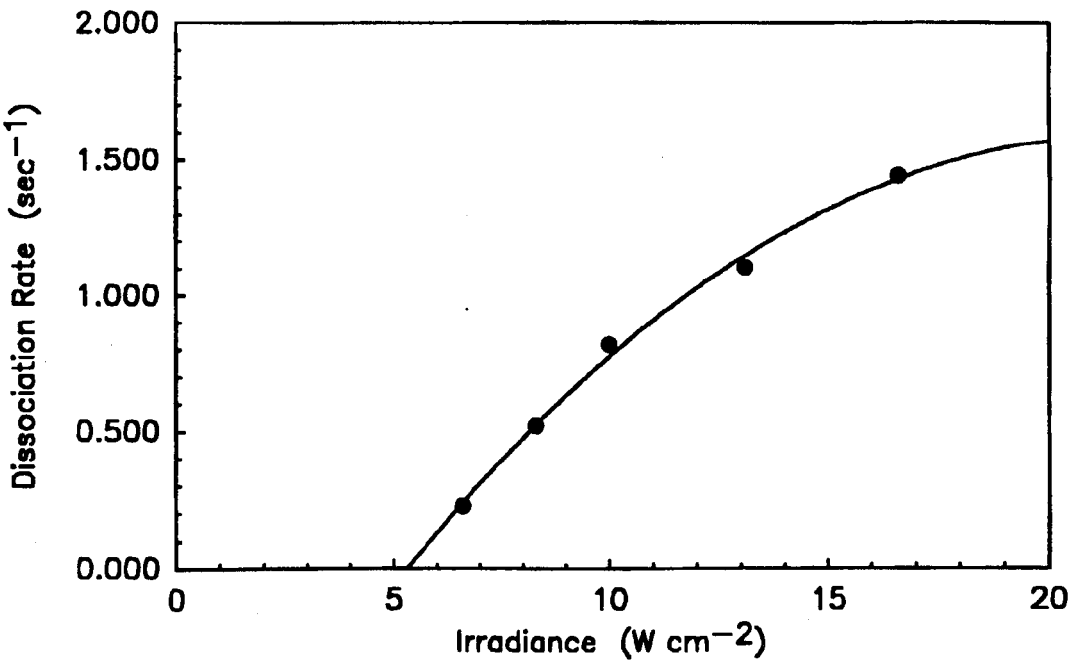
2.000
1.500
1.000
0.500
0.000
Dissociation Rate (sec^{-1})
0
5
10
15
20
Irradiance (W cm^{-2})

Figure 7

Figure 8. RRKM calculations for the rate of dissociation of the proton bound dimer of N-acetyl glycine and alanine. Activation energies for the two processes of 31.7 and 30.0 kcal/mol are assumed, respectively.

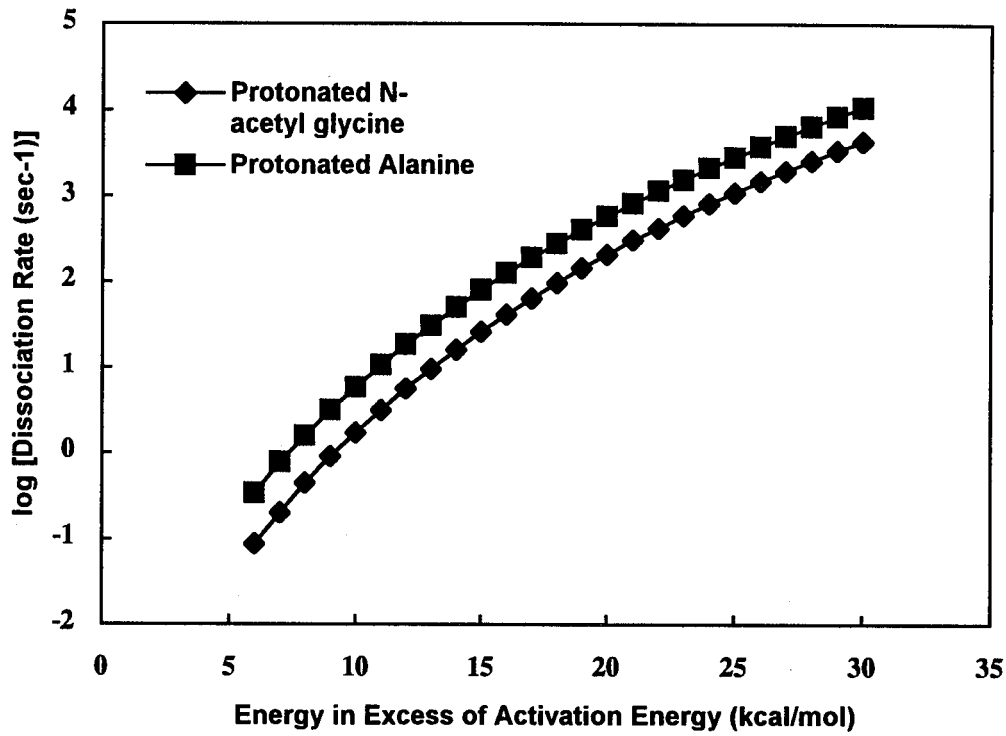
Protonated N-acetyl glycine
Protonated Alanine
log [Dissociation Rate (sec-1)]
5
4
3
2
1
0
-1
-2
0
5
10
15
20
25
30
35
Energy in Excess of Activation Energy (kcal/mol)

Figure 8

comparison to the difference in activation energy assumed. With 2.7 kcal/mol for each photon, this corresponds to absorption of roughly four photons in excess of the threshold energy requirement. The difference in activation energies assumed for this calculation was chosen to reproduce the observed product ratio. Similar RRKM calculations were carried out for the other heterodimer observed (N-acetyl glycine and glycine) and a proton affinity difference of 1.1 kcal/mol can reproduce the observed product distribution reasonably well. We believe that the more quantitative analysis permitted by the RRKM calculations makes it possible to extract approximate values for the proton affinity that are more accurate than would be yielded by simple bracketing experiments. In some respects these experiments are similar to quantitative analysis of competitive fragmentation processes observed in metastable ion studies.[14]

Conclusions

In this study we have demonstrated a novel application of IRMPD to determine the acid base properties of biological molecules. The proton affinity of N-acetyl glycine has been determined to be intermediate between glycine and alanine, with a value of 213.1 ± 0.5 kcal/mol being more closely determined by RRKM model calculations. By forming solvated adducts of biological molecules with appropriate reference bases, it should be possible to extend these studies to more complex systems. We have recently completed construction of an external ion source FT-ICR spectrometer with a 7 Tesla superconducting magnet. With this system it is possible to separate the regions in

which ion formation and ion trapping occur. This facilitates studies of IRMPD under truly collision free conditions and many such studies are in progress.

This study serves to illustrate the temporal constraints associated with IRMPD using cw infrared lasers. The requirement that dissociation rates exceed 1 sec^{-1} does not sound terribly demanding until one considers what it means for a large biological molecule. We have carried out model calculations which indicate that species in the molecular weight range around 10,000 Daltons typically require over 100 eV internal energy to yield reasonable dissociation rates! Achieving the controlled fragmentation of such molecules presents a formidable challenge.

Acknowledgments

The authors wish to thank K. Irikura for his assistance in designing the sample volatilization source. We are indebted to Dr. Arnold Beckman and the Beckman Institute at Caltech for their support of our studies of biomolecule mass spectrometry. We gratefully acknowledge the financial support of SC from a NIH-NRSA traineeship in Biotechnology. This work was supported in part by the National Science Foundation under grant CHE-9108318.

References

1. Karas, M.; Hillenkamp, F. *Anal. Chem.* **1988**, *60*, 2299.

2. Macfarlane, R. D. *ACS Symposium Series*, Vol. 291, Lyon, P. A. Ed., American Chemical Society, Washington, D.C., **1985**, p. 56.

3. Barber, M.; Bordoli, R. S.; Sedgewick, R. D.; Tyler, A. N. *J. Chem. Soc. Chem. Comm.* **1981**, 325.

4. Fenn, J. B.; Mann, M.; Meng, C. K.; Wong, S. F.; Whitehouse, C. M. *Science* **1989**, *246*, 64.

5. Campbell, S.; Beauchamp, J. L.; Rempe, M.; Licthenberger, D. L. *Int. J. Mass Spectrom. and Ion Processes* **1992**, *117*, 83.

6. Thorne, L. R.; Beauchamp, J. L. *Gas Phase Ion Chemistry*, Vol 3., Bowers, M. T. Ed., Academic Press, New York, **1984**, p. 41.

7. Watson, C. H.; Baykut, G.; Eyler, J. R. *ACS Symposium Series*, Vol. 359, Buchanan, M. V. Ed., American Chemical Society, Washington, D.C., **1987**, p. 140.

8. Robinson, P. J.; Holbrook, K. A. *Unimolecular Reactions*, Wiley-Interscience, Bristol, England, **1972**.

9. Marshall, A. G. *Acc. Chem. Res.*, **1984**, *18*, 316.

10. Wolf, J. F.; Staley, R. H.; Koppel, I.; Taagepera, M.; McIver, R. T.; Beauchamp, J. L.; Taft, R. W. *J. Am. Chem. Soc.* **1977**, *99*, 5417.

11. Woodin, R. L.; Beauchamp, J. L. *Chem. Phys.* **1979**, *41*, 1.

12. Shin, S. K.; Beauchamp, J. L. *J. Am. Chem. Soc.* **1990**, *112*, 2057.

13. Meot-Ner, M. *J. Am. Chem. Soc.* **1984**, *106*, 278.

14. Bojesen, G. *J. Am. Chem. Soc.* **1987**, *109*, 5578.

CHAPTER 4

Proton Affinities and Photoelectron Spectra of Phenylalanine and N-Methyl- and N,N-Dimethylphenylalanine. Correlation of Lone-Pair Ionization Energies with Proton Affinities and Implications for N-Methylation as a Method to Effect Site Specific Protonation of Peptides.

Proton Affinities and Photoelectron Spectra of Phenylalanine and N-Methyl- and N,N-Dimethylphenylalanine. Correlation of Lone-Pair Ionization Energies with Proton Affinities and Implications for N-Methylation as a Method to Effect Site Specific Protonation of Peptides.

Sherrie Campbell, Elaine M. Marzluff, M. T. Rodgers and J. L. Beauchamp*

Contribution No. 8878 from the Arthur Amos Noyes Laboratory of Chemical Physics

California Institute of Technology, Pasadena, California 91125

and

Margaret E. Rempe, Kimberly F. Schwinck and D. L. Lichtenberger

The Laboratory for Electron Spectroscopy and Surface Analysis

Department of Chemistry, University of Arizona, Tucson, Arizona 85721

Abstract

A Fourier transform ion cyclotron resonance (FT-ICR) technique for measuring gas phase proton affinities is presented which utilizes collisional dissociation of proton-bound clusters by off-resonance translational excitation. A simplified RRKM analysis relates unimolecular dissociation rates to proton affinities. This technique is used to

measure values for the proton affinities of phenylalanine, N-methyl- and N,N-dimethylphenylalanine of 220.3, 223.6, and 224.5 kcal/mol, respectively (relative to the proton affinity of NH_3=204.0 kcal/mol). The proton affinity measured for phenylalanine is in excellent agreement with reported literature values. The photoelectron spectra of these three molecules are also presented and analyzed. Assignments of bands to specific ionization processes are aided by comparison with model compounds such as methyl-substituted amines and 2-phenylethylamines. These data are employed to examine the correlation of adiabatic nitrogen lone-pair ionization energies with gas phase proton affinities for phenylalanine, N-methylphenylalanine, and N,N-dimethylphenylalanine in comparison to correlations for other amino acids and selected aliphatic amines. Although amine nitrogen methylation increases the potential for localizing charge at the amine terminus of protonated peptides by increasing the gas phase proton affinity, the present study establishes that the increase is not sufficient to compete with protonation of some of the more basic side chains in peptides.

Introduction

The number of investigations into chemical reactivities, proton affinities, and dissociation mechanisms of biological molecules in the gas phase has increased dramatically during recent years. This is due in part to the advances in experimental methodology for the desorption and ionization of thermally fragile high molecular weight molecules. Desorption of an amino acid or larger biological sample from a matrix using laser desorption,[1] plasma desorption,[2] or fast atom bombardment (FAB)[3]

has become an efficient method for producing charged species. Additionally, electrospray[4] and thermospray[5] ionization techniques are used to produce multiply charged gas phase biological species. The attachment of a proton or cation to a peptide may occur at a number of sites due to the many basic functional groups within the molecule. This is a complex process since folding of the molecule allows several basic sites to simultaneously interact with and solvate the charge center.[6,7] Covalent attachment of an ionized functional group (such as an ethyltriphenylphosphonium moiety or a quaternary nitrogen) is the only method currently available for positive ions with which one can *select* the specific site of ionization.[8,9]

The present study examines the effect of amine methylation on the proton affinity and ionization energies of phenylalanine. It is known that the attachment of a methyl group to a primary amine (such as ethylamine) increases the proton affinity by roughly 6 kcal/mol.[10] Attachment of a second methyl group increases the proton affinity by an additional 5 kcal/mol. Since the proton affinity of phenylalanine has been reported by several investigators to be between 219 and 221 kcal/mol,[11,12,13,14,15] N-methylation could potentially increase the basicity of phenylalanine to a level greater than many of the most basic unsubstituted amino acids, which typically have proton affinities less than 230 kcal/mol. Incorporation of this modified amino acid into the N-terminus of a peptide could effect the specific site of protonation in the molecule. Additionally, attachment of methyl groups to a primary amine decreases the ionization energy of the nitrogen lone-pair orbital.[16] Amine methylation of phenylalanine should result in the destabilization of the nitrogen lone-pair orbital while leaving all other

molecular orbitals unaffected. Identification of the nitrogen lone-pair orbital in the photoelectron spectra of methyl-substituted phenylalanines should be easy, as it is shifted to lower energies.

A FT-ICR technique for measuring gas phase proton affinities is introduced which utilizes collisional dissociation of proton-bound clusters by off-resonance translational excitation.[17] A simplified RRKM analysis is used to determine proton affinities from product ion abundances. This experimental methodology is similar to that pioneered by Cooks and co-workers[18] for the extraction of thermochemical data from competitive dissociation processes.

We have demonstrated that it is useful when assessing the protonation energetics of molecules to examine the correlations of proton affinities with adiabatic lone-pair ionization energies of basic sites.[19,20] Such correlations can be made even when the site of protonation is not associated with the lowest ionization energy of the molecule. These correlations have been shown to have several applications. If the proton affinity and site of protonation are known, the correlation can be used to estimate the orbital ionization energy of the site, which is useful in assigning bands in complex photoelectron spectra. This is of particular interest for molecules such as phenylalanine, where the amine nitrogen lone-pair and phenyl π orbitals give rise to unresolved overlapping bands. Similarly, if the lone-pair ionization potential of a basic site in a molecule can be determined using photoelectron spectroscopy, then such correlations can be used to predict the intrinsic base strength of that site. The correlation of adiabatic nitrogen lone-pair ionization energies with gas phase proton

affinities for phenylalanine, N-methylphenylalanine and N,N-dimethylphenylalanine is presented with the purposes of identifying the effect of methyl substitution of the amine nitrogen on the base strength of the molecule and assessing the photoelectron band assignments.

Experimental Details

Photoelectron spectra were recorded at the University of Arizona on an instrument featuring a 36-cm radius hemispherical analyzer (10-cm gap) with customized sample cells, excitation sources, detection and control electronics, and data collection methods that have been previously described.[21] Since the amino acids sublime and then deposit on cooler parts of the instrument, the sensitivity and resolution progressively degrade with time during data collection. The data are represented analytically with the best fit of asymmetric Gaussian peaks (GFIT program).[22] The confidence limits of the peak positions and widths are generally ± 0.02 eV. The confidence limit of the area of a band envelope is approximately ± 5%, with uncertainties introduced from the base-line subtraction and fitting in the tails of the peaks. When peaks are strongly overlapping, as in the first ionization band of phenylalanine, the individual parameters of a peak are less significant since they are dependent on the parameters of other peaks in the band. The adiabatic ionization energy (energetic onset of each peak) is estimated to occur at the point twice the half-width at half-maximum from the vertical ionization energy on the low-energy side of the band.

The proton affinities of the samples were determined at Caltech using an external ion source Fourier transform ion cyclotron resonance (FT-ICR) mass spectrometer. A detailed description of this instrument has been previously published.[23] The spectrometer incorporates an external Cs ion bombardment source, octopole ion guide for transferring ions into the high field region of a 7-T superconducting magnet, a standard 2x2x3 inch detection cell, and the electronics required for data acquisition and processing in the Fourier transform mode. The instrument has three regions of differential cryogenic pumping, resulting in a residual background pressure of high 10^{-10} or low 10^{-9} Torr in the detection cell. A specially designed ionization gauge is an integral part of the ICR cell and is accurately calibrated using a capacitance manometer connected directly to the cell through a static port. Collision gases are delivered through stainless steel tubing directly to the ICR cell using computer controlled General Valve pulsed valves or manual Varian leak valves. Typical static N_2 gas pressures used in collision-induced dissociation experiments are (2-5) x 10^{-8} Torr.

Samples are typically prepared by dissolving small amounts of solid (~0.1 mg) directly into a 2-3 μL drop of a mixture of glycerol and trifluoroacetic acid spread onto a copper probe tip. For the generation of proton-bound clusters, equal amounts of both reference bases are thoroughly mixed together, and a small sample is used for the analysis. Several solid samples do not readily dissolve in the glycerol/trifluoroacetic acid matrix and must first be dissolved in water (typically, 0.5 mg/mL). For these mixtures, 1-2 μL of solution are mixed with the matrix on the probe tip. Desorption of

proton-bound clusters from the probe tip is accomplished in the source region of the spectrometer using 6-8 keV Cs ions.

N,N-dimethylphenylalanine was synthesized using the technique described by Bowman and Stroud.[24] The product yield was adequate at 23%. Purity was confirmed by examination of the melting point (218° C) and H^1-NMR of the product. All other samples were commercially available from Sigma Chemical Co. and used as provided without further purification.

Results and Discussion

Most of the naturally occurring amino acids are α-substituted glycine derivatives and can be represented by the general formula H_2N-RCH-COOH, where R represents one of 19 different side chains. Proline is the only amino acid that does not fit this general formula, as it is a cyclic secondary amine. Differences that arise in the photoelectron spectra or gas phase proton affinity values of amino acids primarily show the effect of changing the R group of the molecule. We have detailed in a previous paper the affects of varying the amino acid side chain on gas phase proton affinities and nitrogen adiabatic lone-pair ionization potentials.[20] The present study examines the gas phase properties of the amino acid phenylalanine and its N-methyl derivatives. Differences in the photoelectron spectra and gas phase proton affinities of these species result from the effect of methyl substitution on the amine nitrogen.

Photoelectron Spectra of Substituted Phenylalanines. Typically, the lowest ionization potential observed in the photoelectron spectra of the amino acids results

from ionization out of the amine nitrogen lone-pair orbital (n_N), which has a lower ionization potential by 1 eV than the next closest peak.[25] For amino acids with complex side groups which have orbital energies comparable to the nitrogen lone-pair, such as aromatic rings or sulfur, nitrogen, or oxygen atoms, the lowest ionization potential may result from ionization out of a side-chain orbital. In these systems, the peaks for ionization from the n_N orbital and the side-chain orbital tend to overlap and are unresolved, making it difficult to interpret the photoelectron spectra of several of the amino acids. The amino acid phenylalanine is an α-substituted glycine compound with the side chain R=benzyl. The photoelectron spectrum is shown in Figure 1a. The broad band that spans the low ionization potential region between 8 and 10 eV results from the overlap of three peaks. These peaks result from ionization out of three high-energy molecular orbitals; one contributed from the amine nitrogen lone-pair and two from the side-chain aromatic ring. Cannington and Ham first reported this feature in the photoelectron spectrum of phenylalanine, but were unable to assign ionization energies to the three orbitals, as the broad spectral band was unresolved.[26] An expanded view of the first ionization band of phenylalanine is shown in Figure 2a. This band displays shoulders on the low- and high-energy sides, requiring at least three peaks to suitably model the band profile.

The peaks in the low ionization potential region of phenylalanine can be identified by comparison to appropriate model compounds. In benzene, the degenerate e_{2g} orbital contributes a single peak in this region of the photoelectron spectrum. The vertical ionization potential of the e_{2g} orbital is reported to be 9.25 eV.[27] Substitution

Figure 1. He I photoelectron spectra of (a) phenylalanine, (b) 2-phenylethylamine, (c) N-methyl-2-phenylethylamine, (d) N,N-dimethyl-2-phenylethylamine and (e) p-hydroxy-2-phenylethylamine. The broad band in the 8-10 eV region observed in each spectrum results from the overlap of three peaks from aromatic π_3, π_2, and nitrogen lone-pair (n_N) molecular orbitals. Methyl substitution on the amine nitrogen of c and d shifts the ionization energy of the n_N orbital out from under the broad band, allowing it to be easily identified. Para hydroxylation of the phenyl ring in e shifts only the π_3 orbital, leaving the peaks for the π_2 and n_N orbitals in the region of 9.3-9.5 eV. Spectra b-e were recorded by Domelsmith *et al.*[28]

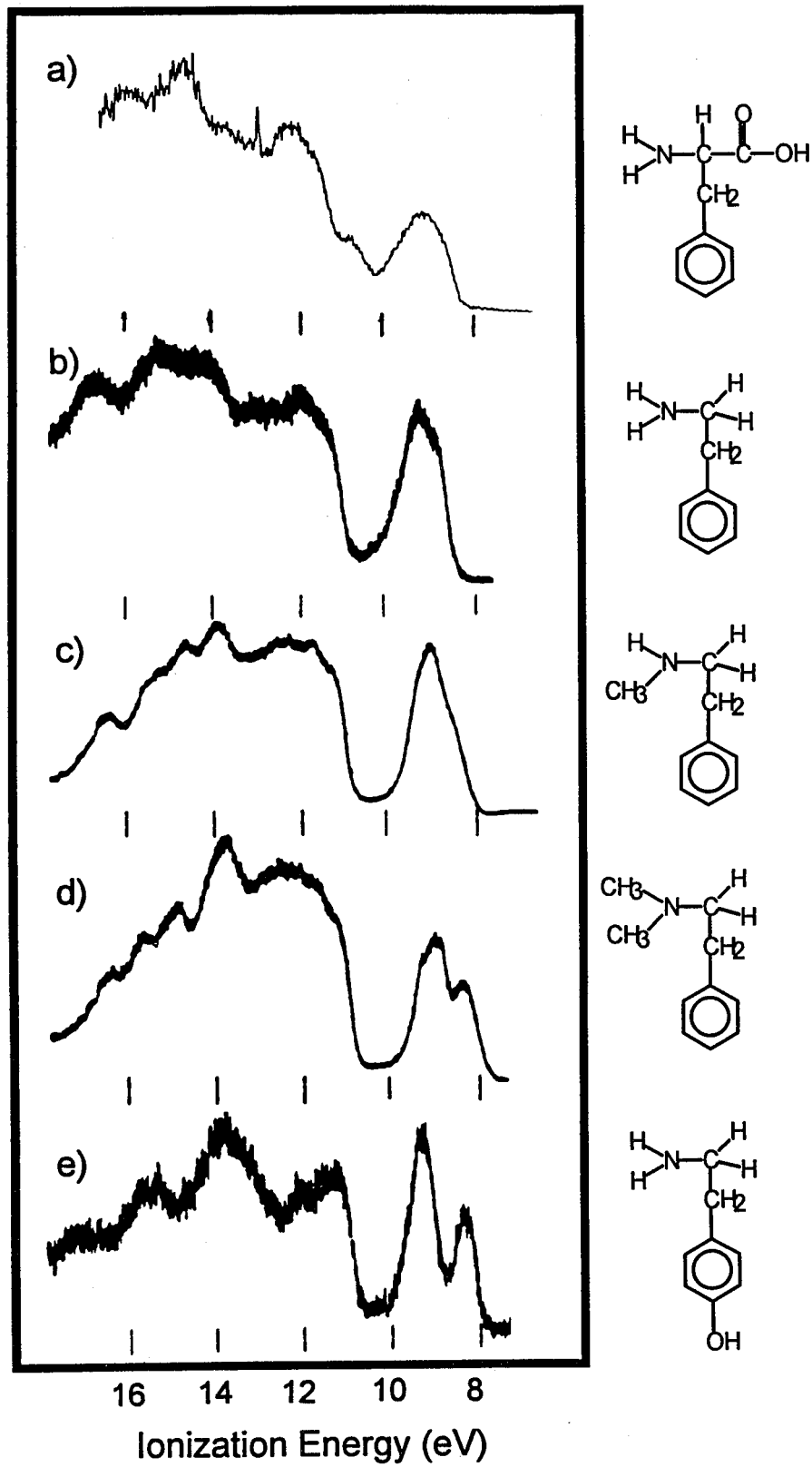

Figure 1

Figure 2. Expansion of the low ionization energy region in the photoelectron spectra of (a) phenylalanine, (b) N-methylphenylalanine and (c) N,N-dimethylphenylalanine. The nitrogen lone-pair orbital peak in phenylalanine (peak II in a) shifts to lower energy upon methylation (peaks I in b and I in c). Peak energy values and identifications are listed in Table 1.

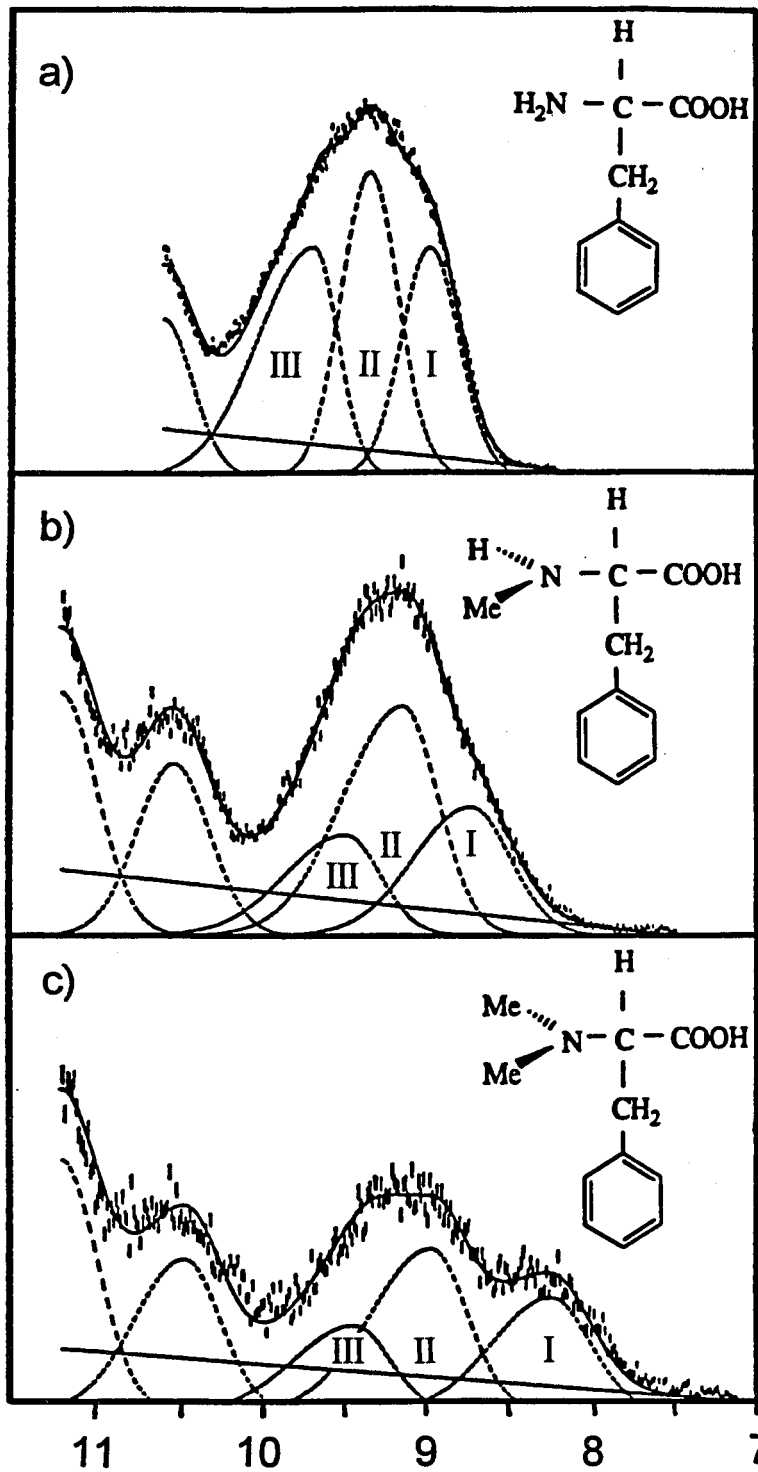
a)
H
H2N – C – COOH
CH2
III
II
I
b)
H
H
N – C – COOH
Me
CH2
II
I
III
c)
H
Me
N – C – COOH
Me
CH2
III
II
I
11
10
9
8
7
Ionization Energy (eV)

Figure 2

of a methyl group on the benzene causes a change in molecular symmetry, creating symmetric (π_3) and antisymmetric (π_2) orbitals. The π_3 orbital is destabilized with respect to the π_2 orbital and yields a lower vertical ionization potential of 8.83 eV, while the π_2 orbital ionization potential of 9.36 eV is slightly higher than that of the e_{2g} orbital of benzene.[27] These ionizations account for two of the three low-energy peaks in the phenylalanine spectrum.

A comprehensive study of the photoelectron spectra and ionization potentials for several substituted 2-phenylethylamines has been reported by Domelsmith *et al.*[28] The aromatic π orbitals of 2-phenylethylamine, as well as those of phenylalanine, are quite similar to those of toluene. The π_3 and π_2 orbitals are not easily distinguished in the photoelectron spectrum of 2-phenylethylamine (Figure 1b), since the amine nitrogen lone-pair orbital appears in the same energy region and creates an unresolved broad band similar to that in the photoelectron spectrum of phenylalanine. Two peak maxima can be identified at 8.99 and 9.35 eV. Determination of the location of the n_N orbital peak, as well as the location of the π_3 and π_2 peaks, is aided by methylation of the amine nitrogen of 2-phenylethylamine. It is expected that the ionization potential of the n_N orbital decreases with each methyl substituent, while the aromatic ionization potentials remain unaffected. This trend in the n_N orbital energies is predicted from the vertical ionization potentials of methylamine, dimethylamine, and trimethylamine decreasing from 9.64 to 8.97 to 8.44 eV, respectively.[16] The n_N peak maximum lies near 8.7 eV in the photoelectron spectrum of N-methyl-2-phenylethylamine (Figure 1c), and this peak is well resolved in the N,N-dimethyl-2-phenylethylamine spectrum at

8.35 eV (Figure 1d). Since secondary amines are predicted to have ionization potentials 0.6-0.8 eV lower than those of primary amines, the n_N orbital peak in the 2-phenylethylamine spectrum should lie in the region between 9.3 and 9.5 eV. The peak near 8.99 eV in the 2-phenylethylamine spectrum is identified as the π_3 orbital, as substitution of a hydroxyl group at the para position of the ring changes only the lowest vertical ionization potential from 8.99 to 8.41 eV and leaves the broad band at 9.35 eV unaffected (Figure 1e).

The photoelectron spectrum of phenylalanine is very similar to that of 2-phenylethylamine. Both have a broad band in the low ionization potential region contributed from aromatic π_3, π_2, and amine nitrogen lone-pair n_N orbital peaks. It is anticipated that methyl substitution on the amine nitrogen of phenylalanine will shift the n_N ionization potential to lower values, without having a significant effect on the phenyl π ionization potentials. The stacked photoelectron spectra of all three methylated phenylalanine species with an expanded low ionization potential region is shown in Figure 2. Table 1 lists the vertical and adiabatic ionization potentials for the numbered peaks in each photoelectron spectrum of Figure 2. The spectrum of N,N-dimethylphenylalanine (Figure 2c) is the easiest to interpret, as substitution of two methyl groups has changed the spectrum dramatically from that of the unsubstituted parent molecule. Peak I, with a vertical ionization potential of 8.2 eV, is contributed from the n_N orbital as the destabilization has lowered its ionization potential and shifted the peak from under the broad band. The π_3 and π_2 vertical ionization potentials (8.9

Table 1: Vertical and Adiabatic Ionization Potentials for Peaks in the Photoelectron Spectra of Phenylalanine, N-methylphenylalanine and N,N-dimethylphenylalanine.

Species	Peak	Vertical IP (eV)	Adiabatic IP (eV)	Orbital assignment
Phenylalanine	I	8.9	8.5	π_3
	II	9.3	8.8	n_N
	III	9.7	9.2	π_2
N-methyl phenylalanine	I	8.7	8.2	n_N
	II	9.1	8.5	π_3
	III	9.4	8.9	π_2
N,N-dimethyl phenylalanine	I	8.2	7.7	n_N
	II	8.9	8.5	π_3
	III	9.3	9.0	π_2

and 9.3 eV, respectively) are relatively unaffected by amine methylation and are similar to the analogous ionization potentials in toluene.

The n_N orbital can be assigned in the N-methylphenylalanine spectrum (Figure 2b) using the following arguments. Secondary amines are expected to have ionization potentials 0.4-0.5 eV higher than tertiary amines; therefore, the n_N orbital peak is predicted to lie in the region between 8.6 and 8.7 eV. The peak with the lowest ionization potential (I) in Figure 2b must arise from the n_N orbital. Table 1 confirms that the vertical and adiabatic ionization potentials of the π_3 and π_2 orbitals (peaks II and III, respectively) remain relatively constant from N-methyl- to N,N-dimethylphenylalanine. Methyl substitution at the amine has little affect on these orbitals.

Comparing the trends in the photoelectron spectrum of phenylalanine to those of 2-phenylethylamine, it is possible to identify the vertical ionization potential for the n_N orbital. Primary amines are expected to have ionization potentials 0.6-0.8 eV higher than secondary amines, so the vertical ionization potential for the n_N orbital of phenylalanine should lie in the region between 9.2 and 9.5 eV. This identifies peak II at 9.3 eV as the n_N orbital. The peak with the lowest ionization potential (I) in Figure 2a is identified as the π_3 orbital, as substitution of a hydroxyl group at the para position of the ring changes only the lowest vertical ionization potential from 8.9 to 8.5 eV, and leaves the broad band at 9.3 relatively unaffected.[26] The π_2 orbital has the highest ionization potential in all three substituted phenylalanines and is always peak III.

The trends in the vertical ionization potentials of the substituted phenylalanines are best summarized in Figure 3. The effect of lowering the n_N ionization potential upon methyl substitution on a primary amine (methylamine) is clearly shown in Figure 3a. This trend is also observed in the n_N ionization potential of substituted 2-phenylethylamines (Figure 3b), while the π_3 and π_2 orbitals remain relatively unchanged. Substituted phenylalanines display the same trends in the n_N and π orbitals as does 2-phenylethylamine, which facilitates the assignment of these orbitals.

Proton Affinities of Substituted Phenylalanines. The gas phase proton affinity of phenylalanine has been determined by numerous investigators to be between 219 and 221 kcal/mol.[11,12,13,14,15] The proton affinity values for methyl-substituted phenylalanines have not been previously reported.

Several experimental methodologies exist for the determination of gas phase proton affinities. Proton-transfer reactions which reach equilibrium at a fixed temperature yield gas phase basicities which can give proton affinities if the entropy of protonation can be estimated using statistical thermodynamics.[29,30] Unfortunately, the use of equilibrium techniques with biomolecules is restricted by their low volatility. The kinetic method, pioneered by Cooks and co-workers,[18] has held the most promise to date for determining proton affinities of relatively nonvolatile molecules. The proton affinity is correlated to the ratio of the product ion abundances in the dissociation of proton-bound dimers. These ions are typically produced by metastable decay of the clusters in the field-free region of a multisector mass spectrometer, but more recently

Figure 3. Trends in the vertical ionization potentials for N-methyl-substituted (a) methylamines, (b) 2-phenylethylamines and (c) phenylalanines. The nitrogen lone-pair (n_N) ionization potential decreases steadily in methyl-substituted amines, while the aromatic π orbitals remain relatively unaffected. Peak assignments for phenylalanine are confirmed by evaluating the trends in the n_N orbital.

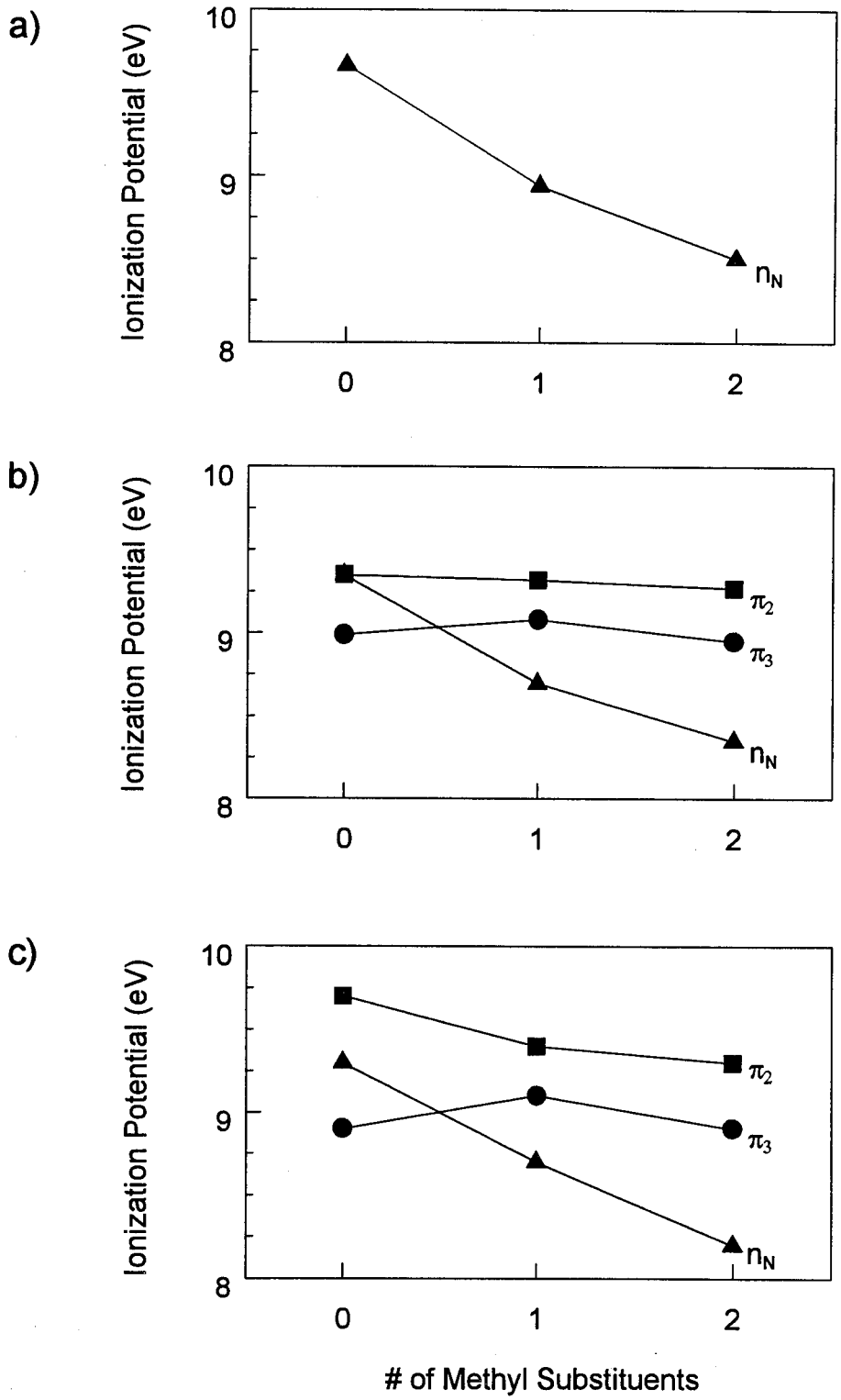
a)
b)
c)
Ionization Potential (eV)
10
9
8
0
1
2
n_N
π_2
π_3
# of Methyl Substituents

Figure 3

have been generated by low-energy collision-induced dissociation of proton-bound clusters in four-sector instruments.[31]

To determine the proton affinity of a base B_2 using the kinetic approach, a proton-bound dimer is formed from a reference base B_1 of known proton affinity and the base B_2. The dissociation of the cluster is dominated by two unimolecular reactions (eq 1). Two assumptions are made in analyzing data from these experiments: (1) if

$$[B_1 — H^+ — B_2] \rightarrow B_1H^+ + B_2 \quad (1a)$$

$$[B_1 — H^+ — B_2] \rightarrow B_1 + B_2H^+ \quad (1b)$$

species B_1 and B_2 are structurally similar, the difference in the entropy of protonation ($\delta\Delta S$) for forming the products is small and (2) the dissociation reactions have zero or very small reverse activation energies. With these assumptions, the difference in activation energies for reactions 1a and 1b, (δE_0), is equal to the difference in proton affinities $PA(B_1)$–$PA(B_2)$.

The kinetic method employs transition-state theory to model unimolecular dissociation rates of the proton-bound dimers. As a result of this approach, dimers are described with a singular effective temperature (T). In reality, both Cooks type experiments and our own deal with a nonthermal internal energy distribution, and the dissociation kinetics are more appropriately analyzed using RRKM theory[32] and averaging over the energy distribution. We start with the simplified RRK[33]

unimolecular dissociation rate described by eq 2, in which ν is the frequency factor for the reaction, E is the total energy of the excited molecule with s vibrational degrees of

$$k(E) = \nu\left(\frac{E - E_o}{E}\right)^{s-1} \tag{2}$$

freedom, and E_0 is the activation energy. If there are two competing dissociation channels for the molecule, as there are for the proton-bound clusters, then the rates of channels 1 and 2 are related by eq 3. Simple mathematical manipulation of eq 3 yields an expression which allows the proton affinity of the unknown base to be extracted

$$\frac{k_1(E)}{k_2(E)} = \frac{\nu_1}{\nu_2}\left(\frac{E - E_o(1)}{E - E_o(2)}\right)^{s-1} \tag{3}$$

from the ratios of the fragment ion abundances (eq 4), provided δE_0 is small compared to $E–E_0$. As stated above, the dissociation rates are proportional to the product ion

$$\ln\frac{k_1(E)}{k_2(E)} = \ln\left(\frac{\nu_1}{\nu_2}\right) - (s-1)\left(\frac{\delta E_o}{E - E_o(2)}\right) \tag{4}$$

abundances and the differences in activation energies are equal to the differences in proton affinities. Plotting the natural log of the ratio of the product ion abundances

versus the reference base proton affinity for a series of bases allows the proton affinity of the unknown species to be determined. The proton affinity of the unknown base is found where the dissociation rates for the reference and unknown base are equal (ln ratio=0). An example of such a plot is shown for N-methylphenylalanine with a series of reference bases later in this section (Figure 6). It should be noted that the inverse of the slope of the plot is equal to the excess internal energy per degree of freedom in the activated complex and can be related to the temperature of the cluster.

Experimental methods which utilize different mass spectrometry techniques have distinctively different time scales and therefore sample ions of differing internal energies. To detect dissociation products using FT-ICR mass spectrometry, molecules must fall apart on a time scale of 100 ms to 1 s, corresponding to rates of 1-10 s^{-1}. In faster MS/MS type experiments of tandem mass spectrometers, molecules dissociate on a time scale of 10^{-4}-10^{-5} s, yielding rates of 10^{4}-10^{5} s^{-1}. RRKM analysis shows that for *similar frequency factors and activation energies,* dissociation rates for systems of varying size are approximately the same when the excess energy per vibrational degree of freedom in the activated complex is comparable. This analysis explains why the kinetic method works as well as it does, since plots of the experimental results give straight lines regardless of the size of the reference base used. Big molecules with large numbers of degrees of freedom require higher internal excitation to dissociate on the same time scale as small molecules. Variation in frequency factors which result from entropic effects obviously complicates the analysis. Hence, it is best to choose reagent bases which are structurally similar, monodentate, and rigid.[31]

Gas phase proton affinities of methyl-substituted phenylalanines were determined by FT-ICR mass spectrometry using the technique described above and have an average uncertainty of ±1 kcal/mol. Proton-bound clusters of reference bases and substituted phenylalanines were generated in the FAB source and transferred into the trapped ion cell of the FT-ICR mass spectrometer. Parent cluster ions were initially isolated by applying resonant frequency ejection pulses to all other species in the cell. The clusters were then translationally excited with sustained off-resonance radio frequency excitation[17] for several seconds and collisionally dissociated against a static pressure of nitrogen ($2x10^{-8}$ Torr).

Ion populations generated in the FAB source and transferred to the detection cell have a wide distribution of energy, since without translational excitation, product ions are observed for dissociation against a static N_2 gas pressure which produces typically one or two collisions per second. Collisional dissociation appears to occur on a time scale faster than collisional or radiative cooling of the cluster ions. Using sustained off-resonance translational excitation, collision conditions are varied from 0 to 4 eV in the center of mass frame to determine if the average relative kinetic energy of the cluster has an effect on fragment product ion distributions. The kinetic energy of a trapped ion obtained from sustained off-resonance radio frequency excitation is described by eq 5, where q is the charge of the ion, E_0 is the amplitude of the applied

$$E_{ion,lab}(t) = \frac{q^2 E_o^2}{2m(\omega - \omega_c)^2} \sin^2\left[\frac{(\omega - \omega_c)t}{2}\right] \qquad (5)$$

electric field, m is the mass of the ion, and $(\omega-\omega_c)$ is the difference between the applied excitation frequency and natural cyclotron frequency of the ion. The time-averaged center of mass kinetic energy of the trapped ion is determined by eq 6. A plot of product ion abundances versus center of mass kinetic energies for the proton-bound

$$\langle E_{ion,cm} \rangle = \frac{m_{gas}}{m_{gas} + m_{ion}} \left[\frac{q^2 E_o^2}{4 m_{ion} (\omega - \omega_c)^2} \right] \qquad (6)$$

dimer of N-methylphenylalanine with 2-aminopyridine is shown in Figure 4. Increasing the center of mass kinetic energy to 2.6 eV produces nearly complete dissociation of the dimer into protonated 2-aminopyridine or protonated N-methylphenylalanine. Both species are produced with similar intensities since they have nearly identical proton affinities. Although the relative ion abundance of each product increases with increasing kinetic energy, the ratio of the product ion abundances is unaffected. A plot of the natural log of the ratio of product ion abundances versus the relative kinetic energy for proton-bound dimers of N-methylphenylalanine with proline, 2-aminopyridine, and trimethylamine is shown in Figure 5. Off-resonance collisional activation is conducted under multiple collision conditions, with sequential encounters resulting in accumulation of sufficient internal excitation to produce dissociation. Increasing the relative kinetic energy allows for more internal excitation to be accumulated per collision, but does not alter the level of internal excitation which produces dissociation. This is in contrast to single-collision excitation, where internal

Figure 4. Variation in relative product ion abundance with center of mass collision energy observed in the collision-induced dissociation of the proton-bound dimer of N-methylphenylalanine and 2-aminopyridine (m/z=274). Protonated N-methylphenylalanine (m/z=180) and protonated 2-aminopyridine (m/z=95) are produced with similar intensities since they have nearly identical proton affinities. Off-resonance excitation is performed for 600 ms using N_2 as the collision gas ($2x10^{-9}$ Torr). Center of mass collision energies vary over the range of 0-2.6 eV.

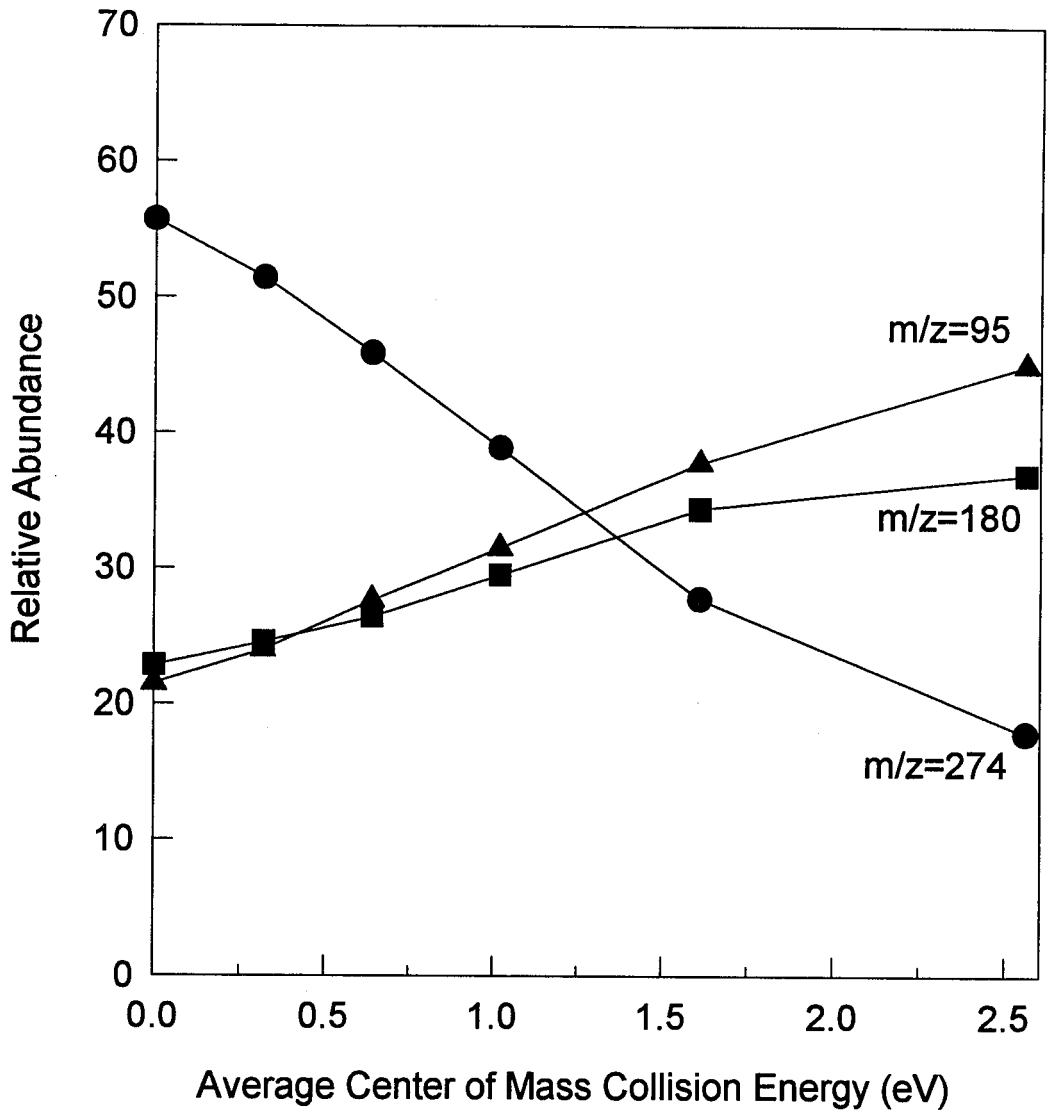
70
60
50
40
30
20
10
0
Relative Abundance
m/z=95
m/z=180
m/z=274
0.0
0.5
1.0
1.5
2.0
2.5
Average Center of Mass Collision Energy (eV)

Figure 4

Figure 5. Ratio of product ion abundances for the collision-induced dissociation of proton-bound dimers of N-methylphenylalanine and reference bases, unaffected by the average relative kinetic energy. Flat slopes in this plot indicate that proton affinities obtained using this technique are independent of collision energies and structural entropic effects.

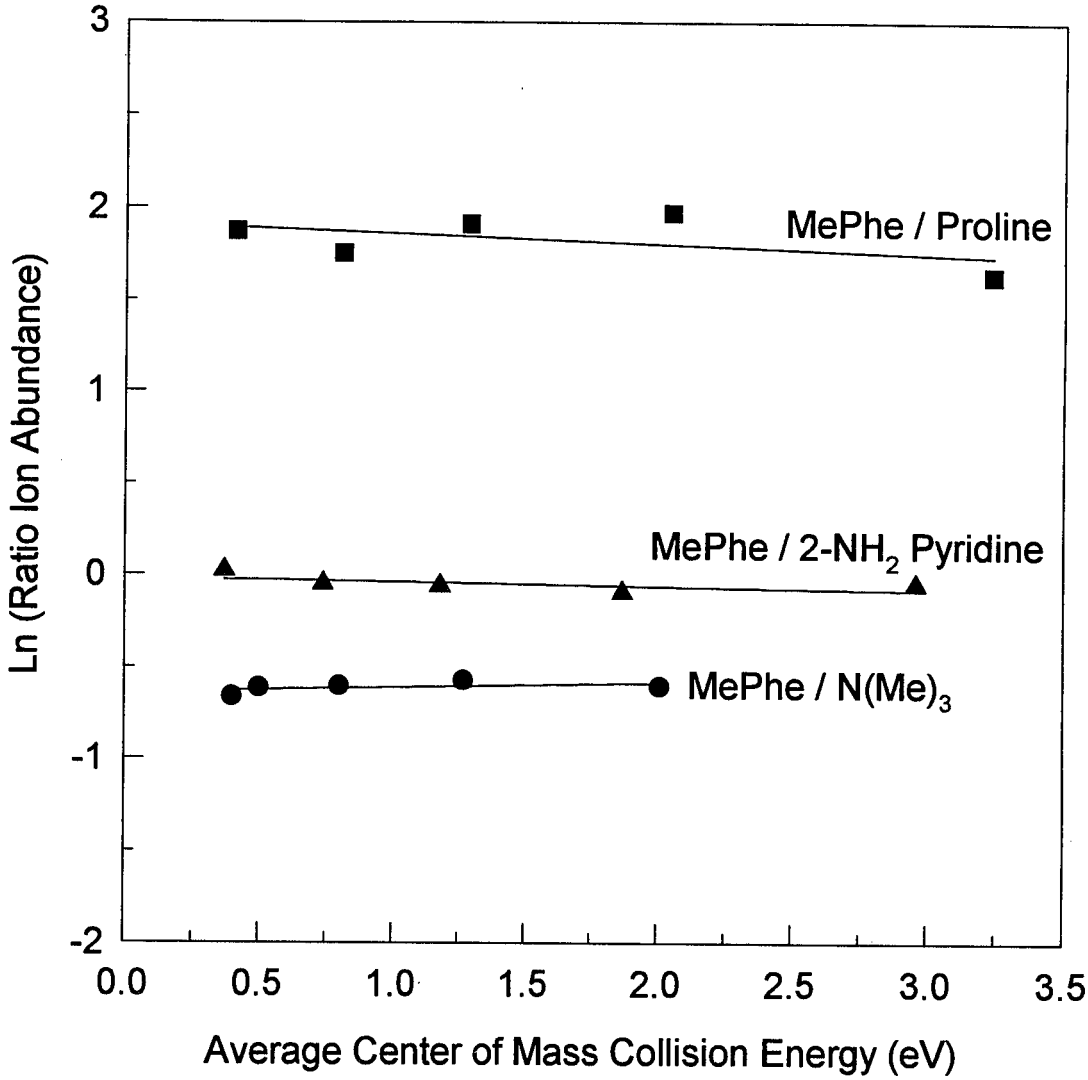
3
2
1
0
-1
-2
0.0
0.5
1.0
1.5
2.0
2.5
3.0
3.5
Ln (Ratio Ion Abundance)
Average Center of Mass Collision Energy (eV)
MePhe / Proline
MePhe / 2-NH2 Pyridine
MePhe / N(Me)3

Figure 5

energies considerably in excess of those required to produce dissociation may result from an individual encounter. As a result, product distributions used to derive proton affinities in these FT-ICR experiments are relatively insensitive to the ion kinetic energies used.

The dissociation technique described above is similar to one we recently developed using cw CO_2 laser irradiation, in which the proton-bound dimer of a reference base and a molecule of interest is subjected to infrared multiphoton dissociation (IRMPD) in an FT-ICR trapped ion cell.[34] Clusters are slowly energized until cleavage occurs selectively along the lowest energy pathway. This process also dissociates the cluster into two intact products, with the species of higher basicity preferentially retaining the proton.

To demonstrate the methodology employed for determining proton affinities, we present a detailed investigation for N-methylphenylalanine. The proton affinity of N-methylphenylalanine was determined by collisionally dissociating proton-bound clusters of five different reference bases with N-methylphenylalanine and evaluating each of their product ion distributions. The data for each experiment is listed in Table 2. The proton affinity of N-methylphenylalanine is bracketed between the values of 223.0 kcal/mol for 6-methylpurine and 223.8 kcal/mol for 2-aminopyridine.[10] A more precise estimate of the value can be made from the data plot in Figure 6. The proton affinity of N-methylphenylalanine extracted from the plot is 223.6 kcal/mol, which is not the median of the bracketed energy difference but is closer to that of 2-aminopyridine.

Table 2: Summary of the Ratios of Product Ion Distributions from the Collision-Induced Dissociation of Proton-Bound Clusters Containing Substituted Phenylalanines and Various Reference Bases

Proton Bound Dimer	# of Trials	Reference Base Proton Affinity[a]	Average Ratio x-Phe/Base	Average ln ratio
Phe with:				
Ile	12	219.3	4.5	1.5
Met	4	221.8	0.1	-2.0
Me-Phe with:				
Pro	11	220.2	6.2	1.8
6-Mepurine	10	223.0	1.2	0.2
2-NH_2 pyridine	15	223.8	0.9	-0.1
$(Me)_3N$	16	225.1	0.6	-0.5
Gln	3	227.4	0.1	-2.0
Me_2-Phe with:				
Me-Phe	3	223.6	1.8	0.6
$(Me)_3N$	4	225.1	0.7	-0.4

a) proton affinities in kcal/mol.

Figure 6. Natural logarithm of (protonated N-methylphenylalanine / protonated reference base) versus reference base proton affinity for five proton-bound dimers. The proton affinity for N-methylphenylalanine extracted from the plot is 223.6 kcal/mol. Data for these experiments are found in Table 2.

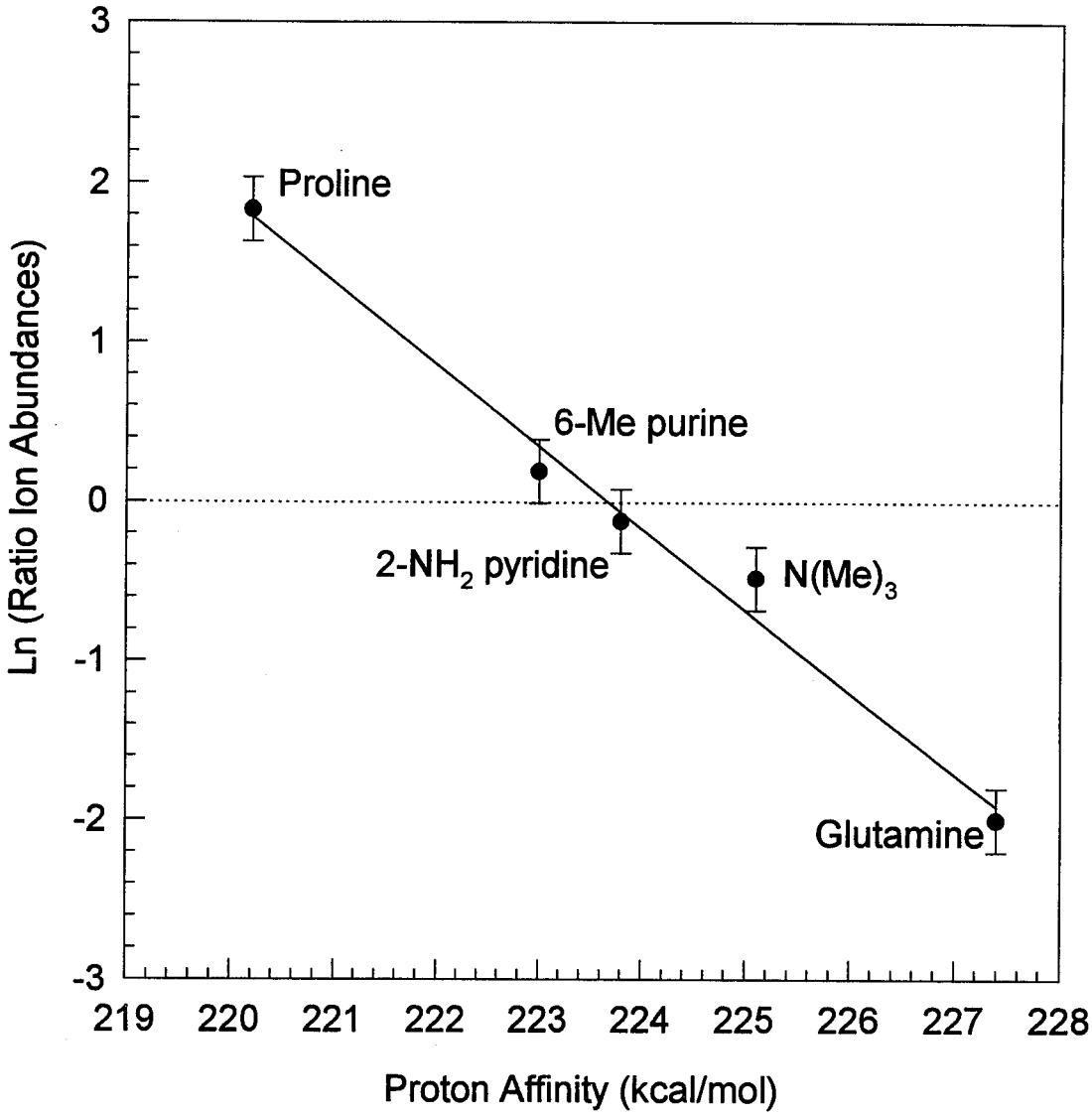
3
2
1
0
-1
-2
-3
Ln (Ratio Ion Abundances)
Proline
6-Me purine
2-NH2 pyridine
N(Me)3
Glutamine
219
220
221
222
223
224
225
226
227
228
Proton Affinity (kcal/mol)

Figure 6

Since the proton affinity of phenylalanine has been published by numerous investigators, phenylalanine can be used as a model compound to test the accuracy of our experimental methods. Proton-bound clusters of phenylalanine with isoleucine and with methionine are isolated and dissociated in the FT-ICR trapped ion cell. In agreement with the N-methylphenylalanine results, the ratios of product ion abundances remain constant over a range of collision energies. A plot of the natural log of the ratio of ion abundances versus the proton affinity of the reference base was generated using the values of 219.3 kcal/mol and 221.8 kcal/mol for the proton affinities of isoleucine and methionine, respectively (data in Table 2).[12] The plot yields a proton affinity for phenylalanine of 220.3 kcal/mol, in excellent agreement with the previously reported range of 219 to 221 kcal/mol. Although determining proton affinities with this technique in theory is quite simple, it can be difficult to generate a variety of proton-bound clusters. Several reference bases with a range of proton affinities were used in the attempt to generate dimers, but most failed to produce any detectable clusters. For reasons not yet understood, we found it easier to generate proton-bound dimers of reference bases with N-methylphenylalanine.

The proton affinity of N,N-dimethylphenylalanine was determined by collisionally dissociating the proton-bound clusters of N,N-dimethylphenylalanine with N-methylphenylalanine and with trimethylamine. As with the above phenylalanine example, N,N-dimethylphenylalanine forms proton-bound dimers with a very select group of reference bases which do not encompass a large range of proton affinities. The proton affinity of N,N-dimethylphenylalanine is bracketed between a range of

223.6 and 225.1 kcal/mol (data in Table 2), and an analysis for these dissociations similar to Figure 6 yields a proton affinity of 224.5 kcal/mol.

Correlations of Adiabatic Nitrogen Lone-Pair Ionization Potentials with Proton Affinities of Substituted Phenylalanines. The proton affinity of a molecule is related to the homolytic bond energy in the conjugate acid $D(B^+-H)$ as indicated by eq 7. If the homolytic bond dissociation energy is constant for a particular functional

$$PA(B) = IP(H) - IP(B) + D(B^+ - H) \qquad (7)$$

group, the proton affinity will exhibit a linear correlation with the quantity IP(H)-IP(B). We have previously reported that a linear correlation exists between the proton affinities and the adiabatic nitrogen lone-pair ionization energies for amino acids which protonate on the amine group.[20] Many of the amino acids correlate well with data for simple primary amines, but the amino acids proline and sarcosine do not. These species, as expected, best fit the correlation for secondary amines. The correlation of the nitrogen lone-pair ionization energy of the amine group with the proton affinity of numerous amino acids, including phenylalanine, N-methyl- and N,N-dimethylphenylalanine is shown in Figure 7. Included in the figure for comparison is the correlation observed for several primary, secondary, and tertiary amines. Deviations from the correlation have been previously explained in detail.[20]

The point for phenylalanine in Figure 7 does not precisely fit the correlation for primary amines. Although it is difficult to interpret the photoelectron spectrum of

Figure 7. Correlation of the amine nitrogen lone-pair adiabatic ionization energy with the proton affinity of numerous amino acids (open circles). Most of the amino acids fit the correlation with the primary amine data (filled circles), which is consistent with the amine group being the preferred site of protonation. Proline, sarcosine and N-methylphenylalanine fail to fit the correlation for primary amines and instead fit the correlation for secondary amines (filled squares). As expected, N,N-dimethylphenylalanine fits the correlation for tertiary amines (filled triangles). Deviations from the correlations are explained in the text. The lines through the points are least-squares fits to the reference aliphatic amine data.

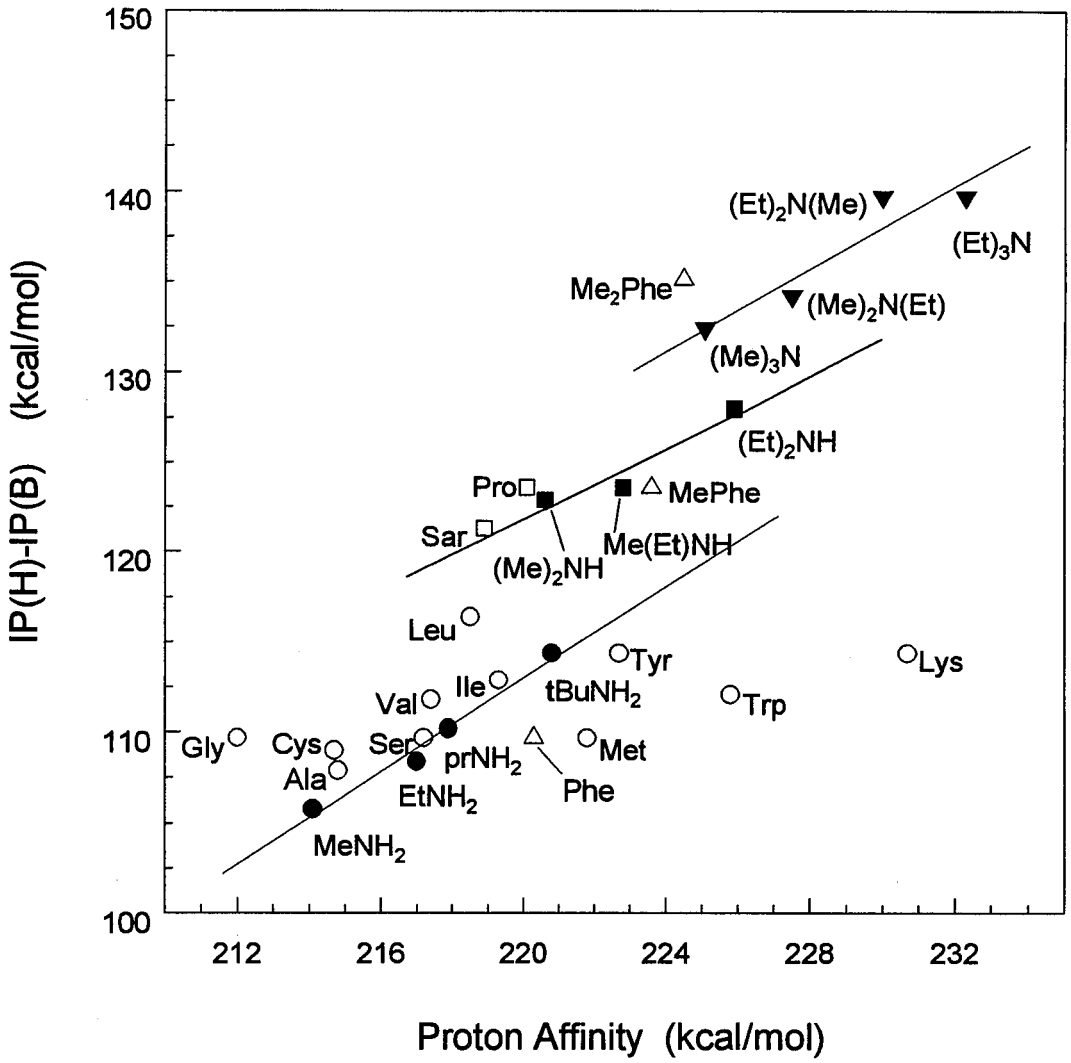
150
140
130
120
110
100
212
216
220
224
228
232
IP(H)-IP(B) (kcal/mol)
Proton Affinity (kcal/mol)
(Et)2N(Me)
(Et)3N
Me2Phe
(Me)2N(Et)
(Me)3N
(Et)2NH
Pro
MePhe
Sar
(Me)2NH
Me(Et)NH
Leu
Tyr
Lys
Val
Ile
tBuNH2
Trp
Gly
Cys
Ser
prNH2
Met
Ala
Phe
EtNH2
MeNH2

Figure 7

phenylalanine (as described above), we are reasonably confident with the assignment of the nitrogen lone-pair as the second band in the photoelectron spectrum. The similar trends observed in the simple amine and 2-phenylethylamine ionization energies resulting from amine methylation support our conclusions (Figure 3). It is noteworthy to mention though, if the peak for the lowest ionization potential (I) in the photoelectron spectrum of phenylalanine is chosen instead of the second peak (II) for the adiabatic nitrogen lone-pair ionization potential, the point for phenylalanine in Figure 7 resides slightly above the correlation line for the primary amines and appears to be in better agreement with many aliphatic amino acids.

Deviation of the phenylalanine point below the primary amine correlation line of Figure 7 implies the proton affinity is larger than the value expected from simple protonation on the amine nitrogen. This enhanced basicity is proposed to result from stabilizing cation-π interactions between the proton on the amine nitrogen and the aromatic ring in the side chain. These interactions are believed to be primarily electrostatic, and previous studies have established that interactions between quaternary ammonium groups and π electrons of aromatic groups (such as benzene) are highly stabilizing.[35,36] Interaction energies for benzene with protonated ammonia, methylamine, and trimethylamine have been reported as 19.3, 18.8 and 15.9 kcal/mol, respectively.[35,36] The large, polarizable ring in the side chain of phenylalanine adopts a geometry which interacts with protons on the amine nitrogen. The net stabilization is not as large as the energies reported above since geometric constraints prevent an optimum interaction and entropic effects due to cyclization must be considered. Recent

molecular mechanics calculations by Gorman and Amster[37] found that dipeptides containing phenylalanine in the C-terminus position displayed considerable stabilization between the protonated N-terminus and the aromatic side chain, yet indicated no significant stabilizing interaction between the proton and aromatic side chain for the isolated amino acid. In contrast, semiempirical calculations using AM1 methodology[38,39] find sizable interactions between the protonated amine and the aromatic side chain of phenylalanine. Geometry optimizations yield two of the amine hydrogens simultaneously pointing directly at the aromatic side chain, polarizing the ring charge distribution to maximize the electrostatic interactions. Fractional charges of 0.272 and -0.137 on two of the amine hydrogens and phenyl carbons, respectively, result in hydrogen bonds that constrain the phenylalanine geometry. The fractional charges on the amine hydrogens decrease upon methylation from 0.272 for phenylalanine to 0.261 for N,N-dimethylphenylalanine. This is accompanied by a decrease in the charge induced on the phenyl carbons. The calculated proton affinities for phenylalanine and N-methyl- and N,N-dimethylphenylalanine are 210.7, 213.8, and 213.1 kcal/mol, respectively, roughly 10 kcal/mol lower than the experimental values. It should only be considered significant that the calculations predict small methyl substituent effects on the proton affinity of phenylalanine. Similar calculations exploring methyl substituent effects on the proton affinities of n-alkyl amines correctly reproduce the observed trend but underestimate the magnitude of observed effects.[40]

The point for phenylalanine is displaced horizontally from the correlation curve of Figure 7 by roughly 3.0 kcal/mol, implying an intrinsic proton affinity (neglecting

intramolecular interactions) of 217.3 kcal/mol. Using the technique of high-pressure mass spectroscopy, Meot-Ner *et al.* determined the proton affinity of phenylalanine to be 216.8 kcal/mol.[41] This measurement was performed at a higher temperature, which would tend to mask stabilizing intramolecular interactions, and is in good agreement with the value predicted by the correlation curve.

The point for N-methylphenylalanine fits the correlation in Figure 7 for secondary amines reasonably well. As with phenylalanine, the point is slightly below the correlation line but is only displaced horizontally by approximately 1.8 kcal/mol. Since the proton affinity of N-methylphenylalanine has not previously been published, there is no high-temperature value available for comparison. Addition of a methyl group on the amine nitrogen increases the proton affinity of that site, but appears to weaken the intramolecular cation-π interaction as the displacement from the correlation line is not as great as in phenylalanine. This observation follows the previously mentioned trend in the interactions of benzene with protonated amines, where interaction energies decreased upon methylation from ammonia to methyl- and trimethylamine. As may be expected from electrostatic considerations, interaction energies decrease as the fractional charge on the amine hydrogens decrease.

The point for N,N-dimethylphenylalanine, in contrast to the above examples, lies to the left of the correlation line for the tertiary amines. As noted above, the addition of a second methyl group on the nitrogen reduces the electrostatic charge on the amine hydrogen and thus reduces the stabilizing effect of the phenyl substituent. Although this molecule does not necessarily fit the tertiary correlation well, it follows

the trend observed for the majority of aliphatic amino acids which fall to the left of the correlations for aliphatic amines.

An additional argument is offered to support the postulate that the proton affinity of phenylalanine reflects cation-π interactions. Substitution of methyl groups onto the nitrogen of primary amines increases the proton affinity substantially, whereas substitution of methyl groups onto the amine nitrogen of phenylalanine does very little to increase the proton affinity. The addition of one methyl group to ethylamine increases the proton affinity by 5.8 kcal/mol. The difference in the measured proton affinities of phenylalanine and N-methyl-phenylalanine, 3.4 kcal/mol, is not as large as expected. If the intrinsic proton affinity estimated from Figure 7 is used for phenylalanine (217.3 kcal/mol), the anticipated proton affinity of N-methylphenylalanine should be 223.1 kcal/mol (217.3 + 5.8). This value is in reasonable agreement with that observed experimentally (223.6 kcal/mol) and suggests that the protonated phenylalanine has additional stabilization.

Conclusions

This study presents a quantitative approach for extracting gas phase proton affinities from cluster dissociation data. A simplified RRKM analysis is used to determine proton affinities from product ion abundances. This methodology is similar to that introduced by Cooks and co-workers[18] for the extraction of thermochemical data from competitive dissociation processes, but varies in the interpretation of the results.

The photoelectron spectra of amino acids with complex side groups can be difficult to interpret since the peaks for ionization from the amine nitrogen lone-pair orbital and side-chain orbitals tend to overlap and are unresolved. The spectrum for phenylalanine clearly displays this problem as the nitrogen lone-pair and aromatic phenyl π orbitals have virtually the same ionization energies. Methyl substitution on the amine nitrogen destabilizes the lone-pair orbital and shifts the peak in the spectrum to a lower ionization potential. This technique is useful in general for identifying orbital peaks which are unresolvable in complex photoelectron spectra.

Methyl substitution onto the amine nitrogen of phenylalanine has also been shown to increase the basicity of the molecule. Although the increase in proton affinity is less than that observed for methylation of simple amines, complete methylation increases the proton affinity of phenylalanine by approximately 4 kcal/mol. This small net difference in proton affinities results from stabilizing intramolecular cation-π interactions which are present in phenylalanine (and to a much lesser extent N-methylphenylalanine) and cause the proton affinity to be higher than if simple protonation occurred on the amine. The proton affinity of N,N-dimethylphenylalanine does not reflect these additional stabilizing interactions and accounts for the small net difference in proton affinities between the parent and dimethylated species.

Due to the varying strengths of intramolecular interactions for the remaining amino acids, it is difficult to predict the effect of amine methylation on proton affinities. The increase could range from a few kilocalories/mol to roughly 11 kcal/mol, that observed for methylation of simple amines. Incorporation of a methylated amino acid

into the N-terminus of a peptide will potentially increase the basicity of that site, but in most cases will not be sufficient to compete with protonation of highly basic side chains or internally solvated amide oxygens.

Acknowledgments

J. L. B. gratefully acknowledges the Beckman Foundation and Institute for the initial funding and continuing support of the research facilities, and the National Science Foundation for their funding (CHE-9108318). We acknowledge the financial support of S. C. from a NIH-NRSA traineeship in Biotechnology, E. M. M. from a NIH-NRSA Human Genome traineeship and Rainin Fellowship, and M. T. R. from a California Institute of Technology Consortium grant. D. L. L. acknowledges support of the Department of Energy (Division of Chemical Sciences, Office of Basic Energy Sciences, Office of Energy Research; Contract No. DE-FG02-86ER13501), the National Science Foundation for assistance in support for instrumentation (CHE-9300841) and for support of K. F. S. under the REU program (CHE-376800), and the Materials Characterization Program (Arizona).

References

1. Karas, M.; Hillenkamp, F. *Anal. Chem.*, **1988**, *60*, 2299.

2. Torgerson, D. F.; Skowronski, R. P.; Macfarlane, R. D. *Biochem. Biophys. Res. Commun.*, **1974**, *60*, 616.

3. Barber, M.; Bordoli, R. S.; Sedgewick, R. S.; Tyler, A. N. *J. Chem. Soc. Chem. Commun.*, **1981**, 325.

4. (a) Meng, C. K.; Mann, M.; Fenn, J. B. *Z. Phys. D.*, **1988**, *10*, 361. (b) Fenn, J. B.; Mann, M.; Meng, C. K.; Wong, S. F.; Whitehouse, C. M. *Science*, **1989**, *246*, 64.

5. (a) Blakely, C. R.; Vestal, M. L. *Anal. Chem.*, **1983**, *55*, 750. (b) Vestal, M. L.; Fergusson, G. J. *Anal. Chem.*, **1985**, *57*, 2373.

6. Meot-Ner, M. *J. Am. Chem. Soc.*, **1984**, *106*, 278.

7. Grese, R.; Cerny, R.; Gross, M. *J. Am. Chem. Soc.*, **1989**, *111*, 2835.

8. Watson, J. T.; Wagner, D. S.; Chang, Y. S.; Strahler, J. R.; Hanash, S. M.; Gage, D. A. *Int. J. Mass Spectrom. and Ion Processes*, **1991**, *111*, 191.

9. Vath, J. E.; Biemann, K. *Int. J. Mass Spectrom. and Ion Processes*, **1990**, *100*, 287.

10. Lias, S. G.; Bartmess, J. E.; Liebman, J. F.; Holmes, J. L.; Levin, R. D.; Mallard, W. G. *J. of Physical and Chemical Reference Data*, **1988**, 17(1).

11. Wu, Z.; Fenselau, C. *Rapid Comm. Mass Spectrom*, **1992**, *6*, 403.

12. (a) Locke, M. J.; McIver, R. T. *J. Am. Chem. Soc.*, **1983**, *105*, 4226. (b) Locke, M. J. Ph.D. Thesis, University of California, 1983 (unpublished results).

13. Bojesen, G. *J. Am. Chem. Soc.*, **1987**, *109*, 5557.

14. Gorman, G. S.; Speir, J. P.; Turner, C. A.; Amster, I. J. *J. Am. Chem. Soc.*, **1992**, *114*, 3986.

15. Proton affinity of NH_3 referenced at 204.0 kcal/mol.

16. Kimura, K.; Katsumata, S.; Achiba, Y.; Yamazaki, T.; Iwata, S. *Handbook of He(I) Photoelectron Spectra of Fundamental Organic Molecules*, Halsted Press, New York, 1981.

17. Gauthier, J. W.; Trautman, T. R.; Jacobsen, D. B. *Anal. Chim. Acta.*, **1991**, *246*, 211.

18. McLuckey, S. A.; Cameron, D.; Cooks, R. G. *J. Am. Chem. Soc.*, **1981**, *103*, 1313.

19. Staley, R. H.; Kleckner, J. E.; Beauchamp, J. L. *J. Am. Chem. Soc.*, **1976**, *98*, 2081.

20. Campbell, S.; Beauchamp, J. L.; Rempe, M.; Lichtenberger, D. L. *Int. J. Mass Spectrom. & Ion Processes*, **1992**, *117*, 83.

21. (a) Lichtenberger, D. L.; Kellogg, G. E.; Kristofzski, J. G.; Page, D.; Turner, S.; Klinger, G.; Lorenzen, J. *Rev. Sci. Instrum.*, **1986**, *57*, 2366. (b) Calabro,

D. C.; Hubbard, J. L.; Blevins, C. H., II; Campbell, A. C.; Lichtenberger, D. L. *J. Am. Chem. Soc.*, **1981**, *103*, 6839.

22. Lichtenberger, D. L.; Fenske, R. F. *J. Am. Chem. Soc.*, **1976**, *98*, 50.

23. Marzluff, E. M.; Campbell, S.; Rodgers, M. T.; Beauchamp, J. L. submitted for publication.

24. Bowman, R.; Stroud, H. *J. Chem. Soc.*, **1950**, 1342.

25. Klasnic, L. *J. Electron Spectrosc. Relat. Phenom.*, **1976**, *8*, 161.

26. Cannington, P.; Ham, N. J. *J. Electron Spectrosc. Relat. Phenom.*, **1983**, *32*, 139.

27. Turner, D.; Baker, C.; Baker, A.; Brundle, C. *Molecular Photoelectron Spectroscopy*; Wiley-Interscience, London, 1970.

28. Domelsmith, L. N.; Munchausen, L. L.; Houk, K. N. *J. Am. Chem. Soc.*, **1977**, *99*, 4311.

29. Aue, D. H.; Bowers, M. T. *Gas Phase Ion Chemistry*, Academic Press, New York, 1979, Vol. 2.

30. Henderson, W. G.; Taagepera, M.; Holtz, D.; McIver, R. T., Jr.; Beauchamp, J. L.; Taft, R. W. *J. Am. Chem. Soc.*, **1972**, *94*, 4728.

31. Cheng, X.; Wu, Z.; Fenselau, C. *J. Am. Chem. Soc.*, **1993**, *115*, 4844.

32. (a) Marcus, R. A.; Rice, O. K. *J. Phys. Colloid Chem.*, **1951**, *55*, 894. (b) Marcus, R. A. *J. Chem. Phys.*, **1952**, *20*, 359.

33. (a) Rice, O. K.; Ramsperger, H. C. *J. Am. Chem. Soc.*, **1928**, *50*, 617. (b) Kassel, L. S. *J. Phys. Chem.*, **1928**, *32*, 1065.

34. Campbell, S.; Beauchamp, J. L. *Proc. SPIE-Int. Soc. Opt. Eng.*, **1992**, *1636*, 201.

35. Deakyne, C. A.; Meot-Ner, M. *J. Am. Chem. Soc.*, **1985**, *107*, 474.

36. MP2/6-31G** calculations of NH_4^+/C_6H_6 give a binding energy of 17.9 kcal/mol. Private communication with D. A. Dougherty.

37. Gorman, G. S.; Amster, I. J. *J. Am. Chem. Soc.*, **1993**, *115*, 5729.

38. AM1 calculations were performed using the Hyperchem™ Computational Chemistry Software Package, Release 3, Autodesk, Inc. 1992.

39. Dewar, M. J.; Zoebisch, E. G.; Healy, E. F.; Stewart, J. J. *J. Am. Chem. Soc.*, **1985**, *107*, 3902.

40. Dewar, M. J.; Dieter, K. M. *J. Am. Chem. Soc.*, **1986**, *108*, 8075.

41. Meot-Ner, M.; Hunter, E. P.; Field, F. H. *J. Am. Chem. Soc.*, **1979**, *101*, 686.

CHAPTER 5

Deuterium Exchange Reactions as a Probe of Biomolecule Structure. Fundamental Studies of Gas Phase H/D Exchange Reactions of Protonated Glycine Oligomers with D_2O, CD_3OD, CD_3CO_2D, and ND_3.

Deuterium Exchange Reactions as a Probe of Biomolecule Structure. Fundamental Studies of Gas Phase H/D Exchange Reactions of Protonated Glycine Oligomers with D_2O, CD_3OD, CD_3CO_2D, and ND_3.

Sherrie Campbell, M. T. Rodgers, Elaine M. Marzluff and J. L. Beauchamp*

Contribution No. 8999 from the Arthur Amos Noyes Laboratory of Chemical Physics

California Institute of Technology, Pasadena, California 91125

Abstract

A Fourier transform ion cyclotron resonance mass spectrometer was used to examine the hydrogen/deuterium exchange reactions of protonated glycine oligomers (Gly_n, n=1-5) with D_2O, CD_3OD, CD_3CO_2D, and ND_3. Exchange rates in this study were monitored over three orders of magnitude, from 10^{-9} to 10^{-12} $cm^3molecule^{-1}sec^{-1}$. Reaction kinetics are highly dependent on peptide structure and the properties of the exchange reagents. The rate and extent of H/D exchange of the protonated oligomers increases with reagent gas basicity, $D_2O<CD_3OD<CD_3CO_2D<ND_3$. ND_3 is the most efficient reagent studied, as it exchanges every labile hydrogen in each of the oligomers. Several distinct mechanisms, supported by semiempirical AM1 and PM3 calculations, are proposed to explain the observed patterns of reactivity. An onium ion mechanism

is proposed for the exchange of N-terminus hydrogens of Gly_nH^+ oligomers with ND_3, in which an endothermic proton transfer from the N-terminus is rendered energetically feasible by simultaneous solvation of the resultant ammonium ion by the neutral peptide. This mechanism is consistent with the observation of multiple exchanges in a single collision event with ND_3. For those reagents whose proton affinities are too low to form solvated onium ion intermediates, a relay mechanism is proposed in which the reagent shuttles a proton from the N-terminus to a slightly less basic site in the molecule. For the glycine oligomers, this site is an amide oxygen. A tautomer mechanism is proposed for the exchange of the amide hydrogens with ND_3. Exchange occurs by proton transfer from the N-terminus to the amide carbonyl in concert with transfer of the amide proton to ammonia, forming an ammonium ion solvated by a tautomerized peptide. Semiempirical calculations suggest that exchange of the C-terminus hydrogen proceeds via formation of a salt bridge with the reagent gas, which deprotonates the C-terminus acid group, with the nearby protonated N-terminus stabilizing the resultant ion pair. Betaine, $[(CH_3)_3N^+\text{-}CH_2CO_2H]$, used in this study to determine the isotopic purity of the exchange reagents, serves as a model for salt bridge formation since it does not possess a labile proton and readily exchanges the carboxylic acid hydrogen. The effect of translational and vibrational excitation on H/D exchange rates was studied for several oligomers using off-resonance collisional activation. For those oligomers that undergo facile H/D exchange with the reagent gases, excitation decreases rates. For those oligomers which do not undergo facile H/D exchange, reactivity is not promoted by collisional activation.

Introduction

Conformational studies of peptides and proteins in solution have long been aided by isotopic labeling techniques.[1] For small peptides, solvent can access all the labile hydrogen sites and readily exchange the hydrogen for deuterium in the molecule. The rates of exchange can differ widely between the sites in the peptide, and have been shown to be a strong function of pH.[2] For large peptides in highly folded conformations, fewer labile hydrogen sites are exposed to the solvent for exchange, since many of the hydrogens are buried in the hydrophobic core of the protein.[3] Incorporation of deuterium at sites such as exposed amine, carboxylic acid, alcohol, and amide groups which react with differing rates has allowed structural determination via NMR spectroscopy.[4]

Although peptide and protein structures can be well characterized in solution, their gas phase structures are virtually unknown as there are relatively few experiments which extract this information. Employing the techniques of mass spectrometry, several research groups have used collision induced dissociation to identify the amino acid composition and sequence of gas phase peptides and proteins.[5] These experiments have been less useful in elucidating secondary structure information.

H/D exchange of biomolecules in solution has been employed to understand biophysical processes, with a recent emphasis on the kinetics and mechanisms of protein folding.[6] For example, in a fast flow mixing system protein folding is initiated by dilution of a denaturant. After a suitable delay, the solution pH is raised to promote H/D exchange of exposed sites. In a final mixing step, the pH is lowered to terminate

the exchange process. NMR, or more recently mass spectrometry,[7] is then used to examine the partially labeled protein molecules. With the advancements made in soft ionization techniques, such as electrospray[8] and fast atom bombardment,[9] examples of solution phase H/D exchange of proteins followed by mass spectrometric analysis are abundant.[10] Although the proteins are detected in the gas phase, the extent of H/D exchange reflects the conformation in solution and does not necessarily have direct implications for gas phase structures.

H/D exchange of simple molecules directly in the gas phase has been used extensively to distinguish between isomeric species,[11,12] to deduce reaction mechanisms,[13,14,15] and more recently to infer structural features of complex biomolecules.[16,17] Earlier studies from our laboratory,[11] using the technique of ion cyclotron resonance mass spectrometry, demonstrated for substituted benzene derivatives reacting with D_2O that the rate of exchange was strongly dependent on the structure of the sample. For example, ortho and para xylene isomers exchanged all their labile hydrogens with rate constants of 10^{-11} $cm^3molecule^{-1}sec^{-1}$, while meta xylene exchanged only one site more slowly. More recently, Ranasinghe *et al.*[12] investigated the H/D exchange of numerous protonated isomeric aromatic compounds in the collision region of a triple quadrupole mass spectrometer and determined that the proximity of the functional groups and the proton affinity difference between the analyte and the reagent gas were important factors in exchanging polyfunctional compounds. They concluded that ND_3 undergoes exchanges with all active hydrogens in the substituted aromatic compounds studied, even those remote from the charge site.

For example, p-amino benzoic acid exchanges all four labile hydrogens with ND_3 under trapped reaction conditions. In contrast, CH_3OD displays proximity effects by only exchanging functional groups at specific orientations, and can be used to distinguish different isomers and functionalities. The same p-amino benzoic acid undergoes only two exchanges with CD_3OD, while o-amino benzoic acid exchanges all four labile sites. More interestingly, they observed that exchange efficiencies for both reagent gases were highest whenever cluster species of the analyte and reagent were higher in abundance than the protonated analyte itself, indicating the importance of a collision complex for exchange.

Long-lived complexes are frequently postulated to account for the emergence of particular products from ion-molecule reactions,[18,19] and a multiple-well potential energy surface[20] to describe H/D reactions has achieved general acceptance. Squires *et al.*[21] used this model over a decade ago to explain multiple H/D exchanges and determine reaction rate constants of anionic bases and neutral acids in flowing afterglow experiments. The potential energy surfaces drawn for simple H/D exchange are highly dependent on the proton affinity difference between the analyte and the deuterating reagent gas. For simple H/D exchange via proton transfer, exchange is most probable when the proton affinities of the reagent and the analyte molecule are similar. Investigations by Ausloos and Lias[14] have shown that for protonated monofunctional compounds, H/D exchange reactions do not occur when the proton affinities differ by more than 20 kcal/mol.

Several exceptions to this 20 kcal/mol limit have been shown for polyfunctional molecules, such as amino acids and peptides. Using the techniques of ion cyclotron resonance mass spectrometry, Gard *et al.*[22] demonstrated that H/D exchange of several protonated amino acids with CH_3OD occurs despite proton affinity differences for the molecules of 30 to 40 kcal/mol. Most interesting is their finding that the exchange of the carboxylic acid occurs 3 to 10 times faster than the exchange of the more basic amino group, with rate constants ranging from $0.6\text{-}1.4\text{x}10^{-10}$ $cm^3molecule^{-1}sec^{-1}$. Cheng and Fenselau[23] investigated the H/D exchange of four protonated peptides, ranging in proton affinity from 234 to ≥255 kcal/mol, with ND_3 in a four sector tandem mass spectrometer. Despite proton affinity differences of greater than 50 kcal/mol, all peptides underwent complete or partial exchange with the reagent gas. Their results from varying collision gas pressure and collision energy reconfirm the importance of a collision complex for H/D exchange.

Winger *et al.*[16] reported perhaps the first gas phase H/D exchange results for protein ions. Multiply protonated bovine proinsulin and α-lactalbumin were generated using electrospray ionization and reacted with D_2O in a "reaction capillary" prior to detection using a triple quadrupole mass spectrometer. The native and disulfide bond reduced forms of the protein displayed different reactivities in the gas phase with the D_2O exchange reagent, allowing the different protein conformations to be distinguished according to their reactivity. Suckau *et al.*[17] probed the gas phase reactivity of multiply protonated cytochrome *c* formed by electrospray ionization with D_2O using an ion cyclotron resonance mass spectrometer. Their exchange results were interpreted to

indicate that more than one molecular conformation can exist for a specific mass to charge species in a spectrum. Suckau *et al.*[17] suggested that gas phase species with distinctive exchange reactivity could be correlated with known solution phase structures.

The rates of H/D exchange for cytochrome *c* were also reported, and varied from $5x10^{-13}$ to $2x10^{-12}$ $cm^3molecule^{-1}sec^{-1}$ depending on the charge state of the ion. Rates increased almost linearly with the number of charges on the molecules. In comparison with the rates of most ion-molecule reactions, these exchange processes are rather slow. We will consider exchange reactions which proceed with rate constants in excess of 10^{-10} $cm^3molecule^{-1}sec^{-1}$ as facile since they take place with fewer than 10 collisions. In contrast, when 10^3 or more collisions are required for exchange (corresponding to rates $\leq 10^{-12}$ $cm^3molecule^{-1}sec^{-1}$), reactions are not facile in that features must be present in the potential energy surface which inhibit access to the transition state for the process during the lifetime of the collision complex.

Distinctive chemical reactivity remains the principal experimental method to probe the structures of complex molecular ions in the gas phase. Other than adduct formation and simple processes such as proton transfer, there is little known about the gas phase ion chemistry of biological molecules. Isotopic hydrogen exchange reactions are the only notable exception. With the limited range of studies that have been performed to date, very little is known about the mechanism and energetics of H/D exchange processes for complex molecules.

We have undertaken a systematic study of isotopic hydrogen exchange using FT-ICR techniques, focusing our attention on simple glycine oligomers (Gly_n, n=1-5) reacting with a series of reagent gases. The glycine oligomers are ideal model systems for understanding the mechanisms of H/D exchange. The glycine residues do not have basic side chains, hence the site of protonation in all the oligomers studied is the N-terminus nitrogen. Additionally, there have been several recent measurements of the gas phase proton affinities for this series.[24,25,26] The proton affinities reported for Gly_1 to Gly_5 via the kinetic method are 211.6, 219.1, 223.1, 227.2, and 231.8 kcal/mol, respectively.[24] The choice of H/D exchange gases reflects our attempt to probe a range of proton affinities and include species which are capable of multiple exchanges in a single encounter.[27] The reagents investigated include D_2O (166.5), CD_3OD (181.9), CD_3CO_2D (190.2), and ND_3 (204.0 kcal/mol).[28] In this article, a kinetic analysis of the deuterium incorporation data for all 5 oligomers with each reagent gas is presented.[29] The simplicity of the glycine oligomers facilitates theoretical studies to better understand our experiments. We have modeled our results using semiempirical AM1[30] and PM3[31] calculations to quantify potential energy surfaces for selected systems. We wish to report findings which assist in elucidating important features of potential energy surfaces for isotopic hydrogen exchange and stable structures of peptides in the gas phase.

Experimental Details

Experiments were performed in an external ion source Fourier transform ion cyclotron resonance (FT-ICR) mass spectrometer. A detailed description of this instrument has been previously published.[32] The spectrometer incorporates a Cs ion bombardment source, octopole ion guide for transferring ions into the high-field region of a 7-T superconducting magnet, a standard 2x2x3 inch detection cell, and the electronics required for data acquisition and processing in the Fourier transform mode. The instrument has three regions of differential cryogenic pumping, resulting in a residual background pressure of high 10^{-10} or low 10^{-9} Torr in the detection cell. A Schulz-Phelps ionization gauge is an integral part of the ICR cell and is calibrated using a capacitance manometer connected directly to the cell through a static port. Uncertainties in pressure measurements are estimated to be ±20%. This is the major source of error in reported rate constants. Comparison of literature rates for several well characterized reactions to measurements made with the new instrument give agreement within this range of uncertainty. Deuterating gases are degassed using several freeze-thaw cycles before introduction directly into the ICR cell using Varian leak valves. Typical static gas pressures used in the exchange reactions are (0.5-1.5)x10^{-7} Torr. Higher pressures lead to significant ion losses at long trapping times.

Samples are typically prepared by dissolving small amounts of solid (~0.1 mg) directly into a 2-3 μL drop of a mixture of glycerol and triflouroacetic acid spread onto a copper probe tip. Protonated peptide ions are produced by Cs ion bombardment of the acidic matrix, and are transported and loaded into the ICR cell for 100 ms. Species

are isolated within 20 ms of the ion loading period by applying rf excitation at the resonance frequencies of all unwanted higher and lower mass ions in the ICR cell. Fast ion bombardment can generate ions with a full range of excess vibrational energy. Evidence for this has been provided by various experiments which reported the metastable decay of large ions over several milliseconds.[33] In our experiments, the peptide ions were not observed to decompose after isolation. The effects of excess vibrational and translational energies of reactant ions are further considered below.

To avoid off-resonance excitation[34] of the reactant ion, carbon-13 isotopes of the protonated glycine oligomers were not ejected from the cell. All isotopic contributions were subtracted from the raw data (according to their natural abundances) prior to calculating the reaction rate constants. H/D exchange reaction times were varied from a minimum of 130 ms up to 20 seconds.

Methyl esters of the glycine oligomers were synthesized by dissolving the peptides in a solution of methanol and triflouroacetic acid (99:1), and stirring overnight. Reaction yields did not exceed 75%, but products could be easily isolated in the FT-ICR experiments. Structures of the products were confirmed using collision induced dissociation techniques. All other peptide samples were commercially available from Sigma Chemical Co. and used as provided without further purification. The deuterating reagents D_2O (99.9 atom % deuterium), CD_3OD (99.8 atom % deuterium), and CD_3CO_2D (99.91 atom % deuterium) were also purchased from Sigma Chemical Co. ND_3 was obtained from Matheson with a purity of 99.0 atom % deuterium.

Since our FT-ICR instrument is not exclusively used for H/D exchange reactions, the vacuum chamber is primed overnight with deuterating gas at approximately 10^{-6} Torr to allow for the complete exchange of all surfaces. Although the reagent gases have high isotopic purity (>99 atom %) prior to introduction into the mass spectrometer, the percent deuterium of the reagent gases in the vacuum chamber is not as high. A unique molecule for probing the percent deuterium of each reagent gas in the vacuum chamber is betaine (Structure 1). Since betaine contains one labile hydrogen which exchanges fairly rapidly, the product ion distribution after complete H/D exchange indicates the actual atom percent deuterium of the reagent gas in the vacuum chamber. For all the reagent gases studied, the percent deuterium ranged from 90-95 atom %.

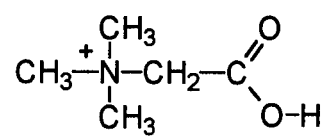

1

Semiempirical calculations were performed with Hyperchem[35] to obtain model structures and energetics for the protonated glycine oligomers and the reagent exchange gases. Both the AM1[30] and PM3[31] semiempirical methods were employed. In all of the calculations, starting structures for the molecules were obtained using the standard amino acid templates provided with Hyperchem. Structures for the

protonated species were obtained by attaching a proton to a basic site. The structure was then annealed using molecular mechanics and energy-minimized using semiempirical methods. The site of protonation and initial geometry was varied to determine the differences in the structure and stability of various conformations of the protonated parent molecules. Geometries of the protonated peptide/reagent gas adducts, neutral peptides, and reagent gases were obtained in a similar manner. Since both the AM1 and PM3 methods give a very poor estimate of the heat of formation of H^+, the experimental value 365.7 kcal/mol was used.[28]

Results

Reactions with D_2O. D_2O, with a proton affinity of 166.5 kcal/mol,[28] is the least basic exchange reagent used in this study. The differences in proton affinity between D_2O and the glycine oligomers (n=1-5) range from 45.1 to 65.3 kcal/mol.[24] Gly_1H^+, with the smallest difference in proton affinities, is virtually unreactive with D_2O, displaying one slow exchange of a labile hydrogen during the 10 second reaction period (Figure 1a). Gly_2H^+ is more reactive with D_2O, since all five of its labile hydrogens are observed to exchange (Figure 1b). Three of five H/D exchanges are fairly fast, proceeding within the first three seconds of reaction, while the remaining exchanges are slower. The reaction of Gly_3H^+ with D_2O is slightly less efficient than that of Gly_2H^+, since only five of six labile hydrogens are observed to exchange (Figure 1c). $(Gly_3\text{-}OMe)H^+$ exchanges all five of its labile hydrogens with D_2O, possibly indicating the unreactive sixth site on Gly_3H^+ is the C-terminus hydroxyl. For the larger

Figure 1. Time plots of the H/D exchange products of Gly_nH^+ with D_2O ($1.0x10^{-7}$ Torr). (a) $GlyH^+$ exchanges only one hydrogen slowly with D_2O. (b) In contrast, Gly_2H^+ readily exchanges all 5 labile hydrogens. (c) Gly_3H^+ exchanges 5 of 6 labile hydrogens. (d) Facile exchange abruptly halts, as Gly_4H^+ slowly exchanges a single hydrogen. Least square fits (lines) of kinetic equation (see text) to the experimental intensities (points) are shown. The number of deuterium atoms incorporated into each species is indicated as d_n.

a)

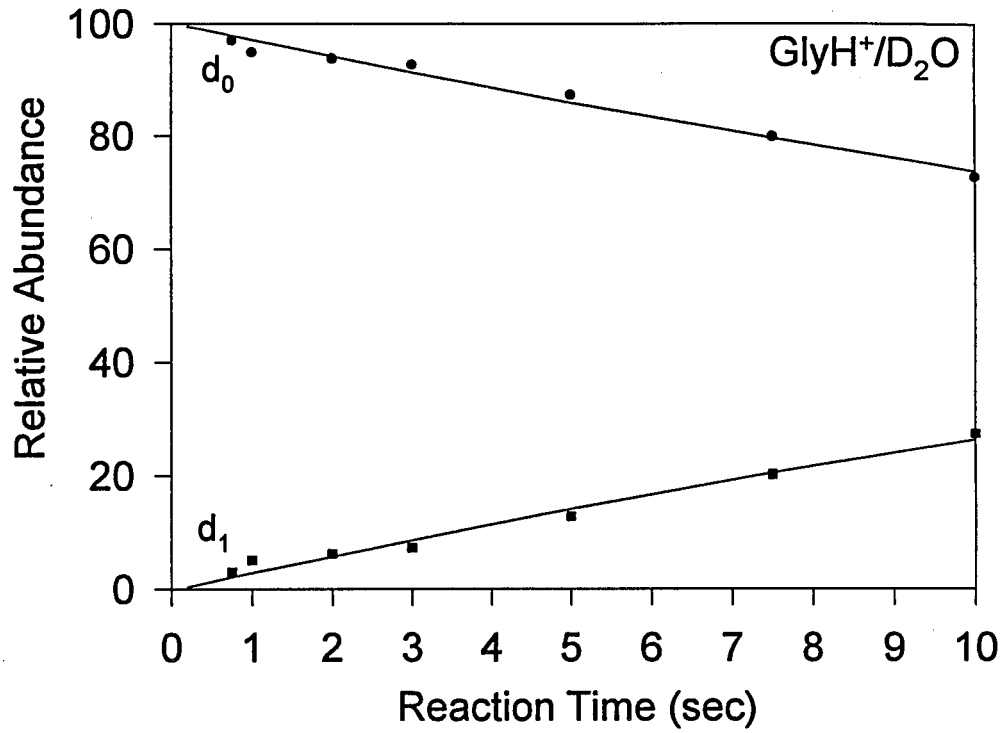
GlyH+/D2O
d0
d1
Relative Abundance
Reaction Time (sec)
0
20
40
60
80
100
0 1 2 3 4 5 6 7 8 9 10

b)

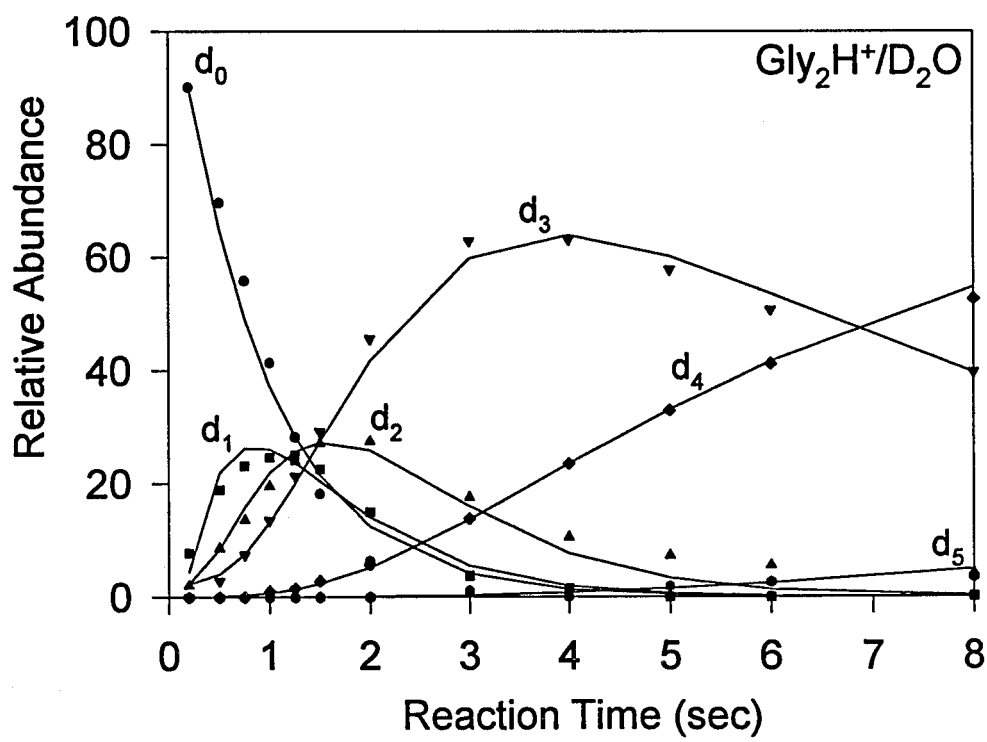
Gly2H+/D2O
d0
d1
d2
d3
d4
d5
Relative Abundance
Reaction Time (sec)
0
20
40
60
80
100
0 1 2 3 4 5 6 7 8

Figure 1

c)

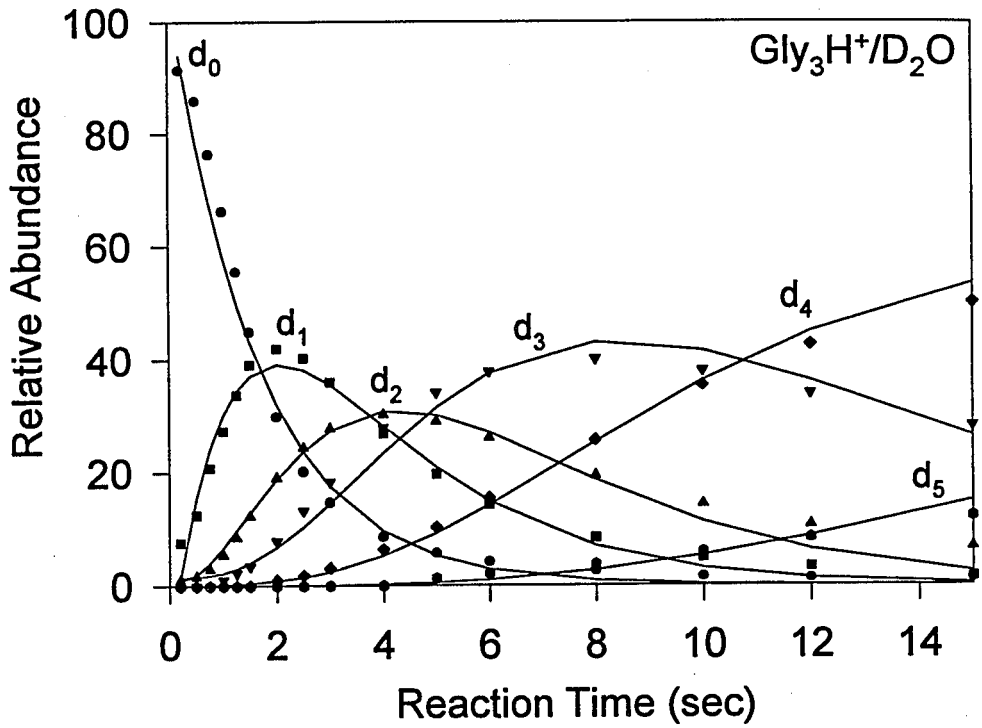
Gly3H+/D2O
d0
d1
d2
d3
d4
d5
Relative Abundance
Reaction Time (sec)
0
20
40
60
80
100
0
2
4
6
8
10
12
14

d)

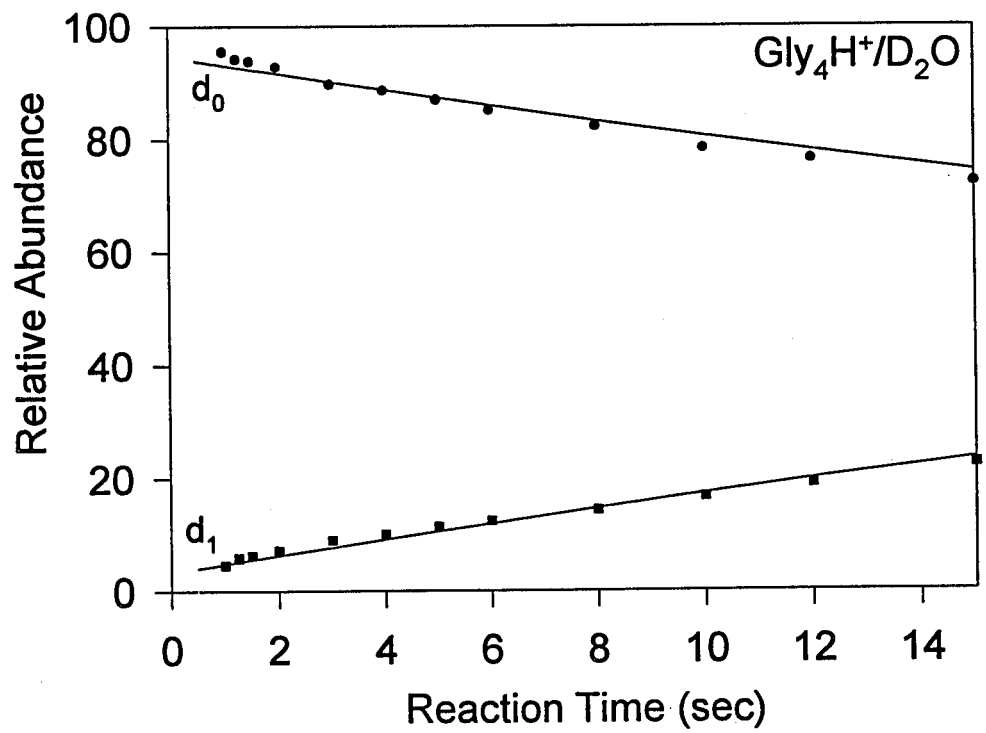
Gly4H+/D2O
d0
d1
Relative Abundance
Reaction Time (sec)
0
20
40
60
80
100
0
2
4
6
8
10
12
14

oligomers Gly_4H^+, $(Gly_4\text{-}OMe)H^+$, and Gly_5H^+ reacting with D_2O, facile exchange abruptly halts and only one deuterium is slowly incorporated into the molecule (e.g., Figure 1d). Since the proton affinity of Gly_4H^+ is reported as 227.2 kcal/mol, an upper limit of 61 kcal/mol can be implied as the largest difference in proton affinities for which H/D exchange occurs with D_2O. Two observations can be made from the exchange data with D_2O. First, excluding glycine, H/D exchange rates decrease with increasing proton affinity of the peptide. Second, a subtle change to the oligomer (addition of a single glycine unit to Gly_3) can cause a dramatic change in reactivity.

It is of interest to explore the occurrence of multiple exchanges in a single collision event. D_2O has the opportunity to exchange two deuteriums during each reactive encounter. Of the glycine oligomers studied, only Gly_2 and Gly_3 exchange more than a single site with D_2O. Figure 2a shows the results of reacting Gly_3H^+ with D_2O for 1 second. Three deuteriums are incorporated into the oligomer during this time period. If the d_1 species (m/z=191, resulting from one exchange) is continuously ejected during the one second time period, no higher mass products are observed (Figure 2b). Under similar experimental conditions, Gly_2H^+ also displays no higher mass products when continuously ejecting the d_1 species. D_2O therefore partakes in predominantly single, sequential exchanges with the glycine oligomers.

Determination of the reaction rate constants for glycine oligomers with D_2O is straightforward. The above experiment provides support for calculating these values using a model of simple sequential deuterium incorporation. The rate constant for the exchange of the nascent reactant MH^+ can be determined from the slope of a semi-log

Figure 2. (a) H/D exchange products of Gly_3H^+ with D_2O ($1.0x10^{-7}$ Torr) after 1 second. (b) Continuous ejection of the d_1 (m/z=191) species during the reaction inhibits formation of higher mass exchange products. D_2O partakes in primarily single, sequential exchanges.

a)

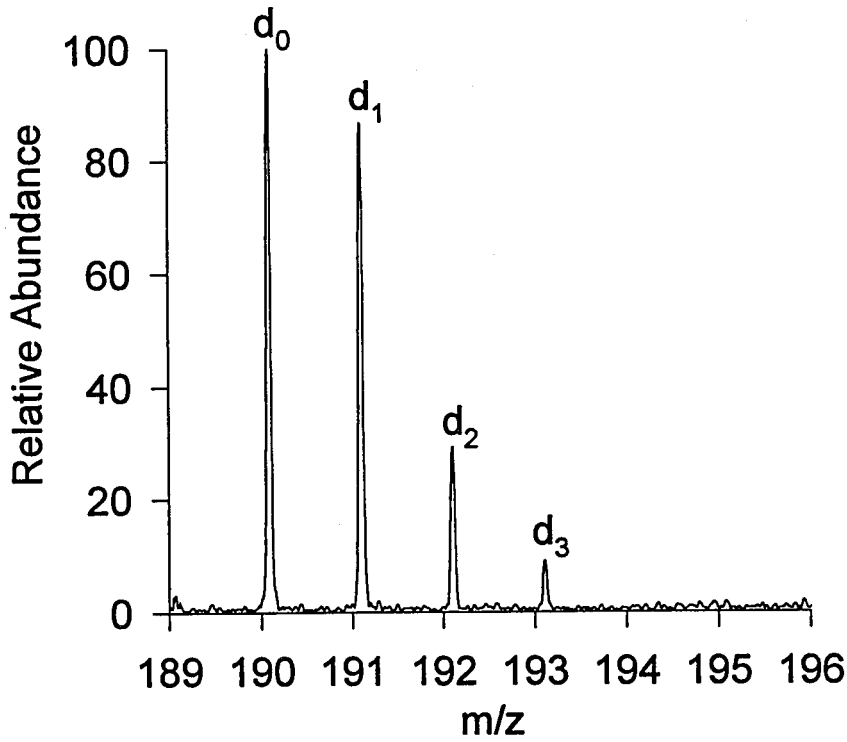
d0
d1
d2
d3
100
80
60
40
20
0
Relative Abundance
189 190 191 192 193 194 195 196
m/z

b)

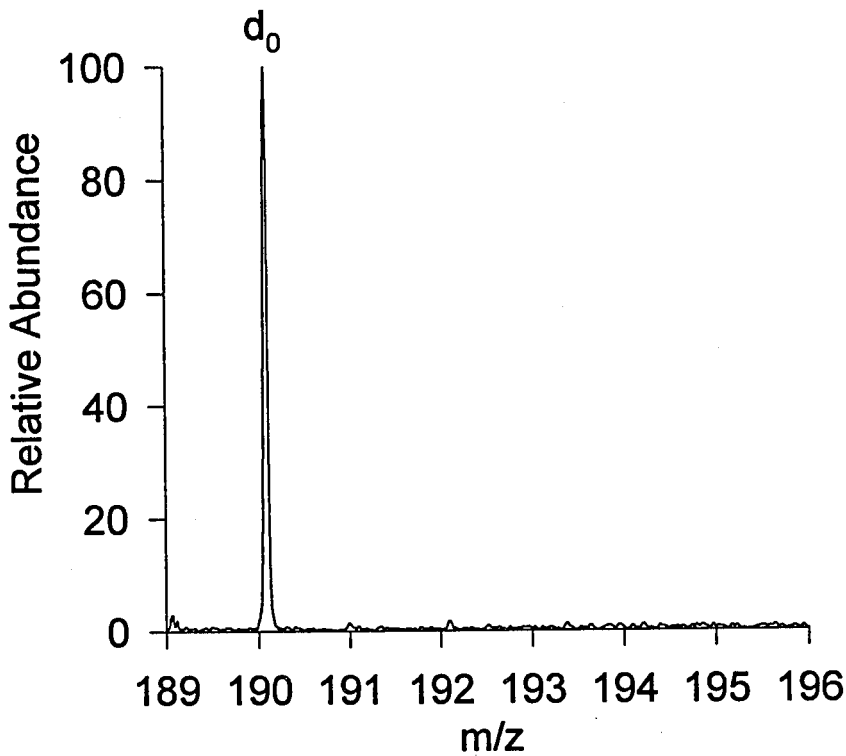
d0
100
80
60
40
20
0
Relative Abundance
189 190 191 192 193 194 195 196
m/z

Figure 2

plot of ion abundance versus reaction time. Data for Gly_nH^+ (n=1-5) are shown in Figure 3. The reaction rate constants for the first exchanges are $1.8x10^{-11}$, $3.7x10^{-10}$, $2.5x10^{-10}$, $1.5x10^{-11}$, and $2.0x10^{-11}$ $cm^3molecule^{-1}sec^{-1}$, for Gly_1H^+ to Gly_5H^+, respectively, taken from limiting slopes for the disappearance of the reactant ion in Figure 3. These results are summarized in Table 1. The curvature of the plots at short times suggests a translationally or vibrationally hot population which reacts slower than thermalized ions.[36] The long time behavior for each plot should approach that of a thermal distribution. There are no indications of an unreactive population in any of the systems, which might suggest that only species with excess energy react.

To determine the reaction rate constants for subsequent sequential exchanges, the data can be fit using mathematical modeling. For n exchangeable hydrogens, a series of n+1 coupled first order differential equations is solved numerically to yield n+1 curves describing the time dependent behavior of the different deuterated species. Rate constants which give a best fit to the experimental data are summarized in Table 1. The equations can be modified to account for reverse reactions which regenerate lower mass hydrogenated peptides if the concentration of HOD is found to be significant in the background gas. Results from calculations which include this correction do not vary significantly from the simpler model, since the isotopic impurities do not typically exceed 5-10 atom %.

As an alternate method, the k_2 and k_3 rate constants of Gly_2H^+ and Gly_3H^+ can be estimated from the exchange time plots in Figure 1b and 1c. The peak in the curve for the d_1 species occurs at a reaction time where product formation and depletion rates

Figure 3. Semi-log plots of ion abundance versus reaction time for Gly_nH^+ with D_2O ($1.0x10^{-7}$ Torr). Reaction rate constants for the first exchange are extracted from the limiting slope of each plot. H/D exchange of Gly_2 and Gly_3 is an order of magnitude faster than that of Gly_1, Gly_4, and Gly_5. Curvature in the slopes at short delays indicates a vibrationally and translationally hot population with decreased reactivity, which cools after approximately 500 ms.

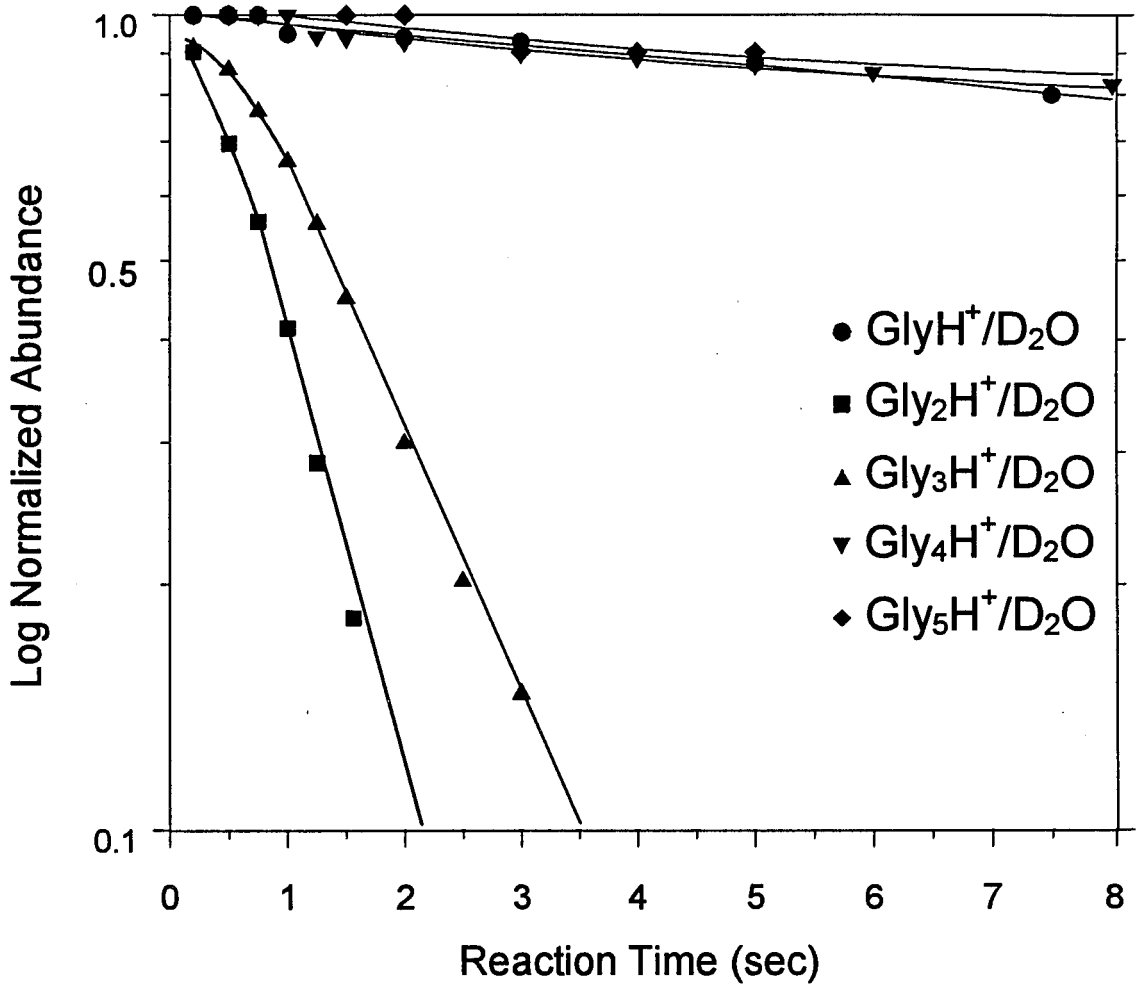
1.0
0.5
0.1
Log Normalized Abundance
0
1
2
3
4
5
6
7
8
Reaction Time (sec)
GlyH+/D2O
Gly2H+/D2O
Gly3H+/D2O
Gly4H+/D2O
Gly5H+/D2O

Figure 3

Table 1: H/D exchange rates for glycine oligomers with reagent gases using a sequential model for deuterium incorporation (rates x10^{10} cm^3/s)

Gas	Gly_n	ADO rate	Number of Observed Deuterium Exchanges							
			D1[a]	D2	D3	D4	D5	D6	D7	D8
D_2O	β–ine	17.2	0.01	-	-	-	-	-	-	-
	1	17.9	0.09 (0.18)	*	*	*	-	-	-	-
	2	17.0	3.1 (3.7)	5.2	3.6	0.47	0.07	-	-	-
	3	16.7	1.8 (2.5)	1.4	1.2	0.47	0.12	*	-	-
	3-Me	16.7	1.6	1.2	1.1	0.36	0.07	-	-	-
	4	16.5	0.05 (0.15)	*	*	*	*	*	*	-
	4-Me	16.5	0.04	*	*	*	*	*	-	-
	5	16.4	0.02 (0.20)	*	*	*	*	*	*	*
MeOD	β-ine	14.7	1.0	-	-	-	-	-	-	-
	1	15.6	1.9 (2.7)	0.78	0.55	0.25	-	-	-	-
	2	14.5	5.0 (6.1)	8.8	5.6	1.7	0.78	-	-	-
	3	14.0	4.3 (4.6)	4.6	3.4	1.2	0.32	0.16	-	-
	3-Me	14.0	2.1	2.3	1.6	0.49	0.13	-	-	-
	4	13.8	0.23 (0.48)	0.21	*	*	*	*	*	-
	4-Me	13.8	0.02	0.04	*	*	*	*	-	-
	5	13.6	0.01 (0.03)	*	*	*	*	*	*	*
AcOD	β-ine	12.9	2.5	-	-	-	-	-	-	-
	1	14.1	4.5	1.5	1.1	0.53	-	-	-	-
	2	12.7	10.2 (11.8)	8.8	5.6	1.9	0.72	-	-	-
	3	12.0	7.4	5.2	4.0	2.0	0.78	0.34	-	-
	4	11.7	1.4 (4.5)	0.43	0.40	0.39	*	*	*	-
	5	11.4	3.5 (5.3)	0.35	0.36	0.40	*	*	*	*
ND_3	β-ine	13.8	2.1	-	-	-	-	-	-	-
	1	14.3	2.7 (3.4)	5.5	3.6	1.1	-	-	-	-
	2	13.7	5.4 (7.4)	8.1	5.0	2.1	0.39	-	-	-
	3	13.4	8.9 (10.3)	14.1	11.9	7.2	2.8	0.47	-	-
	4	13.2	12.3 (14.2)	21.1	13.0	6.5	1.7	0.76	0.62	-
	5	13.1	14.2 (14.5)	21.8	14.7	8.9	3.3	1.3	0.57	0.64

[a]Rate constant in parentheses is determined from the limiting slope of a semi-log plot of ion abundance versus reaction time. *Exchange possible but not observed. -Exchange not expected.

are equal, which happens when Equation 1 is satisfied. This yields k_2 values for Gly_2H^+ and Gly_3H^+ of $5.8x10^{-10}$ and $1.5x10^{-10}$ $cm^3molecule^{-1}sec^{-1}$, respectively, as compared with the values of $5.2x10^{-10}$ and $1.4x10^{-10}$ $cm^3molecule^{-1}sec^{-1}$ in Table 1. The k_3 rate constants can be estimated in a similar manner from the ion abundances at the maximum in the yield of d_2, equation 2. This gives k_3 values for Gly_2H^+ and Gly_3H^+ of $3.9x10^{-10}$ and $1.3x10^{-10}$ $cm^3molecule^{-1}sec^{-1}$, respectively, compared with best fit values of $3.6x10^{-10}$ and $1.2x10^{-10}$ $cm^3molecule^{-1}sec^{-1}$ from Table 1. It is interesting to note that the data for Gly_2H^+ in Figure 1b indicate that k_2 is faster than k_1.

$$k_2 = k_1 \frac{[d_0]}{[d_1]} \qquad (1)$$

$$k_3 = k_2 \frac{[d_1]}{[d_2]} \qquad (2)$$

The calculated ADO reaction rates[37] for each species are included for comparison to the experimental values in Table 1. The species which undergo only a single exchange with D_2O [$GlyH^+$, Gly_4H^+, $(Gly_4\text{-}OMe)H^+$, and Gly_5H^+] all possess similar rate constants in the range of 10^{-11} to 10^{-12} $cm^3molecule^{-1}sec^{-1}$, much slower than the ADO collision limit. Gly_2H^+, Gly_3H^+, and $(Gly_3\text{-}OMe)H^+$ display similar reactivity with three moderately fast exchanges of 10^{-10} $cm^3molecule^{-1}sec^{-1}$, and two slower reactions.

Conceptually it is easy to think that the initial H/D exchange occurs at the most reactive site. In fact, even though some sites have a higher probability of exchange in the first event, the "first" exchange does not necessarily have to occur at any one specific site in the molecule. Since these molecules possess several labile hydrogens, the MH^+-d_1 species is most likely comprised of a distribution of species labeled with deuterium at different sites. The calculated k_1 rate constant more realistically represents the sum of the rate constants for each individual d_1 species and gives the total rate for reaction at all sites. It is therefore important not to over interpret the rates obtained for sequential processes.

Reactions with CD_3OD. With a proton affinity of 181.9 kcal/mol,[28] CD_3OD is 15.4 kcal/mol more basic than D_2O. The differences in proton affinities between CD_3OD and the glycine oligomers range from 29.7 kcal/mol for Gly_1 to 49.9 kcal/mol for Gly_5.[24] With few exceptions, CD_3OD and D_2O display very similar reactivities towards the glycine oligomers. The small oligomers of Gly_2H^+, Gly_3H^+, and $(Gly_3\text{-}OMe)H^+$ are observed to exchange all of their labile hydrogens with CD_3OD. The oligomers larger than Gly_3 exchange at most two labile sites during the 20 second time period, displaying the same distinctive change in reactivity observed for larger molecules with D_2O.

The two main differences between CD_3OD and D_2O are the observed rates of the reactions and the reactivity of Gly_1H^+ with the reagents. Since CD_3OD can only participate in a single deuterium exchange per reactive encounter, the reaction rate constants for the glycine oligomers with CD_3OD are calculated using the sequential

incorporation model discussed above. For Gly_2H^+, Gly_3H^+, and $(Gly_3\text{-}OMe)H^+$, the H/D exchanges with CD_3OD are roughly 1.5 times faster than with D_2O, and the exchange rate for Gly_4H^+ is nearly five times faster with CD_3OD (Table 1). $(Gly_4\text{-}OMe)H^+$ and Gly_5H^+ are still virtually unreactive with the reagent gas, displaying exchange rates of $1\text{-}2x10^{-12}$ $cm^3molecule^{-1}sec^{-1}$. The trends in the reactivity of CD_3OD with the glycine oligomers demonstrate an upper limit to the difference in proton affinities of 50 kcal/mol, which is lower than the 61 kcal/mol limit for D_2O.

The reactivity of Gly_1H^+ displays the biggest difference between the two exchange gases. Where D_2O is able to slowly exchange only one site on Gly_1H^+, CD_3OD is observed to exchange all four labile hydrogens on the molecule. The results for Gly_1H^+ in Table 1 are consistent with those of Gard *et al.*,[22] but are roughly twice as fast as their reported values. This difference could be attributed to the difficulty in accurately measuring gas pressures in the ICR cell. Our experiments utilize a Schulz-Phelps ionization gauge which is an integral component of the ICR cell, calibrated against a capacitance manometer. Gard *et al.* use an externally located ion gauge and adjust their rate constants for back reactions with CH_3OH impurities (up to 30%), during the exchange experiments.

Reactions with CD_3CO_2D. CD_3CO_2D is more efficient at promoting H/D exchange of the glycine oligomers. It has a higher proton affinity (190.2 kcal/mol)[28] compared to the reagents of D_2O and CD_3OD, and demonstrates a smaller difference in proton affinities with the oligomers (21.4 for Gly_1 to 41.6 kcal/mol for Gly_5). CD_3CO_2D is somewhat more reactive with the small oligomers of $n\leq3$ than CD_3OD,

since it is observed to exchange all the labile hydrogens of these oligomers during the 20 second reaction period (Table 1). The larger oligomers of Gly_4H^+ and Gly_5H^+ exchange several, but not all, of their labile hydrogens with CD_3CO_2D. As with the results of the two previous reagents, H/D exchange rates decrease with increasing proton affinity of the glycine oligomer. The overall rates of exchange are faster for CD_3CO_2D than for D_2O and CD_3OD, with the trend in rates following the proton affinity ordering, $D_2O<CD_3OD<CD_3CO_2D$.

Reactions with ND_3. ND_3 is the most basic exchange reagent used in this study. With a proton affinity of 204 kcal/mol,[28] ND_3 demonstrates the smallest differences in proton affinities with the glycine oligomers (ranging from 7.6 kcal/mol with Gly_1 to 27.8 kcal/mol with Gly_5). ND_3 is the most efficient reagent studied for promoting H/D exchange of the glycine oligomers, as it exchanges every labile hydrogen site in each of the oligomers. In the small oligomers, the exchange rates are fast enough to achieve complete deuterium incorporation during a seven second reaction period. A time plot for the H/D exchange of Gly_3H^+ (containing six labile hydrogens) with ND_3 is shown in Figure 4a. It is apparent that the ND_3 reagent gas contains small amounts of NHD_2 impurities, since an equilibrium distribution of incomplete exchange products is approached at long delay times. Analysis of the isotopic product distribution indicates the atom % deuterium in this system is 90%. The larger oligomers (n>3) display similar reactivity with ND_3, exchanging every labile site, but cannot complete the numerous exchanges on the molecule within the time frame of the experiments. Gly_4H^+ is observed to undergo seven exchanges during the

Figure 4. Time plots of the H/D exchange products of Gly_nH^+ with ND_3 ($1.5x10^{-7}$ Torr). (a) Gly_3H^+ exchanges all 6 labile hydrogens rapidly. An equilibrium distribution of species is observed after 3-4 seconds due to a small presence of hydrogen impurities in the exchange gas (10 atom % hydrogen). (b) Gly_4H^+ exchanges all 7 labile hydrogens rapidly, but reaches an equilibrium distribution in which d_5 is the most abundant species. The number of deuterium atoms incorporated into each species is indicated as d_n.

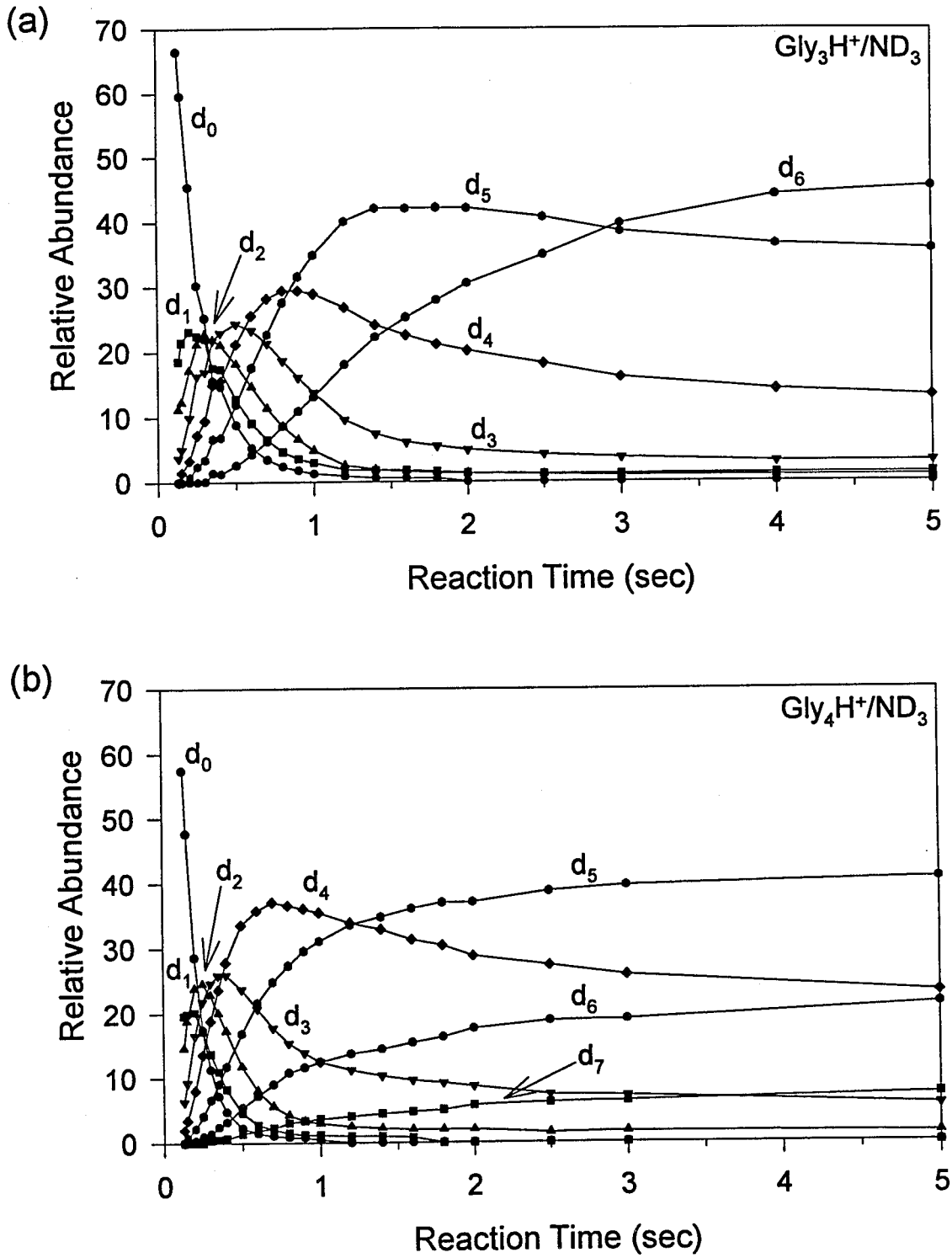
(a)
Gly3H+/ND3
Relative Abundance
Reaction Time (sec)
d0
d1
d2
d3
d4
d5
d6
(b)
Gly4H+/ND3
Relative Abundance
Reaction Time (sec)
d0
d1
d2
d3
d4
d5
d6
d7

Figure 4

seven seconds of reaction with ND_3, but the reaction time plot in Figure 4b clearly demonstrates that the species with five deuteriums incorporated is the dominant species at this detection time.

ND_3 and D_2O are the only two reagent gases studied which have the potential to participate in multiple deuterium exchanges. Experiments were also performed to explore the possibility of multiple exchanges for ND_3 in a single collision event. Figure 5a shows the results of reacting Gly_3H^+ with ND_3 for 1 second. The ND_3 pressure in this experiment was reduced from that in Figure 4a to observe a wider range of species at the 1 second detection time. Five deuteriums are incorporated into the oligomer during this time period. If the d_1 species (m/z=191, resulting from one exchange) is continuously ejected during the reaction, the yield of higher mass ions is diminished but not inhibited (Figure 5b). Comparing the product ion intensities of the two spectra indicates that ND_3 partakes in multiple exchanges during a single collision event 22% of the time. Similar experiments with Gly_2H^+ indicated that multiple exchanges occur 28% of the time.

Semi-log plots of the H/D exchange data for Gly_nH^+ (n=1-5) reacting with ND_3 are shown in Figure 6. Disappearance rate constants are $3.4x10^{-10}$, $7.4x10^{-10}$, $1.0x10^{-9}$, $1.4x10^{-9}$, and $1.4x10^{-9}$ $cm^3molecule^{-1}sec^{-1}$, for Gly_1H^+ to Gly_5H^+, respectively. As with the results for D_2O, these calculated "first" rate constants give the total rate for reaction at all labile sites in the molecule. Additionally, since ND_3 partakes in multiple exchanges, these rate constants include contributions from processes which produce the MH^+-d_1, -d_2, and -d_3 species.

Figure 5. (a) H/D exchange products of Gly_3H^+ with ND_3 ($5.0x10^{-8}$ Torr) after 1 second. (b) Continuous ejection of the d_1 (m/z=191) species during the reaction diminishes the amount of higher mass exchange products, but does not inhibit their formation. ND_3 partakes in multiple exchanges during a single collision event with Gly_3H^+ 22% of the time.

a)

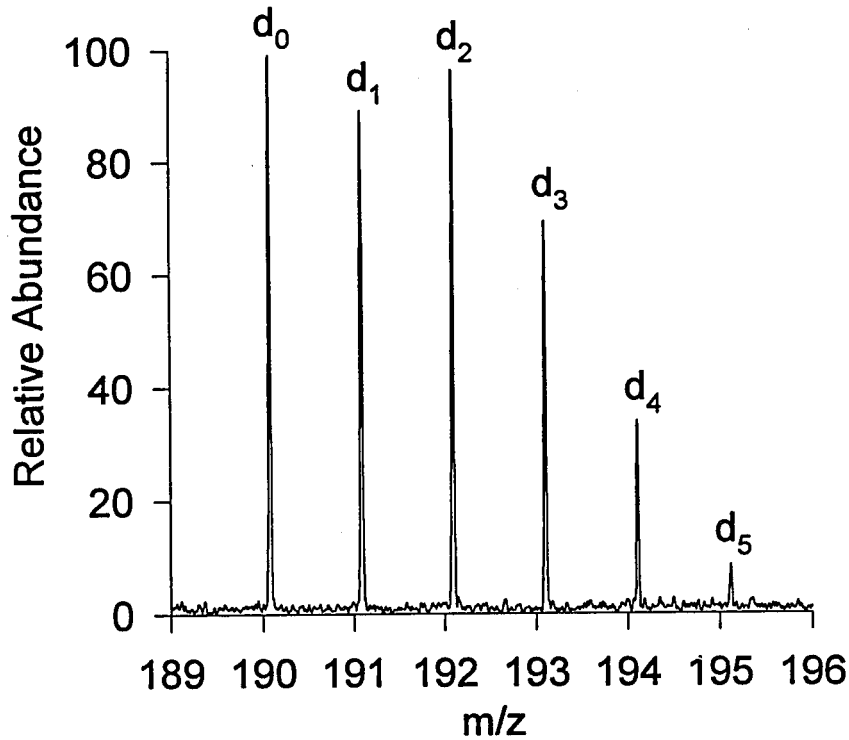
d0
d1
d2
d3
d4
d5
100
80
60
40
20
0
Relative Abundance
189 190 191 192 193 194 195 196
m/z

b)

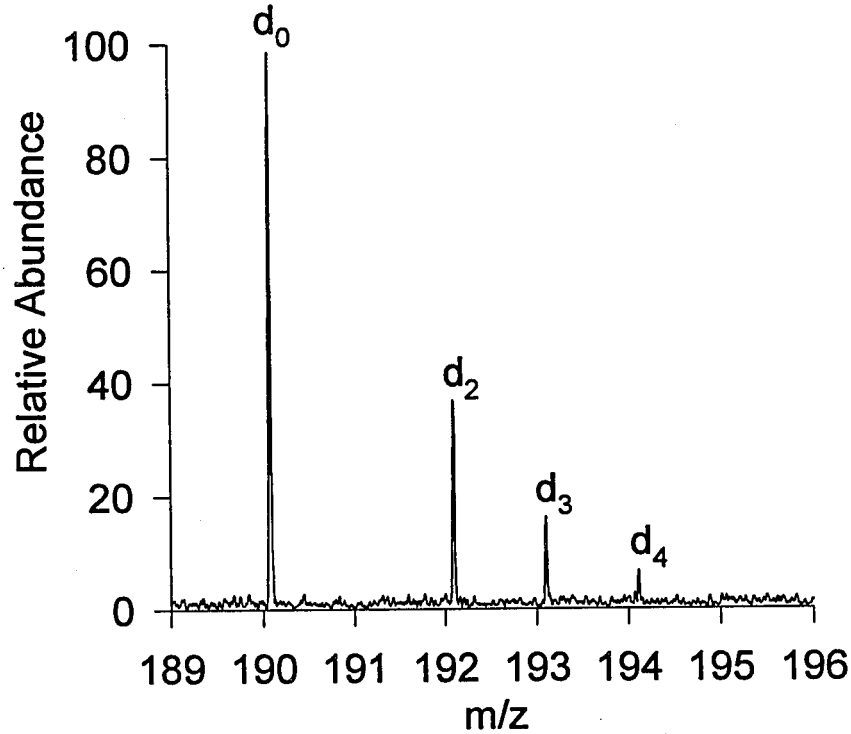
d0
d2
d3
d4
100
80
60
40
20
0
Relative Abundance
189 190 191 192 193 194 195 196
m/z

Figure 5

Figure 6. Semi-log plots of ion abundance versus reaction time for Gly_nH^+ with ND_3. Reaction rate constants for the first exchange are extracted from the limiting slope of each plot. H/D exchange rates increase with oligomer length. Curvature in the Gly_1H^+ slope at short delays indicates a vibrationally and translationally hot population with decreased reactivity, which rapidly cools.

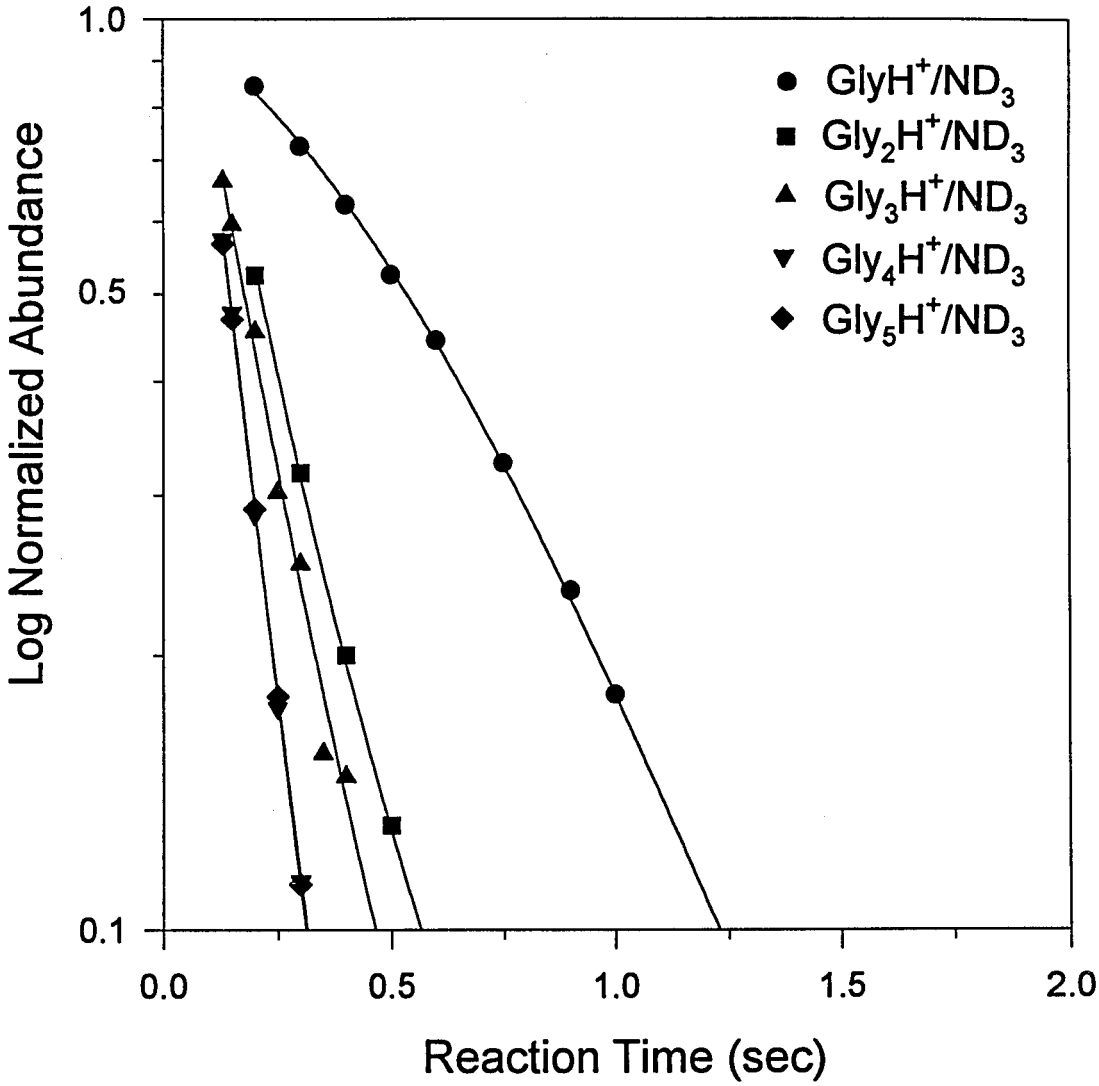
1.0
0.5
0.1
Log Normalized Abundance
0.0
0.5
1.0
1.5
2.0
Reaction Time (sec)
GlyH+/ND3
Gly2H+/ND3
Gly3H+/ND3
Gly4H+/ND3
Gly5H+/ND3

Figure 6

Determination of the subsequent reaction rate constants for the glycine oligomers with ND_3 is more difficult than for D_2O, CD_3OD, and CD_3CO_2D. A model using only sequential incorporation of deuterium (such as that for D_2O) neglects the contributions of roughly a quarter of the reactions which proceed by multiple exchanges. As a result, rate constants calculated from a sequential model will be in error. A product which incorporates three deuteriums will require three exchanges during the specified reaction period using the sequential model, yet more realistically may be formed by multiple exchanges in a smaller number of reaction events. The calculated H/D exchange rate constants for the glycine oligomers with ND_3 using a simple sequential model are listed in Table 1. Although careful selective ion ejection experiments can yield more information, the kinetic data themselves are insufficient to extract all of the rate constants in this system. Only the "first" exchange rate of Gly_nH^+ can be determined with any accuracy from semi-log plots of the experimental data, with the rate reflecting reactions by single and multiple exchange processes.

Off-resonance excitation during H/D exchange. It is of interest to investigate the effects of increased translational and vibrational energy on the rates and extent of H/D exchange. This is of particular interest in systems where exchange is slow or not observed. Off-resonance excitation[34] was used to collisionally activate several oligomers during H/D exchange with D_2O and CD_3CO_2D reagent gases. In the off-resonance excitation experiments, rf excitation is applied at a frequency slightly different from the cyclotron frequency of the ion to be translationally excited. This

causes the ion energy to oscillate with time, with an average given by Equation 3, where q is the charge of the ion, E_o is the amplitude of the applied electric field, and

$$\left\langle E_{ion,cm} \right\rangle = \frac{m_{gas}}{m_{gas} + m_{ion}} \left[\frac{q^2 E_o^{\,2}}{4 m_{ion} (\omega - \omega_c)^2} \right] \qquad (3)$$

$(\omega-\omega_c)$ is the difference between the applied excitation frequency and natural cyclotron frequency of the ion. For all examples in this article, excitation was applied on the high frequency or low mass side of the ion to avoid exciting higher mass exchange products whose cyclotron frequencies are further off resonance. Vibrational excitation of the ions results from sequential multiple collisions (at elevated translational energies) with appropriate gases. D_2O and CD_3CO_2D serve both as exchange and collision gases. The conversion of translational energy into vibrational energy in low energy collisions is predicted to be very efficient for molecules of this size.[38] Excitation levels were adjusted to maximize translational and vibrational excitation, while promoting a minimum amount of collisional dissociation.

The results for Gly_4H^+ reacting with CD_3CO_2D are shown in Figure 7. Exchange reactions were monitored over a period of seconds with and without activation at an average center of mass collision energy of 0.18 eV. During the first 1.5 seconds of the reaction, the H/D exchange rates are slower with off-resonance excitation applied. A decrease in the reaction rate constant with increasing translational energy is often characteristic of exothermic ion-molecule reactions. When Gly_3H^+ is

Figure 7. H/D exchange of Gly_4H^+ with CD_3CO_2D ($7.6x10^{-8}$ Torr), with and without off-resonance collisional activation. Translational and vibrational excitation leads to a lower rate of exchange for the excited species (d_0*). Species labeled as d_n* are exchange products of excited Gly_4H^+.

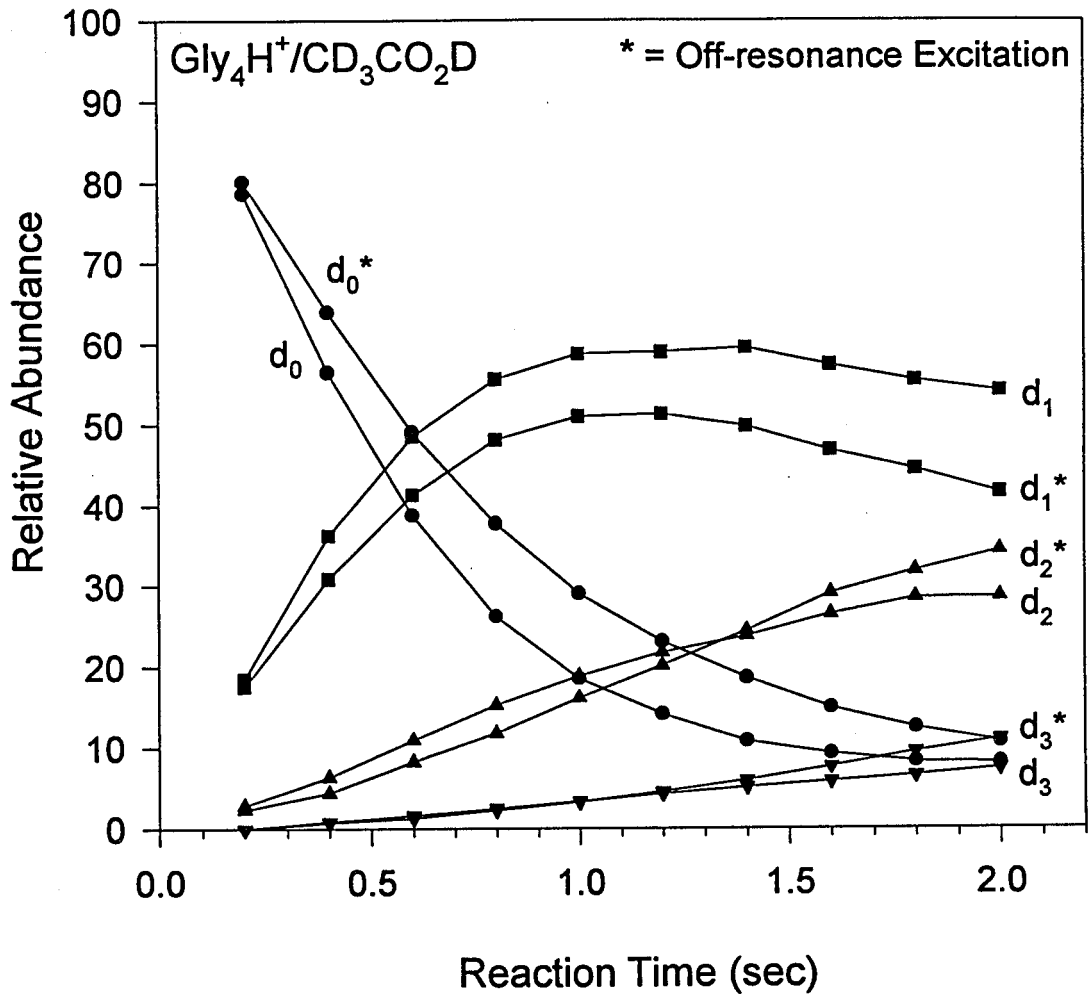
Gly4H+/CD3CO2D
* = Off-resonance Excitation
Relative Abundance
Reaction Time (sec)
d0*
d0
d1
d1*
d2*
d2
d3*
d3
100
90
80
70
60
50
40
30
20
10
0
0.0
0.5
1.0
1.5
2.0

Figure 7

translationally and vibrationally excited using D_2O, the H/D exchange rates also appear to decrease slightly. Under thermal conditions, Gly_4H^+ only undergoes one slow exchange with D_2O (Figure 1d). Collisional activation of Gly_4H^+ does not enhance reactivity. In fact, high excitation levels caused extensive collisional dissociation during the reaction period. The excitation causes no noticeable effect on the rate or extent of H/D exchange in Gly_4H^+.

Discussion

Several recent studies report a correlation between the extent of H/D exchange observed for a molecule and the absolute difference in proton affinities between the molecule and the exchange reagent.[14,22,23] Some researchers have reported that H/D exchange cannot occur between species which differ by more than 20 kcal/mol,[14] while others have observed exchange between species which differ by more than 50 kcal/mol.[23]

Isotopic hydrogen exchange processes are generally initiated by the formation of a strong hydrogen bond between the reactant ion (designated B_1H^+, assuming a protonated species) and the neutral exchange reagent (designated B_2). The energetics of this process can be discussed with reference to the potential energy surface in Figure 8, in which the variation in energy with proton position is shown for several values of the B_1-B_2 separation (determined by the internuclear spacing of the sites of protonation). Figure 8 is adapted from *ab initio* calculations for the system $NH_4^+\cdots OH_2$.[39] At large separations, the well depths approach the limiting values

Figure 8. Potential energy surfaces for proton motion between B_1 and B_2 for several values of the separation of the basic sites in B_1 and B_2. At large separations, curve 1, the surface approximates that of the isolated systems, and the difference in well depths is approximately equal to the difference in proton affinities $\Delta D_0(B\text{-}H^+)$. As the reactants approach, the barrier to proton transfer is reduced (curve 2) and the total energy of the system is lowered. At equilibrium (curve 3), the energy decrease equals the hydrogen bond energy $D_0(B_1H^+\text{-}B_2)$.

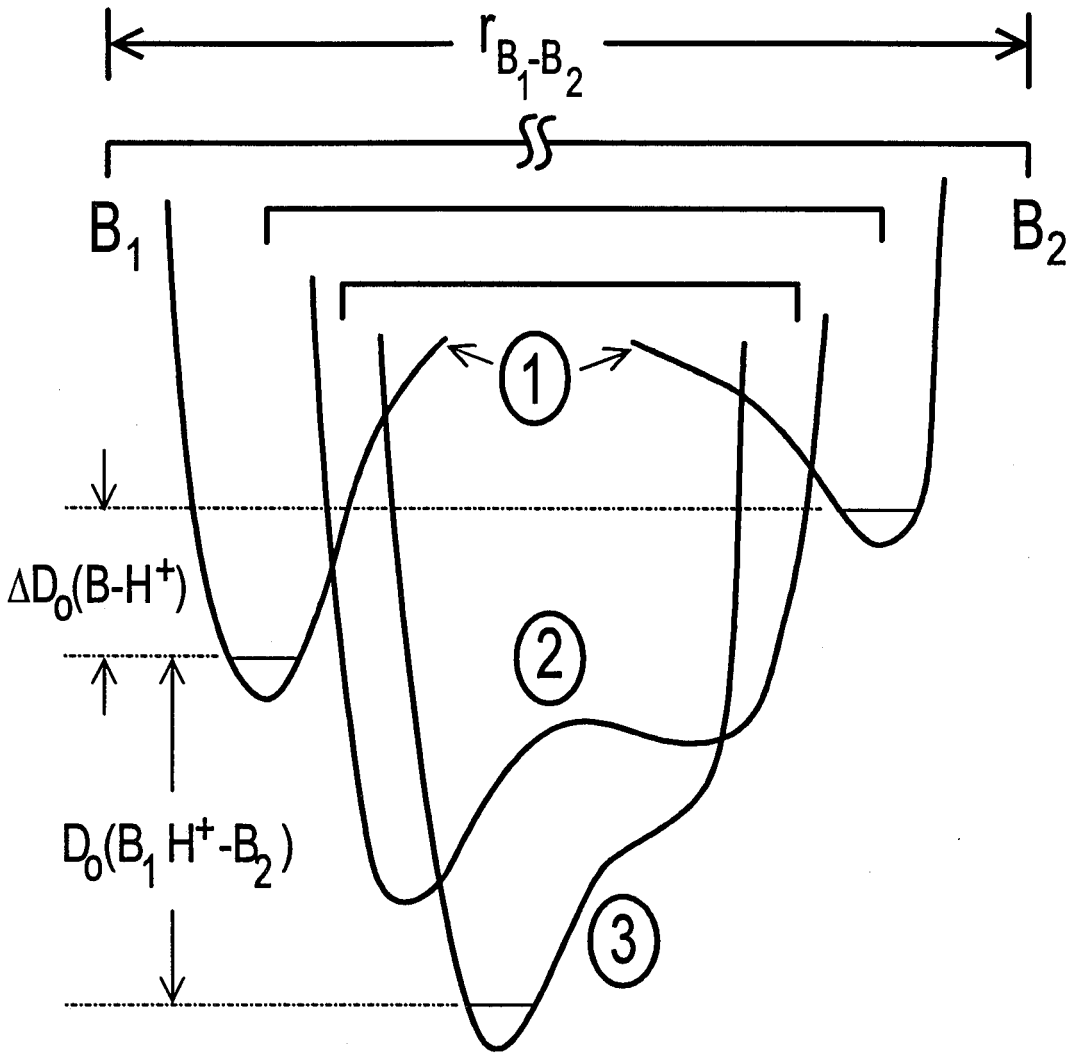

Figure 8

associated with the proton affinities of the isolated bases. As the separation decreases, the total energy of the system decreases to reflect the strength of the hydrogen bond, $DH^{\circ}_{298}[B_1H^+\text{-}B_2]$. Depending on B_1 and B_2 the potential surface may exhibit either single or double minima. If the energy released by formation of a strong hydrogen bond is sufficient to allow the proton motion to sample regions of the potential energy surface in which it approaches within normal bonding distance to B_2, then it is highly probable that this motion can couple with other degrees of freedom and result in facile isotopic hydrogen exchange. Meot-Ner has investigated a large series of complexes in an attempt to quantitate the strengths of typical strong hydrogen bonds.[18] Equations 4 and 5 can be used to determine the hydrogen bond strengths in a dimer containing a protonated amine and an oxygen or nitrogen donor base, respectively, where ΔPA is

$$NH^+\cdots O \qquad DH^{\circ}_{298}[NH^+\text{-}O]=28.3\text{-}0.23\Delta PA \qquad (4)$$

$$NH^+\cdots N \qquad DH^{\circ}_{298}[NH^+\text{-}N]=23.2\text{-}0.25\Delta PA \qquad (5)$$

the difference in proton affinities of B_1 and B_2. If we consider only basic sites involving the heteroatoms N and O and avoid systems where steric effects constrain the approach of the two basic centers, then it is reasonable to assume that the barrier to proton transfer will be either small or non-existent (Figure 8). We can then take the differences in proton affinities of the two bases as an upper limit to the hydrogen bond strength required to permit facile isotopic hydrogen exchange (i.e.,

$DH^{o}_{298}[B_1H^+-B_2]=\Delta PA$). Equations 4 and 5 indicate that this occurs at proton affinity differences of 23 and 19 kcal/mol, respectively, for oxygen and nitrogen bases. These considerations are consistent with the observations that H/D exchange is often not observed between simple species whose proton affinity difference exceeds approximately 20 kcal/mol. In applying it to the present study, this simple mechanistic picture can be used to explain the H/D exchange of species like ND_3 with Gly_1H^+ or Gly_2H^+, whose proton affinity differences are less than 20 kcal/mol, and where folding does not lead to significant stabilization from intramolecular hydrogen bonding in B_1H^+. Unfortunately, the difference in proton affinities between most of the peptides and reagent gases is larger than 20 kcal/mol and this picture does not suffice to explain most of our observations.

Our experimental results for the protonated glycine oligomers indicate H/D exchange can occur between molecules with large differences in proton affinities. D_2O, with a proton affinity of 166.5 kcal/mol, undergoes facile H/D exchange with Gly_3H^+ (PA=223.1 kcal/mol) but is unreactive towards Gly_4H^+ (PA=227.2). This places the upper limit to reactivity between 57 and 61 kcal/mol. Using the same analysis for CD_3OD (PA=181.9) reacting with Gly_4H^+ and Gly_5H^+ (PA=231.8 kcal/mol), the upper limit changes to 45-50 kcal/mol. Additionally, Gly_2H^+ (PA=219.1 kcal/mol) reacts with D_2O, whereas Gly_1H^+ (PA=211.6 kcal/mol) is mostly unreactive. It is clear from these results that the propensity of a specific system to exhibit isotopic hydrogen exchange is dependent on factors other than differences in proton affinities.

To understand the present results, it is useful to have some notion of the potential energy surfaces for H/D exchange with these supposedly "simple" model systems. High quality *ab initio* calculations are not feasible for systems as large as these, however. For this reason, we resort to the use of AM1 and PM3 semiempirical calculations to provide a semi-quantitative assessment of the energetics of postulated reaction intermediates and to construct reaction coordinate diagrams for different proposed mechanisms.

Semiempirical calculations. Semiempirical calculations were performed using Hyperchem[35] computational software to obtain model structures and energetics for the protonated glycine oligomers and reagent exchange gases. The calculations were performed using both the AM1 and the PM3 methods. The proton affinities are found from the calculated heats of formation of the geometry optimized neutral and protonated molecules. Dewar and co-workers[30] have provided a comprehensive comparison of calculated and experimental heats of formations for both neutrals and ions using the AM1 method. The PM3 method has similarly been evaluated.[31] Using the AM1 method, errors in the calculated heats of formation of protonated species are comparable with those in the neutral precursors. With the PM3 method, the average difference between the predicted heats of formation and experimental values for 657 compounds was 7.8 kcal/mol, and for 106 hypervalent compounds, 13.6 kcal/mol. The PM3 method differs from the AM1 method only in the values of the parameters. In the critical area of modeling the strengths and energies of hydrogen bonds, the PM3 method is preferred. Numerous investigations conclude that AM1 geometries are in

poor agreement with *ab initio* calculations, whereas PM3 gives geometries similar to *ab initio* structural results.[40] The main limitations in the PM3 method are the underestimation of hydrogen bond lengths by 0.1-0.2 Å for some systems and the underestimation of reliable experimental hydrogen bond strengths by approximately 1-2 kcal/mol.[40]

Table 2 summarizes the calculated and experimental thermochemical properties for the glycine oligomers considered in the present study. While agreement in most instances is fairly good, there are some obvious problems. Most importantly, the predicted proton affinity of glycine is 200.1 and 200.6 kcal/mol by the AM1 and PM3 methods, respectively, compared to the experimental value of 211.6 kcal/mol.[24] Calculations for ammonia indicate the error is in the opposite direction with predicted values of 207.9 and 209.2 kcal/mol with AM1 and PM3 methods, respectively, being higher than the experimental value of 204.0 kcal/mol. Hence proton transfer from NH_4^+ to glycine is predicted to be endothermic by approximately 8 kcal/mol when it is exothermic by nearly the same amount. ICR experiments which probe the reverse reaction give no evidence for proton transfer from Gly_1H^+ to NH_3.[26]

As a starting point for considering the mechanism of exchange, structures were calculated for the protonated glycine oligomers. In all cases the proton is preferentially bound to the N-terminus and the peptide folds up to solvate the charge site, mainly by forming hydrogen bonds to carbonyl oxygens. The starting point for each structure involves a β-sheet configuration. For Gly_nH^+ (n=2-4) in the folded form, the N-terminus glycine prefers a cis amide bond in the most stable structure. With Gly_5H^+,

Table 2: Calculated and experimental proton affinities[a] for the glycine oligomers.

Species	PA (calculated)				ΔPA (folded-open)		PA (experimental)		
Gly_n Oligomer	AM1		PM3		AM1	PM3	Fenselau[b]	Lebrilla[c]	Cassady[d]
	folded	open	folded	open					
Gly_1	-	200.1	-	200.5	-	-	211.6	210.1	208.3
Gly_2	210.6	205.1	209.4	206.0	5.15	3.4	219.1	218.5	217.4
Gly_3	219.8	206.6	216.3	206.5	13.2	9.8	223.1	219.8	220.6
Gly_4	227.6	207.1	222.0	208.6	20.5	13.4	227.2	219.8	226.0
Gly_5	235.8	209.0	230.1	207.0	26.8	23.1	231.8	221.7	226.3

[a]Proton affinities in kcal/mol. [b]Ref. 24. [c]Ref. 25. [d]Ref. 26. -Gly_1 does not exhibit folding.

structures with the N-terminus glycine in both the cis or trans form were of comparable stability.

Calculated proton affinities[41] of the glycine oligomers are summarized in Table 2 and compared with available experimental results.[42] The comparison is shown graphically in Figure 9. AM1 calculations are known to predict hydrogen bond strengths which are somewhat higher than experimental, whereas the PM3 method gives somewhat better agreement.[40] The results in Figure 9 suggest the same trends, with PM3 giving better results. Both the kinetic and bracketing methods of determining proton affinities have been subjected to critical analysis which will not be repeated here.[43] The lack of agreement between the experimental results from three different laboratories (shown in Figure 9) reflects some of the difficulties with these experimental methodologies. Additionally, the semi-empirical calculations do not directly take into account heat capacities of these molecules, which possess many low frequency vibrational modes, to calculate true 298 K heats of formation. With this in mind, we consider that the agreement indicated in Figure 9 is reasonable and we have selected the PM3 calculations for further considerations.

It is instructive to estimate the contribution which folding makes to the stability of the protonated glycine oligomers. Separate calculations were carried out for the protonated species in the extended β-sheet and in the compact hydrogen bonded configurations. Results of these calculations are given in Table 2. Whereas the proton affinities of the compact, hydrogen bonded oligomers display a smooth increase from Gly_1 to Gly_5, the proton affinities of the linear oligomers stay relatively constant.

Figure 9. Comparison of the experimental and calculated proton affinities of the glycine oligomers relative to Gly_1. AM1 calculations appear to overestimate the proton affinity differences between the oligomers, whereas experimental results by Lebrilla[25] appear to underestimate the differences in large oligomers. Fenselau[24] and Cassady[26] predict similar trends in proton affinities using different experimental techniques. The PM3 method gives better agreement with experimental results than does AM1.

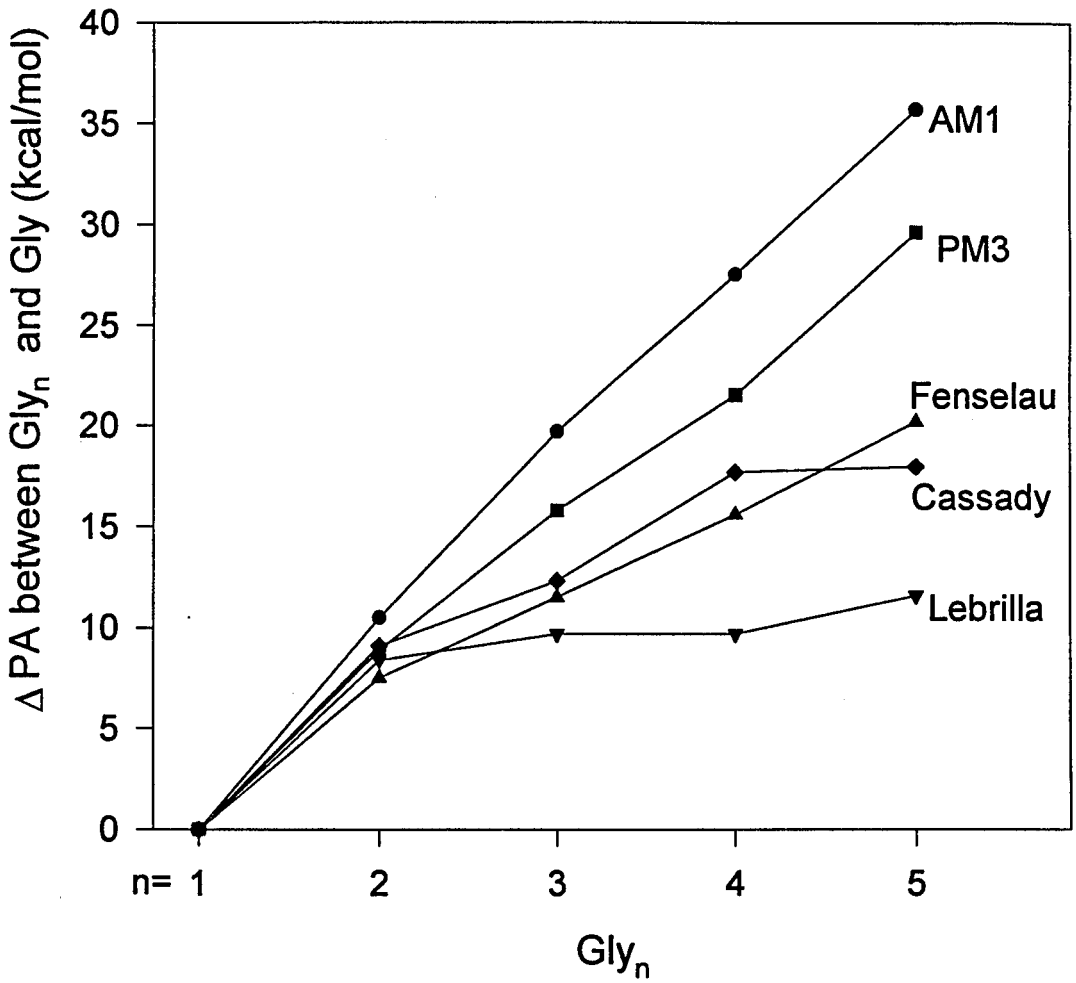
40
35
30
25
20
15
10
5
0
ΔPA between Gly$_n$ and Gly (kcal/mol)
n= 1
2
3
4
5
Gly$_n$
AM1
PM3
Fenselau
Cassady
Lebrilla

Figure 9

Figure 10 indicates that the extended form experiences a sizable increase in proton affinity only in proceeding from Gly_1 to Gly_2. The regular increase in proton affinity predicted and observed for the glycine oligomers comes mainly from the folding contribution to solvate the charge site. In the case of Gly_5, this accounts for 83% of the increase relative to glycine.

Do glycine oligomers form zwitterions (salt bridges) in the gas phase? The unusual change in reactivity observed for Gly_3H^+ and Gly_4H^+ with D_2O caused us to consider the possibility of forming zwitterions in the gas phase. Peptides are known to exist in solution in their zwitterionic forms. To form a zwitterion in the gas phase is energetically unfavorable without solvent stabilization.[44] However, the molecular structures obtained from semiempirical calculations indicated that the addition of one glycine unit to the Gly_3 polymer is enough to allow the peptide ends to interact. An intriguing possibility for the gas phase structure of Gly_4H^+ is a zwitterion in which the ionic ends can approach each other, forming a salt bridge, and allow for the resulting coulombic attraction to compensate for the nominally endothermic process of forming an isolated ion pair.[45] The labile proton would be attached to a basic amide oxygen. Such a species might be feasible for Gly_4H^+ and not Gly_3H^+.

Consider Reaction 1 for glycine, in which an isolated ion pair is formed. This is predicted by PM3 calculations to be endothermic by 141.6 kcal/mol. From gas phase proton affinity and acidity measurements, the experimental value is endothermic by 130.0 kcal/mol.[28] Most of the error in the calculated value is in the proton affinity calculation as noted above. Calculations were first performed to determine if the

Figure 10. Calculated proton affinities for linear (unfolded) and hydrogen bonded (folded) glycine oligomers using the PM3 method. Proton affinities of the unfolded molecules are relatively constant. The majority of increase in the proton affinity of the oligomers comes from folding to solvate the charge center.

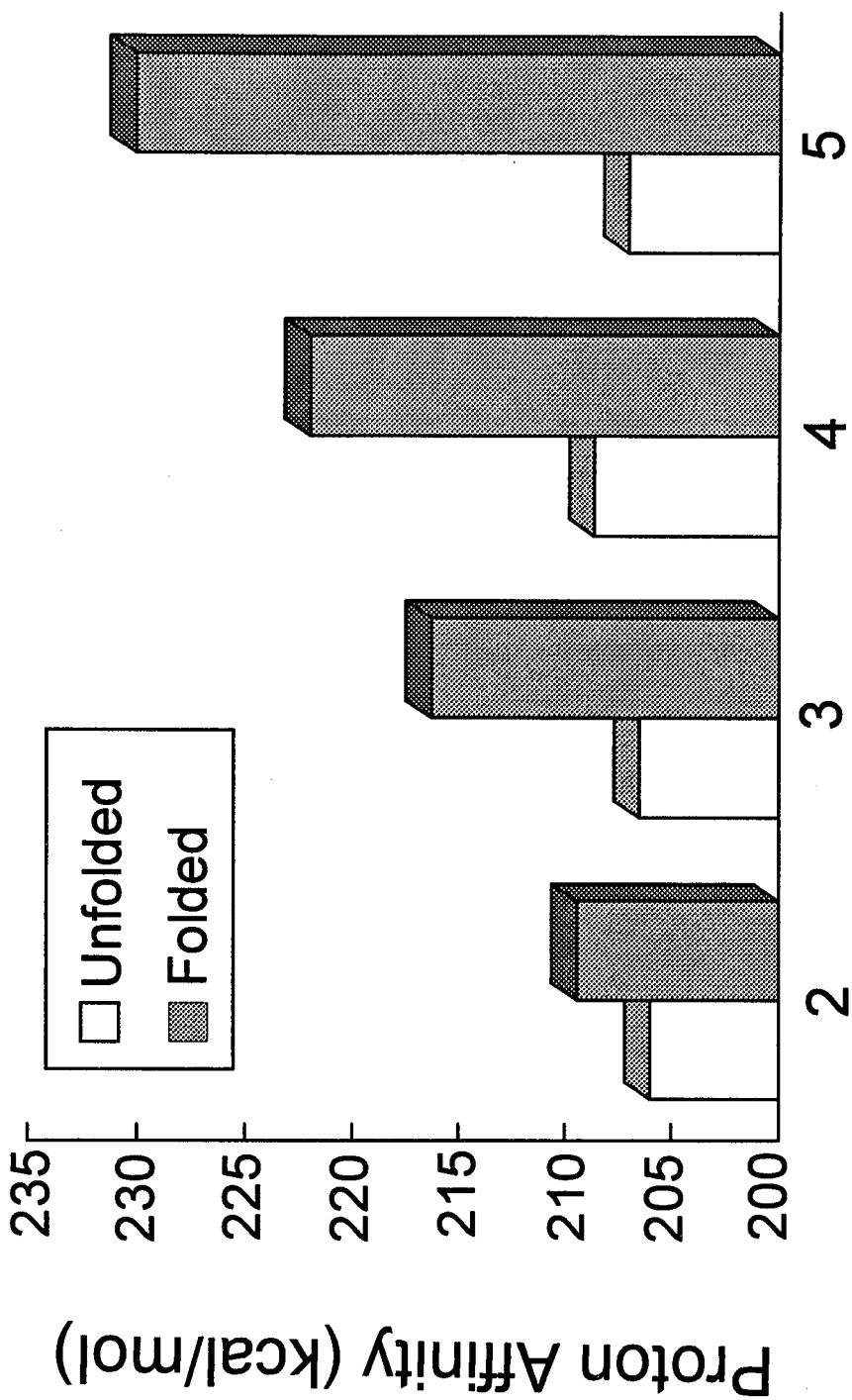
Proton Affinity (kcal/mol)
235
230
225
220
215
210
205
200
Unfolded
Folded
2
3
4
5
Gly n

Figure 10

$$2\,NH_2CH_2CO_2H \rightarrow {}^{+}NH_3CH_2CO_2H + NH_2CH_2CO_2^{-} \qquad (1)$$

longer, more flexible chain of Gly_5 neutral could possibly form a stable salt bridge in the gas phase. Structures which possessed neutral termini were always found to be lower in energy. The most stable Gly_5 zwitterion was estimated to be 20 kcal/mol less stable than the neutral β-sheet configuration.

Addition of a proton to the salt bridge form of neutral Gly_5 occurs on the amide oxygen adjacent to the C-terminus, to give the salt bridge shown in Structure **2**. PM3 results indicate that this species is 17.4 kcal/mol less stable than the folded Gly_5H^+ (Structure **3**). Similar calculations for Gly_4H^+ and Gly_3H^+ exhibit increasingly less stable salt bridge forms relative to the folded structures, protonated on the N-terminus. Experimental results with the methyl esters support the theoretical calculations. The H/D exchange of $(Gly_4\text{-OMe})H^+$ with D_2O displays the same results as Gly_4H^+ with

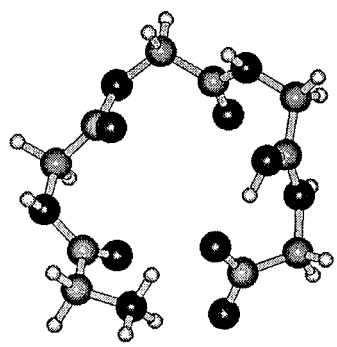

2

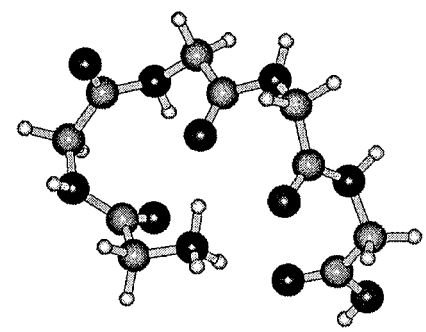

3

only one deuterium incorporated. If Gly_4H^+ had been a salt bridge, methylation of the C-terminus should have disrupted the structure and varied the observed exchange pattern.

Mechanism of exchange for betaine. Before considering exchange mechanisms for the protonated glycine oligomers, it is of interest to reflect on the mechanism by which our probe molecule, betaine (**1**), exchanges its single labile hydrogen with the reagents used in this study. Betaine is unusual in that with the quaternary nitrogen, the molecule does not possess a labile proton. Even so, facile exchange occurs with ND_3, CD_3CO_2D, and CD_3OD, as shown by the rates in Table 1. D_2O is two orders of magnitude slower. Betaine represents a model system for better understanding what might occur in exchange of the carboxyl hydrogen in the protonated glycine oligomers.

Calculations at the PM3 level indicate that NH_3 forms a relatively strong hydrogen bond to betaine (12.6 kcal/mol). Furthermore, proton transfer to NH_3, forming a salt bridge, is actually *exothermic* by 18 kcal/mol (Scheme 1)! The potential energy surface is shown in Figure 11 along with the structures of the exchange

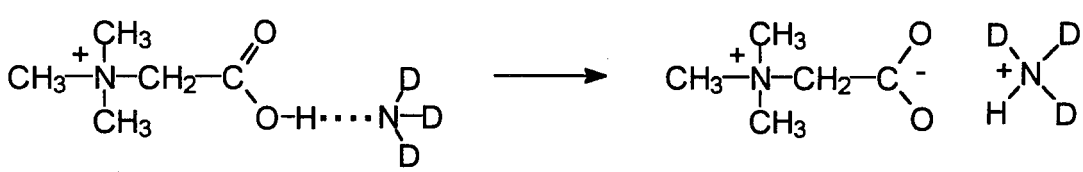

Scheme 1

Figure 11. Potential energy surface for the H/D exchange of betaine with ND_3 via a salt bridge mechanism. A strong hydrogen bond is formed as the reagent base approaches the carboxylic acid group. Proton transfer to ND_3 forming a stable salt bridge is highly favorable and results in facile exchange of the carboxylate.

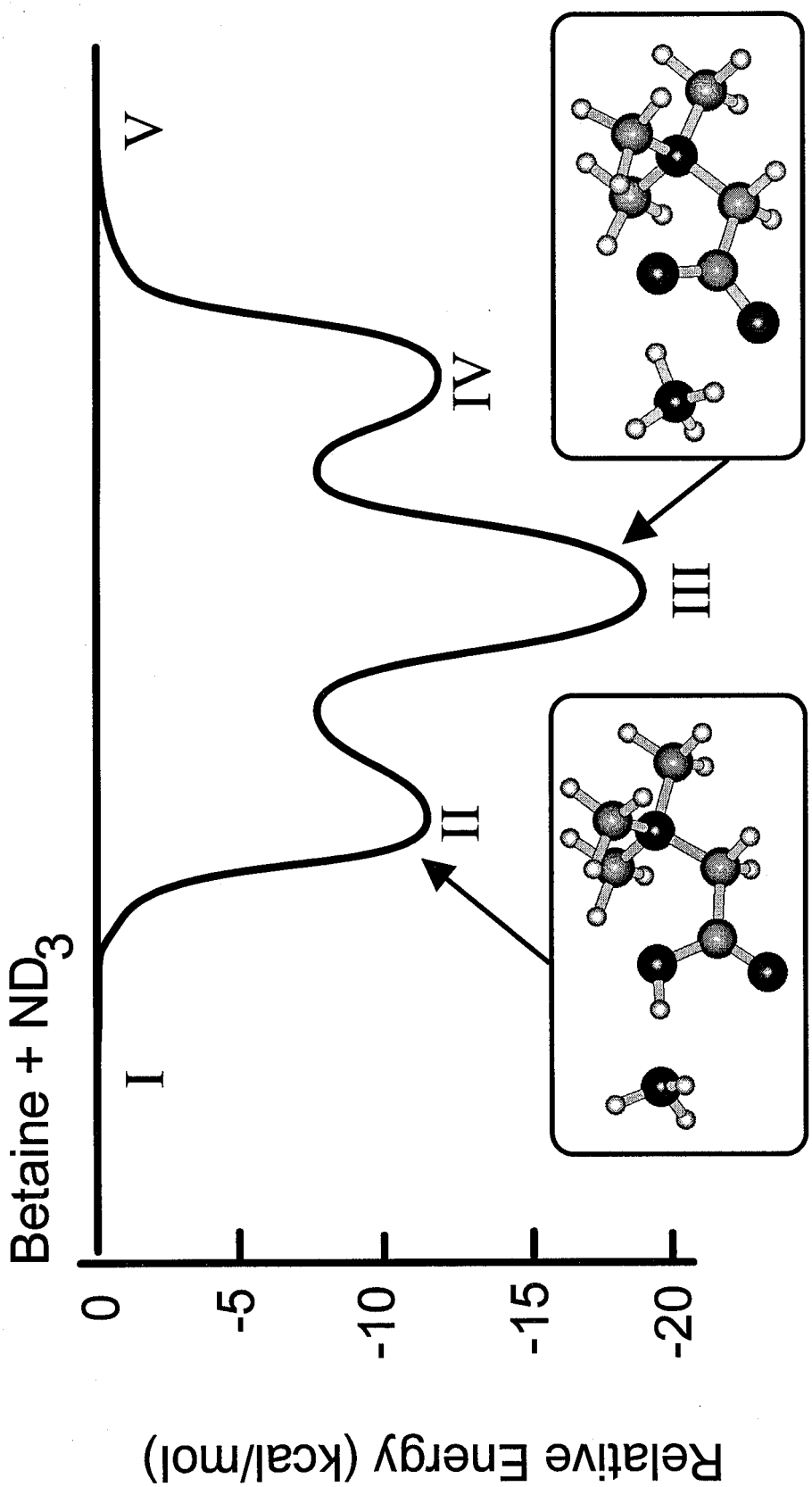

Figure 11

intermediates. Similar calculations for CH_3CO_2H indicate that salt bridge formation with betaine is feasible since the hydrogen bonded intermediate is lower in energy by 12.0 kcal/mol than the separated reagents, and proton transfer from betaine to acetic acid is slightly exothermic (0.1 kcal/mol). Salt bridge formation is not favorable with D_2O and CD_3OD, presumably due to the lower proton affinities compared to NH_3.

It is more difficult to evaluate the possibility of multicenter "flip-flop" exchange intermediates such as those shown in Scheme 2. The barriers for these processes may be high compared to the chemical activation available from complex formation. A possible exception is acetic acid, where barriers for exchange in symmetric hydrogen bonded acid dimers are known to be 10-12 kcal/mol.[46]

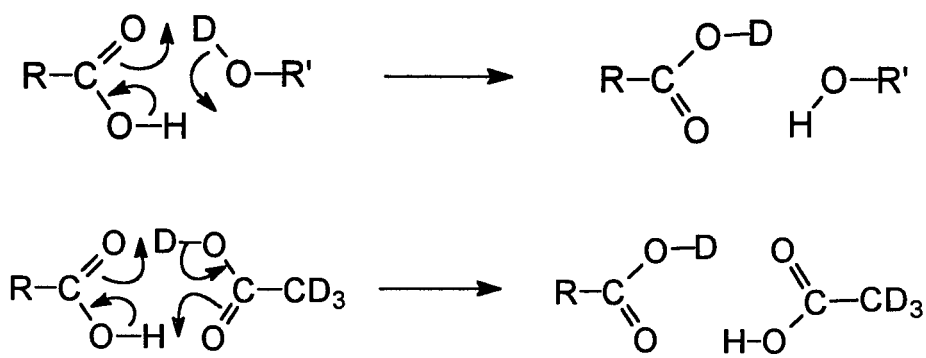

Scheme 2

The results with betaine are perhaps not surprising if one considers the gas phase acidity of the ion (ΔH for Reaction 2). PM3 calculations yield a value of 241.3 kcal/mol, which suggests that it should be possible to deprotonate betaine with strongly

basic neutral species. For comparison, the acidity of glycine is 341.6 kcal/mol.[28] The nearby positive charge center significantly stabilizes the carboxylate anion in deprotonated betaine.[47]

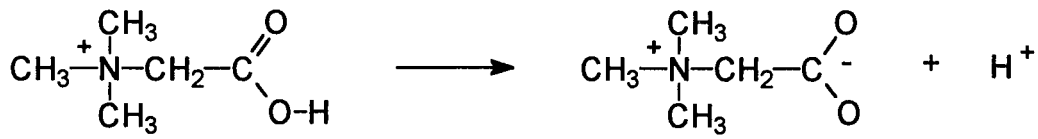

(2)

Mechanisms of exchange for ND_3. A reaction intermediate comprising a chemically activated hydrogen bonded complex is initially invoked (Scheme 3). From experimental proton affinities, it is predicted that proton transfer from a glycine oligomer to an ammonia molecule should be moderately unfavorable. We propose that

$$\underset{\text{I}}{MH^+} + ND_3 \rightarrow \underset{\text{II}}{[MH^+\cdot\cdot ND_3]} \rightarrow \underset{\text{III}}{[M\cdot\cdot HND_3^+]} \rightarrow \underset{\text{IV}}{[MD^+\cdot\cdot HND_2]} \rightarrow \underset{\text{V}}{MD^+} + HND_2$$

Scheme 3

the mechanism of facile H/D exchange for the glycine oligomers with ND_3 involves molecular choreography in which an endothermic proton transfer is rendered energetically feasible by solvation of the resultant ammonium ion (Scheme 4). Solvation of this ion by the oligomer compensates for the loss of folding stabilization in

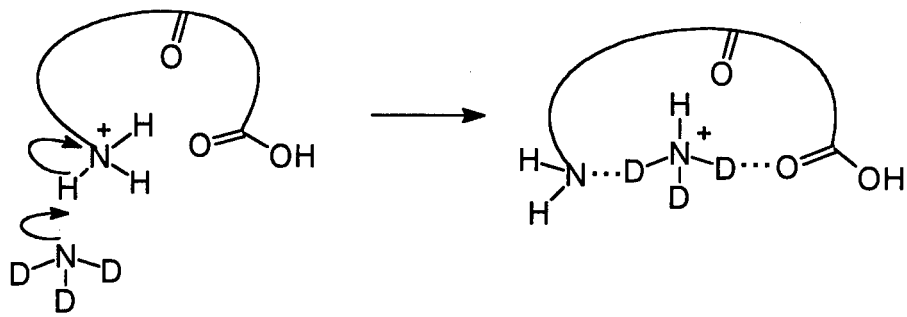

Scheme 4

the parent species (I). PM3 calculations show the onium ion mechanism for H/D exchange is especially favorable for ammonia, as the solvated ammonium ion complex (species III) with Gly_3, Gly_4, and Gly_5 is 25.1, 23.9, and 19.3 kcal/mol more stable than the separated reactants, respectively. As a result, ND_3 is a highly effective reagent for promoting H/D exchange with these oligomers. The calculated potential energy surface for the exchange of Gly_3H^+ with ND_3 is shown in Figure 12, with the intermediates numbered as in Scheme 3. It should be obvious from the potential energy surface of Figure 12 that multiple exchanges are possible with ND_3, since the intermediates can rattle around in the several wells before dissociating to products.

H/D exchange of the amide and carboxylic hydrogens in the glycine oligomers by ND_3 requires further considerations. The energetics of several possible mechanisms were evaluated with semiempirical calculations. Only one viable pathway was discerned which is nearly as energetically favorable as the exchange of the N-terminus hydrogens. The mechanism proposed for exchanging the amide hydrogen involves proton transfer from the N-terminus to the amide carbonyl in concert with transfer of

Figure 12. Potential energy surface for the H/D exchange of Gly_3H^+ with ND_3 via an onium ion mechanism. Proton transfer from the N-terminus to ND_3 is accompanied by simultaneous solvation of the ammonium ion by the carbonyl oxygens of the peptide.

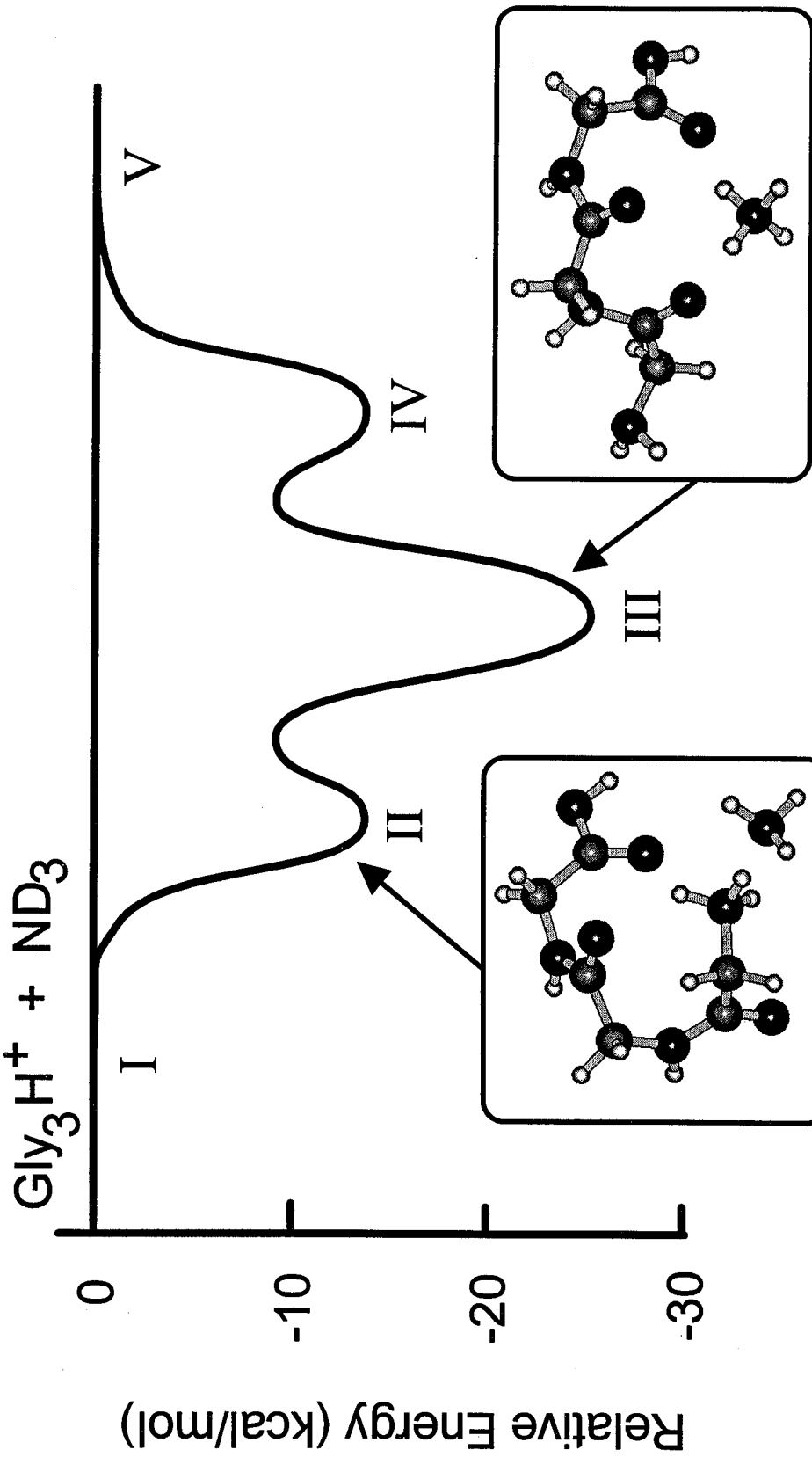

Figure 12

the amide proton to ammonia to form an ammonium ion solvated by the tautomerized peptide (Scheme 5). The potential energy surface for the amide hydrogen exchange of Gly_3H^+ with ND_3 is shown in Figure 13. The tautomerized intermediate is only 5.2 kcal/mol less stable than the onium ion intermediate in Figure 12, and is 19.9 kcal/mol below the energy of the reactants. We will refer to this process as the tautomer mechanism.

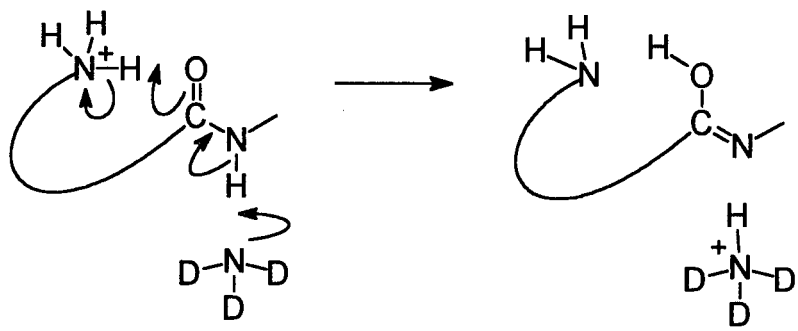

Scheme 5

An intriguing possibility for exchange of the carboxylate hydrogen invokes salt bridge formation. In analogy with the exchange process proposed above for betaine, this process involves proton transfer from the C-terminus to ammonia with concomitant stabilization of the carboxylate anion by the protonated N-terminus (Scheme 6). PM3 calculations suggest favorable energetics for this process as shown in Figure 14. The salt bridge structure involving the C-terminus carboxylic acid is a local minimum on the potential energy surface, but is only 4 kcal/mol lower in energy than the reactants. This

Figure 13. Potential energy surface for the H/D exchange of amide hydrogens of Gly_3H^+ with ND_3 via a tautomer mechanism. Proton transfer from the N-terminus to an amide carbonyl occurs in concert with transfer of the amide proton to ammonia.

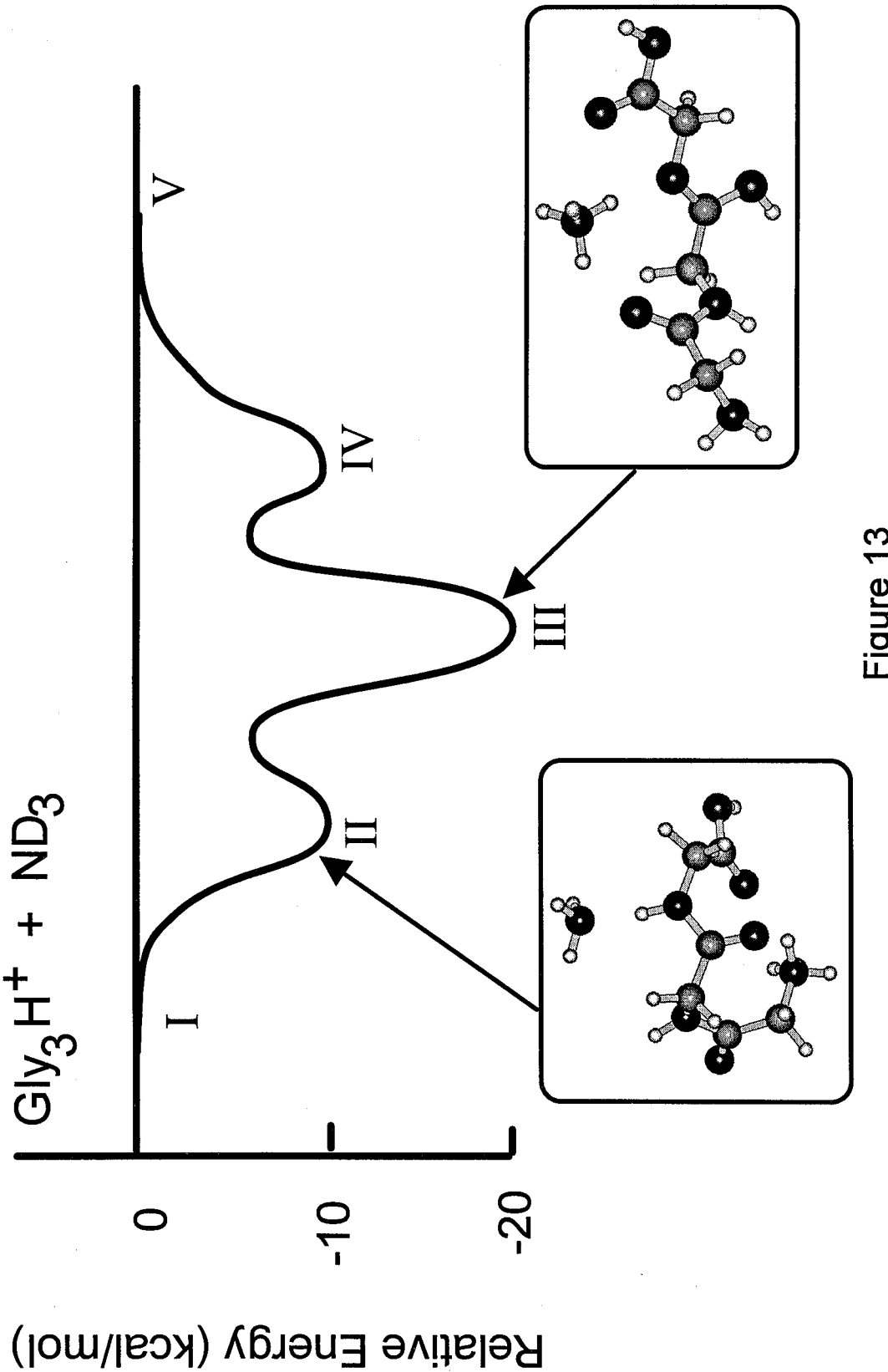

Figure 13

Figure 14. Potential energy surface for the H/D exchange of the C-terminus of Gly_3H^+ with ND_3 via a salt bridge mechanism. Proton transfer from the C-terminus to ND_3 and formation of a salt bridge structure is facilitated by the stabilizing effect of the nearby positively charged N-terminus.

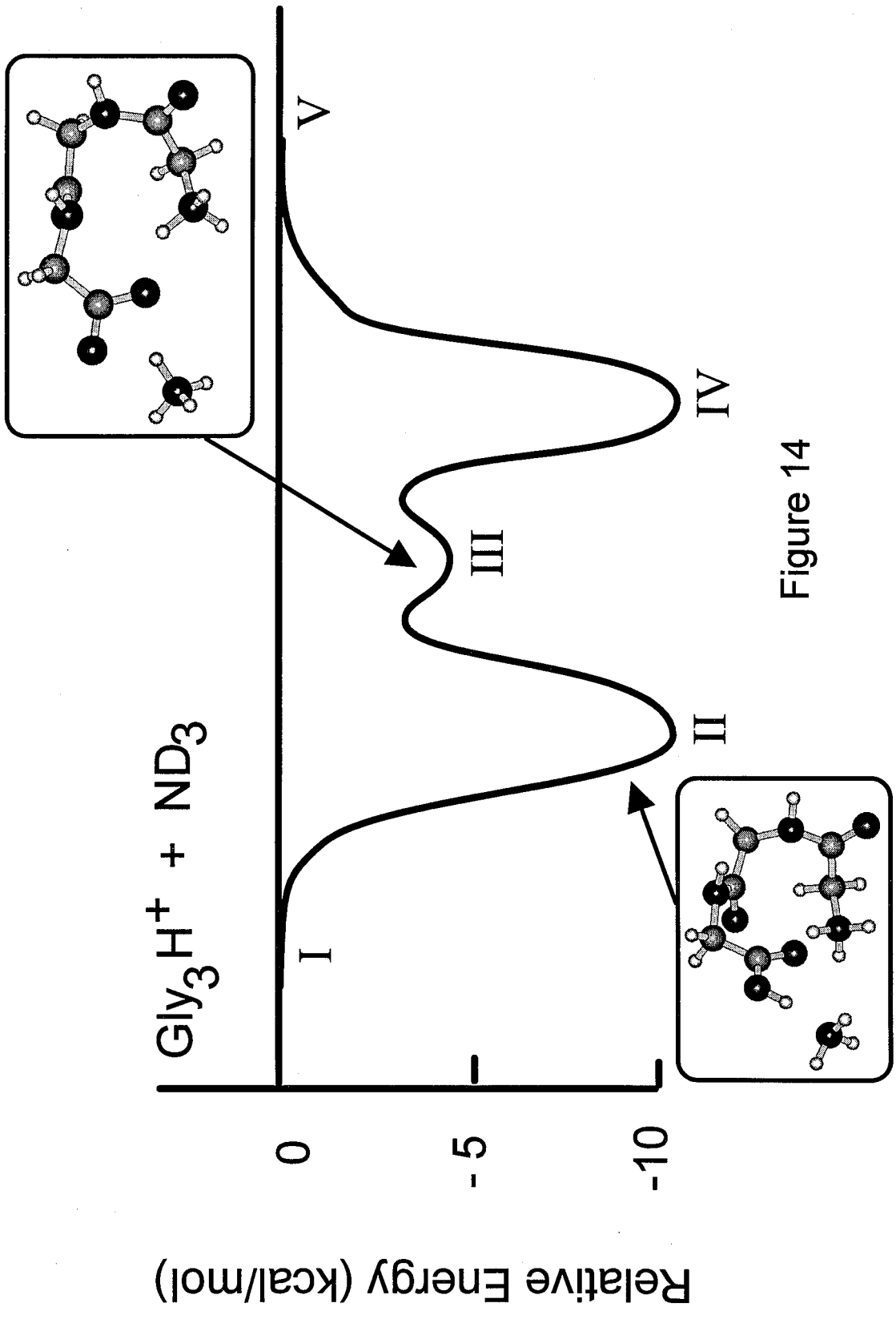

Figure 14

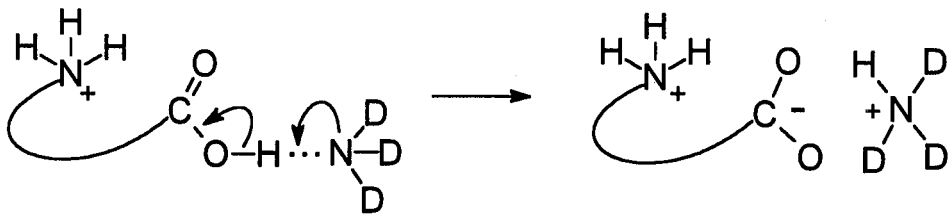

Scheme 6

species will have a tendency to collapse to the significantly more stable onium ion (Figure 12) by transferring a proton from the N-terminus to the carboxylate anion, and the end result can be considered a degenerate tautomer mechanism. Even so, it appears to provide a viable pathway to eventually exchange the C-terminus hydrogen.

Mechanism of exchange for D_2O. For D_2O to undergo H/D exchange with the glycine oligomers, a proton affinity difference of at least 45.1 kcal/mol (for Gly_1) must be overcome. This effectively rules out exchange via simple hydrogen bond formation as in Figure 8, which is inefficient for proton affinity differences greater than 20 kcal/mol. Additionally, exchange by means of a salt bridge mechanism is unlikely since calculations indicate this process is unfavorable for H_2O, due to the much lower proton affinity of H_2O compared to NH_3. Semiempirical PM3 calculations also indicate that H/D exchange by formation of a solvated hydronium ion complex with the glycine oligomers is energetically unfavorable. The proton affinity of D_2O is too low and the energy recovered by solvation of the hydronium ion is insufficient to overcome the endothermicity of proton transfer. The potential energy surface for the H/D exchange

reaction of Gly_3H^+ with D_2O by means of an onium ion mechanism is shown in Figure 15, with the intermediates labeled similarly to those of Scheme 3. Although the hydrogen bonded complex of Gly_3H^+ with D_2O is a local minimum, transfer of the proton to D_2O is unfavorable by 2.1 kcal/mol compared to the separated starting species.

We propose a relay mechanism for facile H/D exchange of protonated peptides with D_2O in which a proton is shuttled from the site of protonation in the hydrogen bonded complex onto D_2O in concert with the transfer of a deuteron from D_2O to a distant, slightly less basic site on the molecule (Schemes 7 and 8). For the glycine oligomers, this corresponds to the labile charge being shuttled from the N-terminus nitrogen (species II) to a less basic amide oxygen (III). The potential energy surface

$$\underset{\text{I}}{MH^+} + D_2O \rightarrow \underset{\text{II}}{[MH^+\cdot\cdot D_2O]} \rightarrow \underset{\text{III}}{[(MD^+)^*\cdot\cdot DOH]} \rightarrow \underset{\text{IV}}{[MD^+\cdot\cdot DOH]} \rightarrow \underset{\text{V}}{MD^+} + DOH$$

Scheme 7

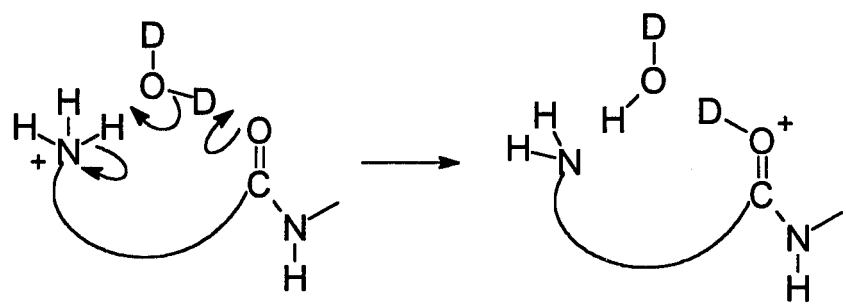

Scheme 8

Figure 15. Potential energy surfaces for the H/D exchange of Gly_3H^+ with D_2O via relay and onium ion mechanisms. Proton transfer to H_2O and formation of a hydronium ion intermediate (dashed line) is unfavorable due to the low proton affinity of H_2O. Instead, exchange occurs via a relay mechanism (solid line) in which a proton is shuttled by D_2O from the N-terminus to an amide carbonyl, leaving the charge site on the peptide.

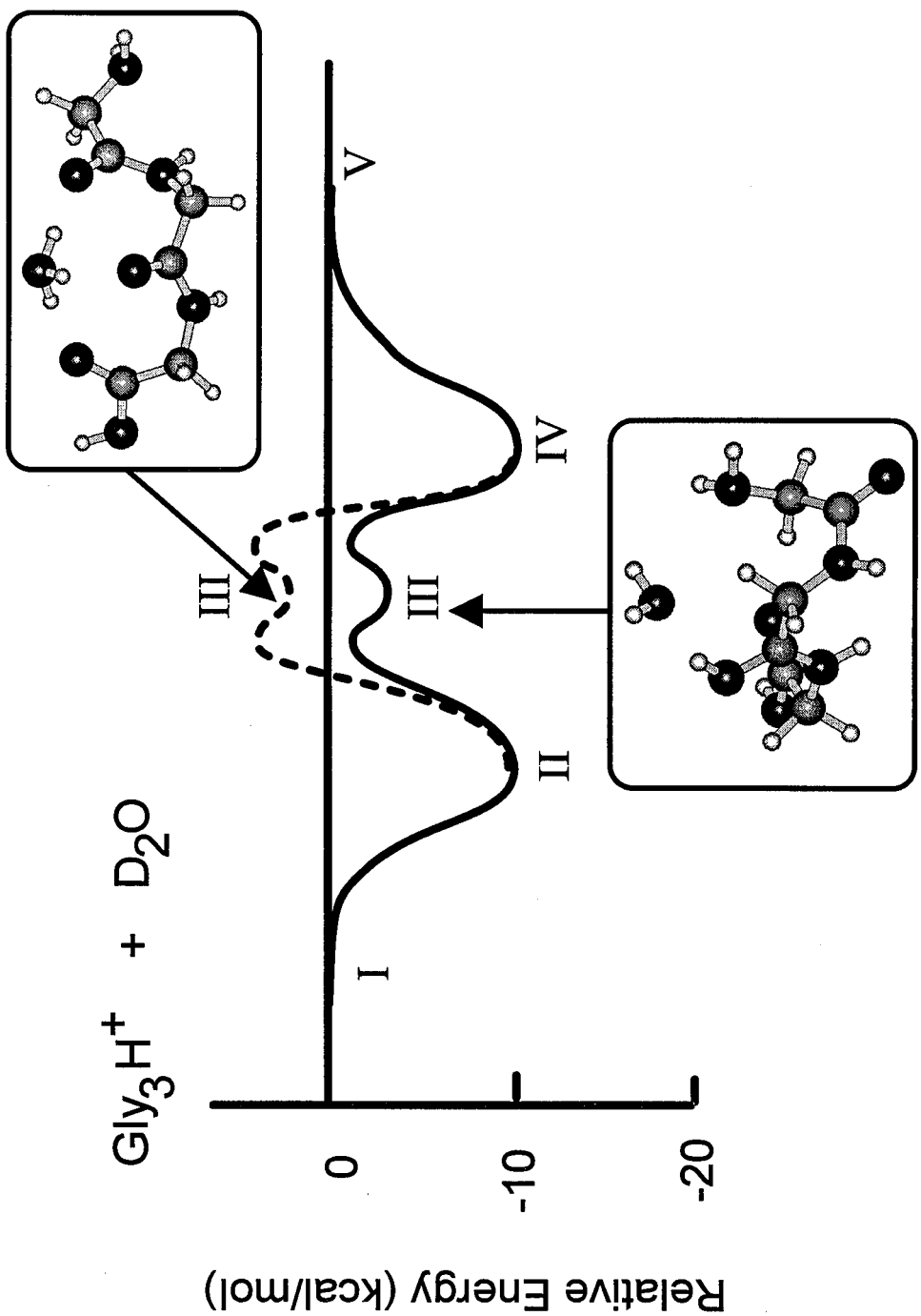

Figure 15

calculated for the H/D exchange of Gly_3H^+ with D_2O via the relay mechanism is shown in Figure 15, with the intermediates numbered as in Scheme 7. Deuteron transfer from the relay intermediate (III) back to the N-terminus nitrogen (IV) and dissociation to products completes the reaction process. The relay mechanism makes proton transfer viable within a molecule using the chemical activation provided by hydrogen bonding.

Although it is possible for reactants to traverse the potential energy surface several times, it seems reasonable that the relay surface for D_2O is less conducive to multiple exchanges than the onium ion surface for ND_3 in Figure 12. PM3 calculations were performed to identify if ND_3 undergoes H/D exchange with the glycine oligomers via the relay mechanism. Calculations indicate that with ND_3, relay intermediates are energetically feasible but readily collapse to the more stable solvated ammonium ion (III, Figure 12).

Differences in reactivity between the oligomers. There are two unusual features observed in the reactivity of the glycine oligomers with the exchange reagents. The first is the lack of reactivity of Gly_1 with D_2O while Gly_2 exchanges all labile hydrogens. The second is the lack of reactivity of oligomers larger than Gly_3 with D_2O and to a lesser extent CD_3OD.

Reactions of the oligomers with D_2O proceed via the relay mechanism. The mechanism makes viable reactions that are nominally endothermic by forming hydrogen bonds between D_2O and the exchange sites. For exchanges to occur, the energy gained by forming hydrogen bonds must be larger than the difference in the proton affinities of the exchange sites and the energy lost by opening the internally solvated structure.

Gly_2H^+ easily exchanges with D_2O via the relay mechanism since very little folding energy is lost by forming the intermediate (Figure 10), and the difference in proton affinity between the N-terminus nitrogen and the amide oxygen is small (8.1 kcal/mol).[48] Gly_1H^+ cannot easily exchange with D_2O via the relay mechanism since the two sites for shuttling the proton are the N-terminus nitrogen and the acid carbonyl. The difference in proton affinities between these sites is calculated to be 13.4 kcal/mol, which is more than the amount recovered by forming a hydrogen bonded intermediate. The one slow exchange observed for Gly_1H^+ probably occurs at the acid hydroxyl, remote from the charge center via a multicenter exchange intermediate similar to Scheme 2.

For Gly_3H^+ and Gly_4H^+ the difference in folding energies probably accounts for the observed difference in reactivity with D_2O. Molecular dynamics simulations[49] show that when D_2O hydrogen bonds to Gly_3H^+, the secondary structure of the molecule is disrupted in less than a picosecond at 300 K. The rupturing of the internal hydrogen bonds exposes labile hydrogen sites and facilitates exchange by the relay mechanism. The energy recovered by forming the exchange intermediate compensates for the loss in intramolecular folding energy. The proton affinity of Gly_4 is larger than that of Gly_3 due to more extensive solvation of the charge site. This effectively increases the disparity in proton affinities between the solvated N-terminus and amide oxygens in the molecule, thereby reducing the effectiveness of the relay mechanism for exchange. Molecular dynamics simulations show that the more extensive intramolecular hydrogen bonding in Gly_4H^+ cannot be disrupted by bonding D_2O to the oligomer and the

complex dissociates on a picosecond timescale at 300 K. Hence, the relay mechanism cannot be invoked for Gly_4H^+ and D_2O is unable to promote facile H/D exchange of this (or any larger) oligomer.

Effects of off-resonance excitation on H/D exchange. The effect of off-resonance excitation on the rate and extent of H/D exchange was studied for several oligomers with D_2O and CD_3CO_2D. For Gly_3H^+ reacting with D_2O and Gly_4H^+ reacting with CD_3CO_2D, initial activation of the protonated parent appears to decrease the rate of deuterium exchange. This is consistent with exchange mechanisms that proceed via long lived collision complexes. High translational and vibrational energies of the protonated oligomer reduce the likelihood of forming a hydrogen bound collision complex.[23] The failure of collisional activation of Gly_4H^+ to promote exchange with D_2O is consistent with this viewpoint. The excess excitation that opens the solvated oligomer by breaking the intramolecular bonds also inhibits hydrogen bond formation to the D_2O exchange agent. Without adduct formation, exchange does not occur.

Conclusions

We have examined the H/D exchange of protonated glycine oligomers with D_2O, CD_3OD, CD_3CO_2D, and ND_3 in a Fourier transform ion cyclotron resonance mass spectrometer. Although it is not the sole determining factor, the rate and extent of isotopic hydrogen exchange increases with increasing basicity of the exchange reagent, $D_2O<CD_3OD<CD_3CO_2D<ND_3$. D_2O is the more discriminant reagent, while ND_3 exchanges all of the labile hydrogens of all the species studied. For those glycine

oligomers whose proton affinities differ from the deuterating reagents by less than 20 kcal/mol, H/D exchange predominantly occurs via formation of a strong hydrogen bonded species. For those oligomers whose proton affinities differ from the reagents by significantly more than 20 kcal/mol, the exchange mechanisms are more subtle.

Five mechanisms are proposed for the H/D exchange of protonated glycine oligomers with reagent bases: the onium ion, relay, salt bridge, flip-flop, and tautomer mechanism. These processes are summarized in Figure 16. An onium ion mechanism is proposed for protonated glycine oligomers exchanging with basic reagents (such as ND_3), in which a nominally endothermic proton transfer from the N-terminus is accompanied by simultaneous solvation of the resultant onium ion (i.e., ammonium ion). For reagents such as D_2O whose proton affinity is too low to overcome the endothermicity of proton transfer from the peptide, a relay mechanism in which the deuterating reagent shuttles a proton from the N-terminus to a slightly less basic site (amide oxygen) is proposed. Semiempirical calculations indicate that exchange of the amide hydrogens is slightly less favorable than exchange of the N-terminus. A tautomer mechanism is proposed in which a proton is transferred from the N-terminus to an amide carbonyl in concert with transfer of the amide proton to the reagent base. This mechanism is highly favorable for ND_3, in which the ammonium ion is solvated by the tautomerized peptide. Exchange of the C- terminus hydrogen using basic reagents occurs via a salt bridge mechanism, in which the hydroxyl proton is transferred to the exchange gas, creating an ion pair stabilized by a nearby charge center. Exchange of

Figure 16. Summary of the proposed H/D exchange mechanisms for the glycine oligomers with reagent bases.

Onium Ion Mechanism	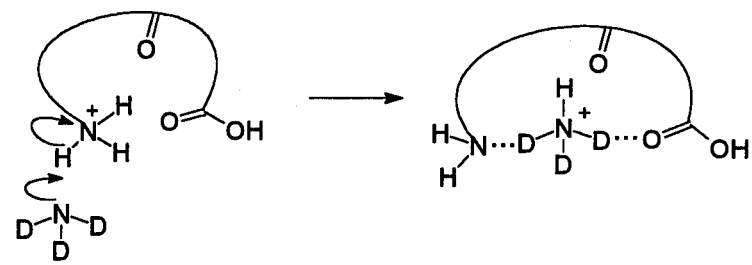
Relay Mechanism	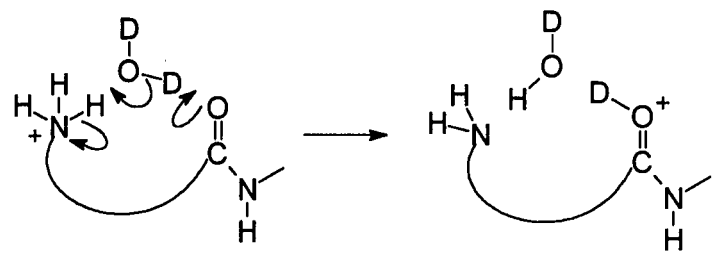
Salt Bridge Mechanism	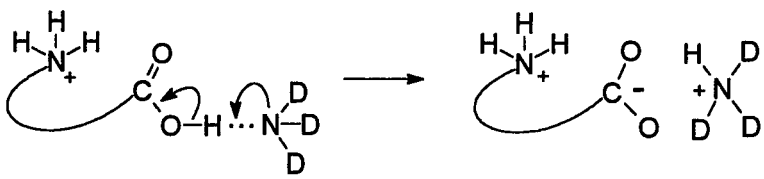
Flip-Flop Mechanism	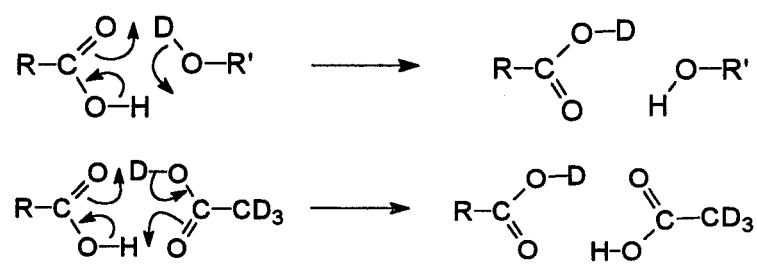
Tautomer Mechanism	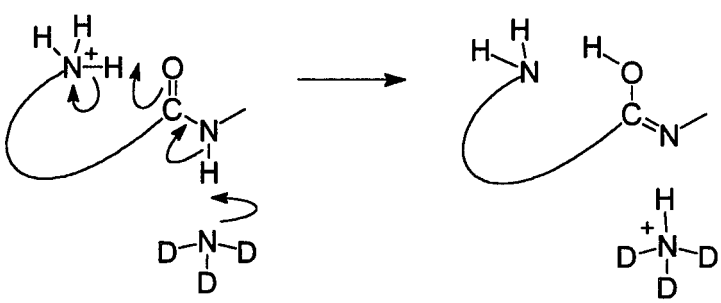

Figure 16

the C-terminus using less basic reagents is slow and probably occurs via a multicentered flip-flop mechanism.

There has been considerable interest in the structural and functional roles of salt bridges in proteins. Charged amino acids have been implicated as factors contributing to protein stability, as driving forces for protein-protein interactions, and as key factors in enzyme mechanisms.[50] The question of salt bridge formation in the gas phase is an interesting one. We believe that H/D exchange intermediates proposed for betaine are perhaps the first examples of salt bridge formation in the gas phase. We also estimate that it is energetically feasible for the C-terminus hydroxyl of betaine and the glycine oligomers to undergo H/D exchange via an intermolecular salt bridge with the deuterating reagent. The systems in which we have invoked salt bridges as viable reaction intermediates involve proton transfer in an acid-base complex to form an ion pair which is stabilized by a nearby charge center.[47] Semiempirical calculations, however, indicate that salt bridges in the isolated glycine oligomers considered in this study are unlikely. This conclusion is supported by the exchange results of oligomers methylated at the C-terminus, which exhibit no difference in reactivity from the unmethylated oligomers. In contrast, the presence of very basic residues such as arginine (whose side chain has a proton affinity 30 kcal/mol greater than the N-terminus) in peptides may allow the formation of intramolecular gas phase salt bridges in peptides with appropriate arrangements of amino acids.

It is particularly interesting to note that D_2O does not undergo facile exchange with the Gly_nH^+ oligomers with n>3. However, McLafferty and co-workers[17] report

that multiply protonated peptides (+6 to +18) of cytochrome *c*, myoglobin, and ubiquitin undergo extensive deuterium exchange with D_2O. They observe H/D exchange rates in the range from $2x10^{-13}$ to $4x10^{-12}$ $cm^3molecule^{-1}sec^{-1}$, with the highest charge states exhibiting the fastest exchange. For peptides with a charge state of +7 or +6, the exchange rates were $<10^{-12}$ $cm^3molecule^{-1}sec^{-1}$, which is slower than the range of rates monitored in our experiments. The coulomb repulsion between charge sites in a multiply protonated peptide effectively reduces the proton affinity of the species. Williams and co-workers[51] have recently examined the deprotonation energetics of multiply charged cytochrome *c* ions. They observe that the gas phase basicities range from 234 kcal/mol for the +3 charge state to 192 kcal/mol for the +15 charge state. Hence, exchange of hydrogen for deuterium with D_2O becomes energetically more favorable. The extent to which protonation sites in these complex molecules are stabilized by intramolecular hydrogen bonding remains uncertain, making it difficult to assess details of H/D exchange mechanisms with different reagent gases.

H/D exchange processes involving even simple model peptides are highly complex processes. As a result, any temptation to assign gas phase structures of biological molecules from H/D exchange results must be approached with caution. With a thorough understanding of the gas phase structures and H/D exchange mechanisms of simple glycine oligomers, it is appropriate to proceed with the investigation of larger, more complex protonated peptides. The incorporation of strongly basic amino acid residues, such as arginine and histidine, into the peptides should complicate simple mechanistic pictures of H/D exchange, due to their high

proton affinities. The resultant disparity in functional group basicities will mitigate against the relay mechanism for H/D exchange. Exchange via the onium ion mechanism will only be viable when the energy recovered by solvating the onium ion exceeds the combined energy lost from unfolding the peptide and transferring the proton to the reagent gas.[52] We are currently undertaking investigations to elucidate the H/D exchange mechanisms of more complex protonated peptides.

Acknowledgments

We gratefully acknowledge the financial support of SC from a NIH-NRSA traineeship in Biotechnology, of MTR from a California Institute of Technology Consortium grant, and of EMM from a Rainin Fellowship and NIH-NRSA Human Genome traineeship. This work was supported in part by the National Science Foundation under grant CHE-9108318. Funds for instrument development have also been provided by ARPA and DoD-URI programs under grant ONR-N0014-92-J-1901. We are indebted to the Beckman Foundation and Institute for the initial funding and continuing support of the research facilities.

References

1. Werstiuk, N. H. *Isotopes in the Physical and Biomedical Sciences*, Vol. 1, Elsevier, Amsterdam, **1987**, p. 122.

2. Wuthrich, K. *NMR of Proteins and Nucleic Acids*, Wiley-Interscience, New York, **1986**.

3. (a) Englander, S. W.; Kallenbach, N. R. *Q. Rev. Biophysics* **1984**, *16*, 521. (b) Roder, H. *Methods Enzymol.* **1989**, *176*, 446.

4. See, for example: Roder, H.; Elove, G. A.; Englander, S. W. *Nature* **1988**, *335*, 700 or Hughson, R. M.; Wright, P. E.; Baldwin, R. L. *Science* **1990**, *249*, 1544.

5. (a) Biemann, K. *Methods in Enzymology*, Vol. 193; McCloskey, J., Ed.; Academic Press; San Diego, California, **1990**, p. 351. (b) Johnson, R. S.; Martin, S. A.; Biemann, K. *Int. J. Mass Spectrom. Ion Processes* **1988**, *86*, 137. (c) Hunt, D. F.; Yates, J. R., III; Shabanowitz, J.; Winston, S.; Hauer, C. R. *Proc. Natl. Acad. Sci. U.S.A.* **1986**, *83*, 6233. (d) Schwartz, B. L.; Bursey, M. M. *Biol. Mass Spectrom.* **1991**, *21*, 92.

6. Englander, S. W. *Science* **1993**, *262*, 848.

7. Miranker, A.; Robinson, C. V.; Radford, S. E.; Aplin, R. T.; Dobson, C. M. *Science* **1993**, *262*, 896.

8. (a) Fenn, J. B.; Mann, M.; Meng, C. K.; Wong, S. F.; Whitehouse, C. M. *Science* **1989**, *246*, 64. (b) Smith, R. D.; Loo, J. A.; Loo, R. R. O.; Busman, M.; Udseth, H. R. *Mass Spectrom. Rev.* **1991**, *10*, 359.

9. (a) Barber, M.; Bordoli, R. S.; Sedgwick, R. D.; Vickerman, J. J. *J. Chem. Soc., Faraday Trans.* **1982**, *78*, 1291. (b) Barber, M.; Bordoli, R. S.; Sedgwick, R. D.; Tyler, A. N. *J. Chem. Soc., Chem. Commun.* **1981**, 325.

10. (a) Katta, V.; Chait, B. T. *Proceeding of the 39th Conference Mass Spectrometry and Allied Topics*, Nashville, TN; ASMS: East Lansing, MI, **1991**; p. 1247. (b) Katta, V.; Chait, B. T. *Rapid Commun. Mass Spectrom.* **1991**, *5*, 214. (c) Katta, V.; Chait, B. T. *J. Am. Chem. Soc.* **1993**, *115*, 6317. (d) Verma, S.; Pomerantz, S. C.; Sethi, S. K.; McCloskey, J. A. *Anal. Chem.* **1986**, *58*, 2898. (e) Sepetov, N. F.; Issakova, O. L.; Lebl, M.; Swiderek, K.; Stahl, D. C.; Lee, T. D. *Rapid Commun. Mass Spectrom.* **1993**, *7*, 58. (f) Guarini, A.; Guglielmetti, G.; Andriollo, N.; Vincenti, M. *Anal. Chem.* **1992**, *64*, 204.

11. Freiser, B. S.; Woodin, R. L.; Beauchamp, J. L. *J. Am. Chem. Soc.* **1975**, *97*, 6893.

12. Ranasinghe, A.; Cooks, R. G.; Sethi, S. K. *Org. Mass Spectrom.* **1992**, *27*, 77.

13. Squires, R. R.; Bierbaum, V. M.; Grabowski, J. J.; DePuy, C. H. *J. Am. Chem. Soc.* **1983**, *105*, 5185.

14. (a) Ausloos, P.; Lias, S. G. *J. Am. Chem. Soc.* **1981**, *103*, 3641. (b) Lias, S. G. *J. Phys. Chem.* **1984**, *88*, 4401.

15. Hunt, D. F.; Sethi, S. K. *J. Am. Chem. Soc.* **1980**, *102*, 6953.

16. Winger, B. E.; Light-Wahl, K. J.; Rockwood, A. L.; Smith, R. D. *J. Am. Chem. Soc.* **1992**, *114*, 5897.

17. Suckau, D.; Shi, Y.; Beu, S. C.; Senko, M. W.; Quinn, J. P.; Wampler, F. M.; McLafferty, F. W. *Proc. Natl. Acad. Sci.* **1993**, *90*, 790.

18. Meot-Ner, M. *Molecular Structures and Energetics*, Vol. 4, VCH Publishers, New York, **1986**, p. 71.

19. (a) Bohme, D. K. *Interactions Between Ions and Molecules*, Plenum, New York, **1975**, p. 489. (b) Farneth, W. E.; Brauman, J. I. *J. Am. Chem. Soc.* **1976**, *98*, 7891.

20. (a) Olmstead, W. N.; Brauman, J. I. *J. Am. Chem. Soc.* **1977**, *99*, 4219. (b) Asubiojo, O. I.; Brauman, J. I. *J. Am. Chem. Soc.* **1979**, *101*, 3715.

21. Squires, R. R.; Bierbaum, V. M.; Grabowski, J. J.; DePuy, C. H. *J. Am. Chem. Soc.* **1983**, *105*, 5185.

22. (a) Gard, E.; Willard, D.; Green, M. K.; Bregar, J.; Lebrilla, C. B. *Org. Mass Spectrom.* **1993**, *28*, 1632. (b) Gard, E.; Green, M. K.; Bregar, J.; Lebrilla, C. B. *J. Am. Soc. Mass Spectrom.* **1994**, *5*, 614.

23. Cheng, X.; Fenselau, C. *Int. J. Mass Spectrom. Ion Processes* **1992**, *122*, 109.

24. Wu, Z.; Fenselau, C. *J. Am. Soc. Mass Spectrom.* **1992**, *3*, 863.

25. Wu, J.; Lebrilla, C. *J. Am. Chem. Soc.* **1993**, *115*, 3270.

26. Zhang, K.; Zimmerman, D. M.; Chung-Phillips, A.; Cassady, C. *J. Am. Chem. Soc.* **1993**, *115*, 10812.

27. For examples of multiple exchanges in a single collision event, see: Grabowski, J. J.; DePuy, C. H.; Van Doren, J. M.; Bierbaum, V. M. *J. Am. Chem. Soc.* **1985**, *107*, 7384.

28. A compilation of gas phase basicities and proton affinities can be found in: Lias, S. G.; Bartmess, J. E.; Liebman, J. F.; Holmes, J. L.; Levin, R. D.; Mallard, W. G. *J. Phys Chem. Ref. Data* **1988**, *17(1)*.

29. Preliminary results have been previously presented, see: Campbell, S.; Rodgers, M. T.; Marzluff, E. M.; Beauchamp, J. L. *J. Am. Chem. Soc.* (in press).

30. (a) Dewar, M. J. S.; Zoebisch, E. G.; Healy, E. F.; Stewart, J-J. P. *J. Am. Chem. Soc.* **1985**, *107*, 3902. (b) Dewar, M. J. S.; Dieter, K. M. *J. Am. Chem. Soc.* **1986**, *108*, 8075.

31. (a) Stewart, J. J. P. *Method J. Comput. Chem.* **1989**, *10*, 209. (B) Stewart, J. J. P. *Method J. Comput. Chem.* **1989**, *10*, 221.

32. (a) Campbell, S.; Marzluff, E. M.; Rodgers, M. T.; Beauchamp, J. L.; Rempe, M. E.; Schwinck, K. F.; Lichtenberger, D. L. *J. Am. Chem. Soc.* **1994**, *116*, 5257. (b) Marzluff, E. M.; Campbell, S.; Rodgers, M. T.; Beauchamp, J. L. *J. Am. Chem. Soc.* **1994**, *116*, 7787.

33. (a) Ngoka, L. C.; Gal, J. F.; Lebrilla, C. B. *Anal. Chem.* **1994**, *66*, 692. (b) Ngoka, L. C.; Lebrilla, C. B. *J. Am. Soc. Mass Spectrom.* **1993**, *4*, 210.

34. Gauthier, J. W.; Trautman, T. R.; Jacobson, D. B. *Anal. Chim. Acta.* **1991**, *246*, 211.

35. Hyperchem Computational Software Package, Ver. 4.0 (Hypercube Inc., 1994). For a review of this computational package, see: Froimowitz, M. *Biotechniques* **1993**, *14*, 1010.

36. Examples of this behavior have been previously reported in: Blint, R. J.; McMahon, T. B.; Beauchamp, J. L. *J. Am. Chem. Soc.* **1974**, *96*, 1269.

37. Bowers, M. T. *Gas Phase Ion Chemistry*, Vol. 1, Academic Press, New York, **1979**, ch. 3.

38. Marzluff, E. M.; Campbell, S.; Rodgers, M. T.; Beauchamp, J. L. *J. Am. Chem. Soc.* **1994**, *116*, 6947.

39. Jaroszewdki, L.; Lesyng, B.; Tanner, J. J.; McCammon, J. A. *Chem. Phys. Lett.* **1990**, *175*, 282.

40. See, for example: (a) Zheng, Y.; Merz, K. M. *J. Comp. Chem.* **1992**, *13*, 1151. (b) Jurema, M. W.; Shields, G. C. *J. Comp. Chem.* **1993**, *14*, 89.

41. Neutral heats of formation were evaluated with the glycine oligomers in an extended β-sheet configuration. Folded configurations did not have significantly different energies.

42. All experimental results are reported relative to the proton affinity of NH_3 as 204.0 kcal/mol.[28] Values which were reported in the literature using the recent scale by Meot-Ner (Meot-Ner, M.; Sieck, L. W. *J. Am. Chem. Soc.* **1991**, *113*, 4448) have been adjusted using their NIST gas phase basicities[28] and adding the appropriate $T\Delta S$ terms estimated by each investigator.

43. (a) Bliznyuk, A. A.; Schaeffer, H. F.; Amster, I. J. *J. Am. Chem. Soc.* **1993**, *115*, 5149. (b) Bojesen, G.; Breindahl, T. *J. Chem. Soc. Perkin Trans. 2*, **1994**, 1030.

44. Locke, M. J.; McIver, R. T., Jr. *J. Am. Chem. Soc.* **1983**, *105*, 4226.

45. It has been shown that acid-base complexes can form ion pairs in the gas phase. See, for example: Legon, A. C. *Chem. Soc. Rev.*, **1993**, *22*, 153.

46. Shida, N.; Barbara, P. F.; Almlof, J. *J. Chem. Phys.* **1991**, *94*, 3633.

47. The effects of nearby charges on the energetics of proton transfer reactions have been considered by: Sanhueza, J. E.; Tapia, O. *J. Mol. Struct.* **1982**, *89*, 131.

48. PM3 calculations predict a protonated N-terminus Gly_2H^+ is 8.1 kcal/mol more favorable than a species with the amide oxygen protonated and solvated.

49. Molecular dynamics calculations were performed with Hyperchem.[35]

50. Rashin, A. A.; Honig, B. *J. Mol. Biol.* **1984**, *173*, 515.

51. Williams, E. R., private communication.

52. Campbell, S.; Beauchamp, J. L. (to be published).

CHAPTER 6

Structural and Energetic Constraints on Gas Phase Hydrogen/Deuterium Exchange Reactions of Protonated Peptides Possessing Strongly Basic Residues with ND_3 and CF_3CO_2D.

Structural and Energetic Constraints on Gas Phase Hydrogen/Deuterium Exchange Reactions of Protonated Peptides Possessing Strongly Basic Residues with ND_3 and CF_3CO_2D.

Sherrie Campbell, John McDunn and J. L. Beauchamp

Contribution No. 9000 from the Arthur Amos Noyes Laboratory of Chemical Physics

California Institute of Technology, Pasadena, CA 91125

Abstract

A Fourier transform ion cyclotron resonance mass spectrometer was used to examine the hydrogen/deuterium exchange reactions of protonated peptides possessing strongly basic residues with ND_3 and CF_3CO_2D. Exchange rates in this study were monitored over three orders of magnitude, from 10^{-9} to 10^{-12} $cm^3molecule^{-1}sec^{-1}$. Leucine enkephalin (YGGFL), a pentapeptide lacking basic side chains, exchanges nine of nine labile hydrogens with ND_3 with rate constants ranging from $4x10^{-10}$ to $4x10^{-11}$ $cm^3molecule^{-1}sec^{-1}$. This behavior is consistent with that observed for H/D exchange of simple protonated glycine oligomers, and we propose that the mechanisms of exchange for leucine enkephalin with ND_3 are analogous to those of the glycine oligomers. Exchange occurs at the N-terminus via an onium ion mechanism, at the C-terminus via

a salt bridge mechanism, and at the amide hydrogens via a tautomer mechanism. Introduction of basic residues such as arginine into peptides shifts the site of protonation in the gas phase from the N-terminus to the side group. Leucine enkephalin arginine (YGGFLR), with 14 labile hydrogens, exhibits quite different exchange behavior with ND_3, exchanging five hydrogens fairly rapidly and one more slowly. Semiempirical calculations suggest that an onium ion mechanism can explain the exchange of the five labile hydrogens of the arginine side chain. Bradykinin (RPPGFSPFR), a nonapeptide with two arginine residues, does not exchange any of its 18 labile hydrogens with ND_3. Semiempirical calculations predict two possible gas phase structures for the protonated peptide with comparable energy. One has a salt bridge in which both arginine side chains are protonated and bridged by the C-terminus carboxylate. In the other conformation, a protonated arginine side chain is encapsulated by the remainder of the peptide. Arguments are presented which suggest neither structure would be expected to undergo facile exchange with ND_3. Gramicidin S (-LFPVOLFPVO-), a cyclic decapeptide, exchanges 3 of 13 labile hydrogens with ND_3. Protonation occurs on the ornithine side chain, but constraints imposed by the cyclic structure prevent the peptide from folding to strongly solvate the charge center. H/D exchange of the side chain via an onium ion mechanism is only moderately favorable since the peptide cannot efficiently solvate the ammonium ion intermediate. As a result, exchange processes for this peptide are slow. It appears that sufficiently large singly protonated peptides possessing residues with strongly basic side groups

will encapsulate the charge site and inhibit H/D exchange, reducing the utility of such experiments as a structural probe.

Introduction

Deuterium exchange has been used extensively in mass spectrometric studies to determine the number of labile sites in simple molecules,[1] and more recently to infer structural features of complex biomolecules.[2,3] While examples of solution H/D exchange of biomolecules followed by mass spectrometric analysis are abundant,[4] fewer studies have considered H/D exchange in the gas phase. Winger *et al.*[2] reported perhaps the first gas phase H/D exchange results for protein ions. Multiply protonated bovine proinsulin and α-lactalbumin were generated using electrospray ionization and reacted with D_2O in a "reaction capillary" prior to detection using a triple quadrupole mass spectrometer. The native and disulfide bond reduced forms of the protein displayed different reactivities in the gas phase with the D_2O exchange reagent, allowing the different protein conformations to be distinguished according to their reactivity. Suckau *et al.*[3] probed the gas phase reactivity of multiply protonated cytochrome *c* formed by electrospray ionization with D_2O using an ion cyclotron resonance mass spectrometer. Their exchange results were interpreted to indicate that more than one molecular conformation can exist for a specific mass to charge species in a spectrum. Suckau *et al.*[3] suggested that gas phase species with distinctive exchange reactivity could be correlated with known solution phase structures.

Cheng and Fenselau[5] investigated the H/D exchange of four relatively small protonated peptides (< 2000 Dalton) and found the extent of deuterium incorporation to be highly dependent on the amino acid composition of the molecule. Peptides with basic residues such as arginine exchanged more slowly and more selectively with the exchange reagent. Their results suggested that possible conformational effects in the gas phase influenced the H/D exchange processes.

In a more fundamental study, Gard *et al.*[6] probed the H/D exchange of several protonated amino acids with CH_3OD to understand the relationship between proton affinity and deuterium incorporation. Surprisingly, they did not find a direct correlation between proton affinity and H/D exchange. Glycine (with a proton affinity of 211.6 kcal/mol) exchanges all of its labile hydrogens with CH_3OD, while alanine (proton affinity of 214.8 kcal/mol) exchanges only two sites rather slowly. The highly basic amino acids of lysine and histidine readily exchange all hydrogens, while arginine (the most basic amino acid, proton affinity of 245.2 kcal/mol)[7] does not exchange a single site with CH_3OD. From their results, Gard *et al.*[5] concluded that the proton affinity difference between remote sites in the molecule, and not the absolute proton affinity of the molecule, controlled H/D exchange processes with CH_3OD. In this regard, lysine (with two primary amine groups of similar basicity) exchanges more readily with CH_3OD than does arginine, which possesses a primary amine and a highly basic guanidine side chain.

With the limited range of studies that have been performed to date, very little is known about the mechanism and energetics of H/D exchange processes for complex

biomolecules. ND_3 is an efficient reagent for promoting H/D exchange of protonated glycine oligomers, as it exchanges every labile hydrogen. We have undertaken a systematic study of isotopic hydrogen exchange using FT-ICR techniques, focusing our attention on several small peptides (leucine enkephalin, leucine enkephalin arginine, bradykinin, and gramicidin S) with ND_3 and CF_3CO_2D. This series was chosen to investigate the effect of introducing the most basic amino acid, arginine, into a peptide. Arginine is expected to shift the site of protonation from the N-terminus to the side group. We have modeled our results using semiempirical calculations to quantify potential energy surfaces of selected systems. We wish to report implications which these studies have for mechanisms of gas phase H/D exchange reactions and stable structures of peptides in the gas phase.

Experimental Details

Experiments were performed in an external ion source Fourier transform ion cyclotron resonance (FT-ICR) mass spectrometer. A detailed description of this instrument[8] and the experimental technique for H/D exchange[9] has been previously reported. Briefly, protonated peptide ions are generated by Cs ion bombardment of an acidic glycerol matrix and transported by the octopole ion guide to the 2x2x3 inch ICR cell in the high-field region of a 7-T superconducting magnet. The peptide ions are isolated from unwanted matrix and fragment ions by resonant rf excitation and reacted with deuterating reagent gases in the ICR cell. Static pressures of the deuterating gases range from 1.0 to 2.5×10^{-7} Torr. The uncertainty in pressure measurements is

estimated to be ± 20%, and is the major source of error in reported rate constants. Product ions are excited with a swept rf pulse and detected at varying lengths of time.

The methyl ester of bradykinin was synthesized by dissolving the peptide in a solution of methanol and trifluoroacetic acid (10:1) and stirring over night. The reaction yield did not exceed 30%, but the product could be identified in FT-ICR experiments. All other peptides were commercially available from Sigma Chemical Co. and used as provided without further purification. ND_3 was obtained from Matheson with a purity of 99.0 atom % deuterium, and CF_3CO_2D was obtained from Aldrich Chemical Co. with a purity of 99.5 atom % deuterium.

Semiempirical calculations were performed with Hyperchem[10] to obtain model structures and energetics for the protonated peptides and reagent exchange gases. Both the AM1[11] and PM3[12] semiempirical methods were employed. In all of the calculations, starting structures for the molecules were obtained using the standard amino acid templates provided with Hyperchem. Structures for the protonated species were obtained by attaching a proton to a basic site. The structure was then annealed using molecular mechanics and energy-minimized using semiempirical methods. The site of protonation and initial geometry was varied to determine the differences in the structure and stability of various conformations of the protonated parent molecules.

Results and Discussion

H/D exchange of leucine enkephalin with ND_3. Protonated leucine enkephalin (YGGFL), a pentapeptide lacking basic amino acid residues, is observed to

exchange nine of nine labile hydrogens with ND_3 during a reaction time of eight seconds. The most abundant exchange species at eight seconds has incorporated six deuteriums, and products resulting from more H/D exchanges are present in smaller abundances. The rate constant for the first exchange of protonated leucine enkephalin with ND_3, determined from the slope of a semi-log plot of ion abundance versus time, is 2.5×10^{-10} $cm^3 molecule^{-1} sec^{-1}$. The reaction rate constants for subsequent H/D exchanges are estimated by fitting the data with first-order differential equations. Rate constants obtained in this method for protonated leucine enkephalin, giving a best fit to the experimental data, range from 4×10^{-10} to 4×10^{-11} $cm^3 molecule^{-1} sec^{-1}$ and are summarized in Table 1. It is interesting to note that previous H/D exchange results for several protonated glycine oligomers indicate that ND_3 partakes in multiple exchanges in a single encounter.[9] Experiments to establish if leucine enkephalin partakes in multiple exchanges with ND_3 have not been performed, but the calculated rate constants for H/D exchange of leucine enkephalin are approximately 3-4 times slower than those of peptides which have been found to undergo multiple exchanges.

Leucine enkephalin is very similar in structure and reactivity to the Gly_5 oligomer.[9] Both species lack basic side chains, protonate on the N-terminus amine, and exchange all labile hydrogens with the ND_3 reagent. Additionally, the gas phase proton affinities of leucine enkephalin[5] and Gly_5 [13] have been reported as 234 and 232 kcal/mol, respectively. Previous results indicate that the relatively high proton affinity of Gly_5 results from folding the peptide to solvate the charge site with intramolecular

Table 1: Calculated H/D exchange rates for several protonated peptides with ND_3 and CF_3CO_2D (rates $x10^{10}$ $cm^3molecule^{-1}sec^{-1}$)

Gas	Peptide	Number of Labile Hydrogen	Number of Observed Deuterium Exchanges								
			D_1	D_2	D_3	D_4	D_5	D_6	D_7	D_8	D_9
ND_3	Leucine Enkephalin	9	2.49	4.33	3.06	1.88	1.08	0.81	0.69	0.37	0.41
	Leucine Enkephalin Arginine	14	0.96	0.75	0.64	0.45	0.31	0.09	*	*	*
	Bradykinin	18	*	*	*	*	*	*	*	*	*
	Bradykinin Methyl Ester	17	*	*	*	*	*	*	*	*	*
	Gramicidin S	13	0.16	0.09	0.22	*	*	*	*	*	*
CF_3CO_2D	Bradykinin	18	0.03	0.03	*	*	*	*	*	*	*
	Bradykinin Methyl Ester	17	0.03	0.03	*	*	*	*	*	*	*

*Exchange not observed

hydrogen bonds.[9] The high proton affinity of leucine enkephalin most likely results from the same process.

Ammonia has a proton affinity 30 kcal/mol lower than that of leucine enkephalin, and H/D exchange of the peptide by means of simple proton transfer to the reagent base should be moderately unfavorable. We propose that the mechanisms of H/D exchange for leucine enkephalin with ND_3 are analogous to those proposed for the exchange of the glycine oligomers. These mechanisms have been previously described in detail[9] and are summarized in Figure 1. Exchange of the N-terminus protons proceeds via an onium ion mechanism, in which an endothermic proton transfer from the N-terminus to ND_3 is rendered energetically feasible by simultaneous solvation of the resultant ammonium ion. Solvation of this ion by the peptide compensates for the loss of folding stabilization (i.e., intramolecular hydrogen bonding) in the parent species. Exchange of the carboxylic hydrogen occurs via salt bridge formation with the exchange reagent. Proton transfer from the C-terminus to ND_3 forming an ion pair is facilitated by stabilizing interactions with the nearby protonated N-terminus. This salt bridge intermediate could exhibit a tendency to collapse to the significantly more stable onium ion by transferring a proton from the N-terminus to the carboxylate anion. Even so, this mechanism appears to provide a viable pathway to eventually exchange the C-terminus hydrogen. Exchange of the amide hydrogens occurs via a tautomer mechanism. Proton transfer from the N-terminus to an amide carbonyl occurs in concert with the transfer of an amide proton to ND_3, forming an ammonium ion solvated by a tautomerized peptide.

Figure 1. Summary of the proposed H/D exchange mechanisms for protonated leucine enkephalin with ND_3. These mechanisms can be applied to all peptides which lack basic amino acid residues and preferentially protonate of the N-terminus.

Onium Ion Mechanism	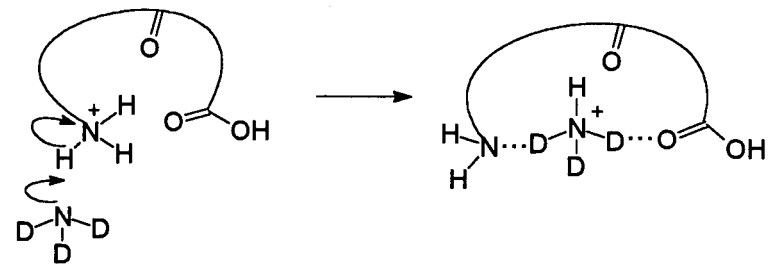
Salt Bridge Mechanism	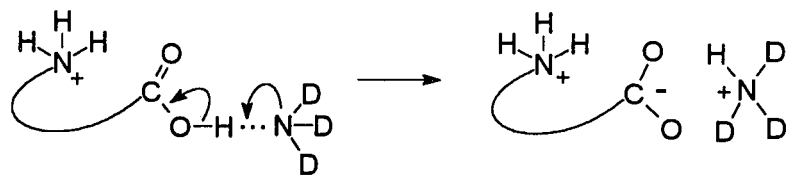
Tautomer Mechanism	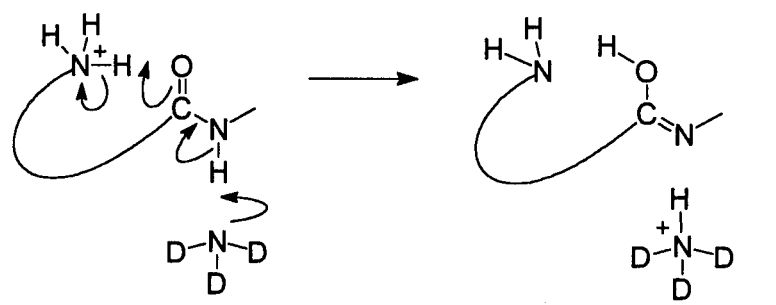
Flip-Flop Mechanism	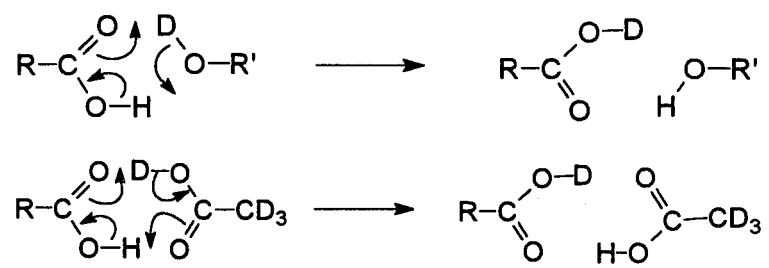
Relay Mechanism	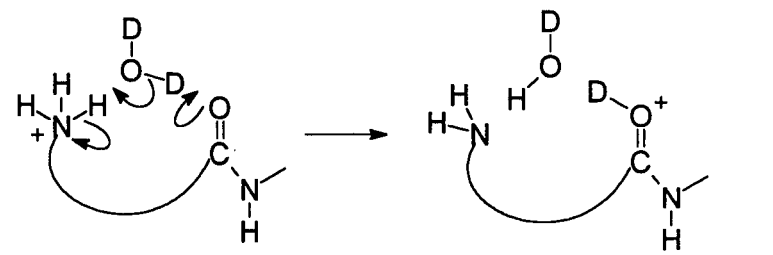

Figure 1

H/D exchange of leucine enkephalin arginine with ND_3. Protonated leucine enkephalin arginine (YGGFLR) exhibits very different exchange behavior with ND_3 than leucine enkephalin. Only 6 of 14 labile hydrogens on the peptide are observed to exchange during a reaction time of 12 seconds. Calculated rate constants are slower than those of leucine enkephalin and range from $9x10^{-11}$ to $9x10^{-12}$ $cm^3molecule^{-1}sec^{-1}$ (Table 1). To better understand the difference in reactivity between these two peptides, the H/D exchange of protonated arginine amino acid was investigated.[14]

The H/D exchange results for protonated arginine reveal that only six of eight labile hydrogens exchange with ND_3 during 60 seconds of reaction. Of these six exchanges, one site exchanges rather quickly and the remaining five are slow. The methyl ester of arginine exhibited no reactivity with ND_3 during a 90 second reaction time, which suggests that a free carboxylic acid is important for promoting the exchange of arginine species! From these results, we propose that the first exchange of arginine occurs at the carboxylic hydrogen and the five slower exchanges occur at the five hydrogens in the protonated guanidine group of the side chain.

It is not obvious with leucine enkephalin arginine which 6 of the 14 labile hydrogens are exchanging, but with the above results for arginine, we propose that the peptide preferentially exchanges the C-terminus and the arginine side chain. The notable differences in reactivity between leucine enkephalin and leucine enkephalin arginine suggest these two peptides do not exchange at similar sites. This is substantiated by the belief that leucine enkephalin arginine protonates on the arginine side chain, while leucine enkephalin protonates on the N-terminus amine.

Strongly basic residues in peptides complicate the simple mechanistic picture of H/D exchange, due to their high proton affinities. Exchange of leucine enkephalin arginine via simple proton transfer to ND_3 is unlikely due to the large difference in proton affinities between the two species (greater than 40 kcal/mol).[5] H/D exchange via a relay mechanism (Figure 1) was previously proposed for the glycine oligomers with reagent gases that were much lower in basicity than the peptides. In the relay mechanism, a proton is shuttled from the site of protonation in a hydrogen bonded complex onto the reagent gas in concert with the transfer of a deuteron from the gas to a distant, slightly less basic site on the molecule. For the glycine oligomers, a proton was shuttled from the N-terminus to an amide carbonyl. For leucine enkephalin arginine, a proton would be shuttled from the arginine side chain to the N-terminus. The large disparity in functional group basicities probably mitigates against this mechanism for H/D exchange.

We propose that the H/D exchange of protonated leucine enkephalin arginine with ND_3 occurs by means of an onium ion mechanism, in spite of the large net difference in proton affinities between the reactants. Semiempirical calculations indicate that ND_3 forms a stable hydrogen bonded complex with protonated leucine enkephalin arginine, which is 4 kcal/mol more stable than the isolated reactants. Furthermore, proton transfer to ND_3 and solvation of the ammonium ion is actually *exothermic* by the same 4 kcal/mol. The potential energy surface is shown in Figure 2 along with the structures of the exchange intermediates.

Figure 2. Potential energy surface for the H/D exchange of leucine enkephalin arginine with ND_3 via an onium ion mechanism. Proton transfer from the arginine side chain to ND_3 is accompanied by simultaneous solvation of the ammonium ion by the carbonyl oxygens of the peptide.

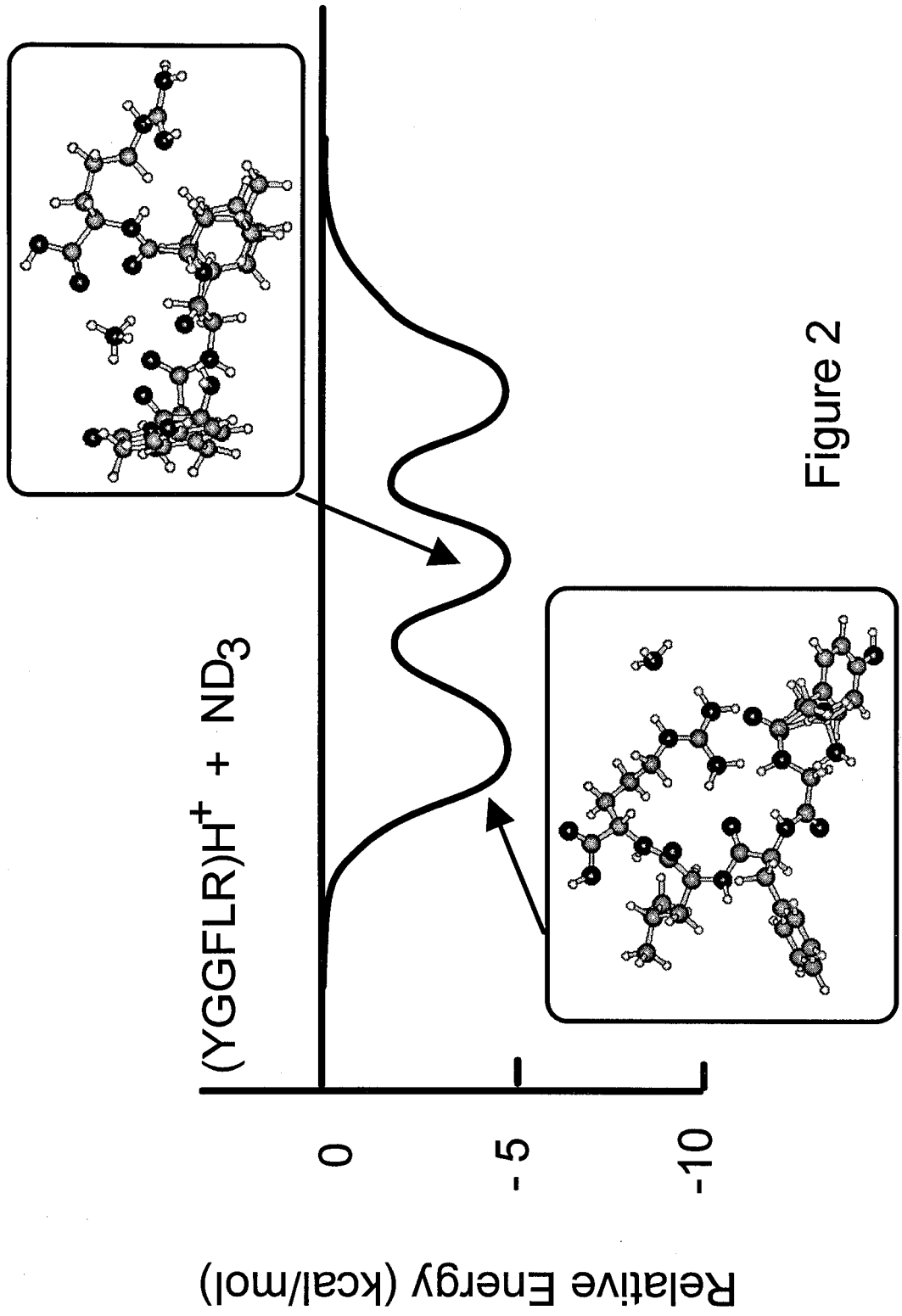

Figure 2

How is it feasible that leucine enkephalin arginine transfers a proton to ND_3? The high proton affinity of the arginine amino acid results from the ability to delocalize charge across the side group. AM1 calculations show the protonated arginine side chain in leucine enkephalin arginine is not strongly solvated by the peptide due to the diffuse nature of the charge site. As a result, intramolecular hydrogen bonding to this side chain is inefficient and there is little folding stabilization in the peptide. In contrast, an ammonium ion has a compact charge distribution compared to the arginine side chain. Semiempirical calculations indicate that endothermic proton transfer from the peptide to ND_3 is a favorable process since the energy recovered by solvating the ammonium ion exceeds that lost from unfolding the protonated peptide and transferring the proton to ND_3. In actuality, the energetic difference in protonating the arginine side chain and solvating the charge center versus protonating the N-terminus and solvating the charge center is not as large as one might predict based on the proton affinities of the isolated amino acids. The difference in part comes from the better solvation of the smaller protonated amine terminus in comparison with the diffuse delocalized charge distribution associated with protonated arginine.

H/D exchange of bradykinin with ND_3. Protonated bradykinin (RPPGFSPFR), a nonapeptide with two arginine residues and 18 labile hydrogens, is not observed to exchange any of its sites with ND_3 during a reaction time of 15 seconds. This result can be rationalized if one considers the proposed structure of the gas phase ion. Semiempirical calculations identify two structures of similar energy for the geometry optimized protonated peptide. In the first structure (**1**), protonation

occurs simply on an arginine side chain and the peptide folds to solvate the charge center. The protonated arginine side chain appears to be completely encapsulated by the peptide and, as a result, is not readily accessible to an approaching ND_3 for exchange. The second structure (**2**) exhibits an intriguing salt bridge interaction, in which the peptide folds and positions the deprotonated C-terminus between two protonated arginine side chains. In the structure below, the salt bridge is observed in the far right region of the molecule, with a protonated arginine side chain as the outermost group. H/D exchange of this configuration via an onium ion mechanism requires the stable, electrostatic salt bridge be disrupted upon proton transfer from the arginine side chain to ND_3. Space filling models additionally show that the remaining labile hydrogens in both peptide geometries are buried within the secondary structure, hindering H/D exchange.

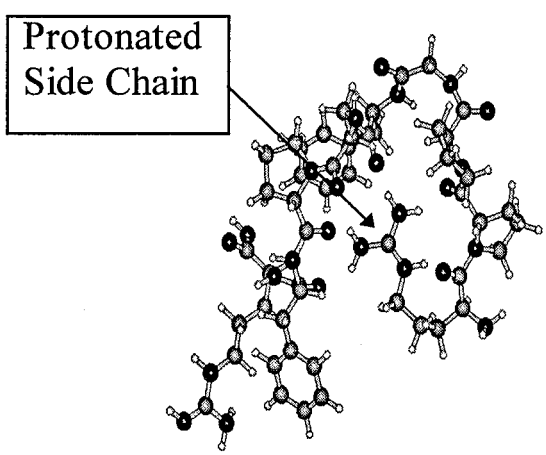

1

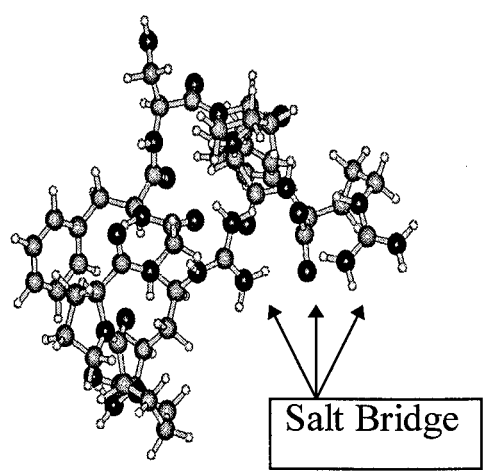

2

The solution phase structure of bradykinin has been predicted by calculations and confirmed by NMR techniques.[15] The most stable conformation of the peptide possesses a salt bridge interaction between the two protonated arginines and a deprotonated C-terminus, and has a net +2 charge from protonating the N-terminus. This agrees well with our second structure, except the gas phase bradykinin lacks the protonated N-terminus. If predictions of a gas phase salt bridge configuration are correct, methylation of the C-terminus should inhibit its formation and we might expect to observe H/D exchange results similar to leucine enkephalin arginine. Unfortunately, the methyl ester of bradykinin also displays no exchange of its labile hydrogens with ND_3. This result does not necessarily provide conclusive evidence for or against one specific structure, since methylation could cause a salt bridged peptide to fold into the alternate structure of similar energy (**1**) with the protonated arginine buried and unreactive.

H/D exchange of bradykinin with CF_3CO_2D. Bradykinin is observed to slowly exchange two labile hydrogens with CF_3CO_2D during a reaction time of 15 seconds, with rate constants of $3x10^{-12}$ $cm^3molecule^{-1}sec^{-1}$. If bradykinin possesses a salt bridged structure in the gas phase, then CF_3CO_2D could exchange the protonated arginine side chain by means of a flip-flop mechanism (Scheme 1). In this method, the acidic exchange gas forms a hydrogen bonded complex to the guanidine group in the side chain. Exchange occurs via a six member intermediate and does not disturb the electrostatics of the salt bridge. It is difficult to evaluate the possibility of multicenter flip-flop exchange intermediates such as those in Scheme 1. The barriers for these

Scheme 1

processes may be high compared to the chemical activation available from complex formation. Previous calculations for acetic acid, though, indicate the barrier for exchange in symmetric hydrogen bonded acid dimers is only 10-12 kcal/mol.[16] Alternately, if bradykinin resembles structure **1** with a single buried charge site, H/D exchange could occur on the more exposed neutral arginine by the same flip-flop mechanism of Scheme 1.

Experimental results of bradykinin methyl ester also indicate that two hydrogens exchange with CF_3CO_2D, with rate constants of $3x10^{-12}$ $cm^3molecule^{-1}sec^{-1}$. The similarity in reaction rate constants between bradykinin and its methyl ester might suggest similar structures for these species, and therefore predict structure **1** (since the methyl ester cannot form the salt bridge). Unfortunately, H/D exchange could likely occur at the N-terminus, which possesses two labile hydrogens, via the same multicenter mechanism and account for the similar reactivities.

H/D exchange of gramicidin S with ND_3. Protonated gramicidin S slowly exchanges 3 of 13 labile hydrogens with ND_3 during a reaction time of 15 seconds. The calculated rate constants for the exchanges range from $2x10^{-11}$ to $9x10^{-12}$ $cm^3molecule^{-1}sec^{-1}$ and are reported in Table 1.

Gramicidin S is a cyclic decapeptide (-LFPVOLFPVO-), and the only molecule investigated which lacks a free N- or C-terminus. Protonation occurs on an ornithine side chain since there are no strongly basic residues in the peptide. Geometric constraints imposed by the cyclic structure prevent the molecule from strongly solvating the ornithine charge center, hence the proton affinity of the ornithine side chain is predicted to be similar to that of a free primary amine. Semiempirical calculations indicate that the protonated ornithine side chain stretches into the central cavity of the peptide ring and tries to interact with amide carbonyls (structure **3**, protonated ornithine at the top of the molecule). The length of the side chain is too short and the conformation of the peptide backbone is too rigid to allow strong hydrogen bonds to form.

We propose that H/D exchange of gramicidin S occurs primarily at the protonated ornithine side chain via a moderately inefficient onium ion mechanism. Endothermic proton transfer from the ornithine side chain to ND_3 is only slightly favorable, since the inflexible peptide cannot effectively solvate the ammonium ion. The endothermicity of proton transfer becomes a limiting factor and, as a result, exchange is slow. Space filling molecular models indicate that the amide hydrogens are

not readily accessible to an approaching ND_3 reagent and H/D exchange occurs only at the exposed ornithine charge site.

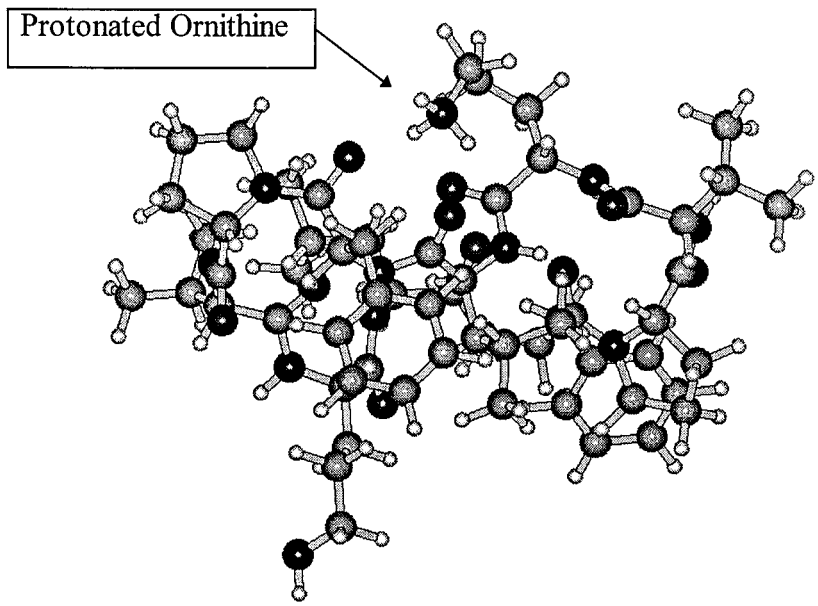

3

Gross and Williams investigated the exchange of singly and doubly protonated gramicidin S with D_2O in an FT-ICR mass spectrometer.[17] At much longer detection times and higher reagent gas pressures, they established that five and six labile hydrogens exchange in the singly and doubly protonated peptides, respectively. A similar conclusion was reached from their results, in that protonation and H/D exchange occurs predominantly on the ornithine side chain. Gross and Williams further concluded that the neutral ornithine side chain in the singly protonated species could be

exchanged by deuterium scrambling within the molecule. No evidence for H/D scrambling was observed during the shorter time frame of our experiments with ND_3.

Conclusions

We have examined the H/D exchange of several protonated peptides with ND_3 in a Fourier transform ion cyclotron resonance mass spectrometer. Peptides which lack basic residues, such as leucine enkephalin and the glycine oligomers, exchange all labile hydrogens with ND_3. For these species, H/D exchange can be used as an efficient probe for counting the number of labile sites in the peptide. This technique could later prove to be useful in predicting the amino acid composition in unknown peptides. The introduction of strongly basic residues, such as arginine, into a peptide has a significant impact. Leucine enkephalin arginine undergoes limited exchange with ND_3 (6 of 14 sites) and bradykinin (with two arginine residues) does not exchange a single hydrogen. It is clear from these examples that H/D exchange will be less useful for counting labile hydrogens and predicting the amino acid composition in peptides of these sorts.

There has been considerable interest in the structural and functional roles of salt bridges in proteins. Charged amino acids have been implicated as factors contributing to protein stability, as driving forces for protein-protein interactions, and as key factors in enzyme mechanisms.[18] The lack of gas phase reactivity between a peptide and deuterating reagent could be an indication of a stabilizing secondary structure which inhibits exchange. The presence of very basic residues may allow the formation of intramolecular gas phase salt bridges in peptides with the appropriate arrangement of

amino acids. We have considered the possibility of salt bridge interactions in the peptides currently investigated. Semiempirical calculations indicate that bradykinin could exist in the gas phase with a salt bridge configuration, but also identify a second simpler conformation of equal stability. Further investigations are needed to elucidate the gas phase structure.

Assigning configurations to biological molecules from gas phase H/D exchange results is a difficult task, even for these relatively small but functionally diverse peptides, and attempts to do so must be approached with caution. The utility of H/D exchange for predicting the molecular conformation of large peptides and proteins is uncertain since larger molecules might not exhibit exchange with the reagent gases. Further investigations are necessary to elucidate the H/D exchange mechanisms of more complex protonated peptides with a variety of reagent gases.

Acknowledgments

We gratefully acknowledge the financial support of SC from a NIH-NRSA traineeship in Biotechnology, and of JM from a Caltech Summer Undergraduate Research Fellowship. This work was supported in part by the National Science Foundation under grant CHE-9108318, and by ARPA and DoD-URI programs under grant ONR-N0014-92-J-1901. We are indebted to the Beckman Foundation and Institute for the initial funding and continuing support of the research facilities.

References

1. See, for example: Ranasinghe, A.: Cooks, R. G.; Sethi, S. K. *Org. Mass Spectrom.* **1992**, *27*, 77 or Hunt, D. F.; Sethi, S. K. *J. Am. Chem. Soc.* **1980**, *102*, 6953.

2. Winger, B. E.; Light-Wahl, K. J.; Rockwood, A. L.; Smith, R. D. *J. Am. Chem. Soc.* **1992**, *114*, 5897.

3. Suckau, D.; Shi, Y.; Beu, S. C.; Senko, M. W.; Quinn, J. P.; Wampler, F. M.; McLafferty, F. W. *Proc. Natl. Acad. Sci.* **1993**, *90*, 790.

4. See, for example: Verma, S.; Pomerantz, S. C.; Sethi, S. K.; McCloskey, J. A. *Anal. Chem.* **1986**, *58*, 2898. or Katta, V.; Chait, B. T. *Rapid Commun. Mass Spectrom.* **1991**, *5*, 214.

5. Cheng, X.; Fenselau, C. *Int. J. Mass Spectrom. Ion Process.* **1992**, *122*, 109.

6. Gard, E.; Green, M. K.; Bregar, J.; Lebrilla, C. B. *J. Am. Soc. Mass Spectrom.* **1994**, *5*, 614.

7. Wu, Z.; Fenselau, C. *Rapid Commun. Mass Spectrom.* **1992**, *6*, 403.

8. (a) Campbell, S.; Marzluff, E. M.; Rodgers, M. T.; Beauchamp, J. L.; Rempe, M. E.; Schwinck, K. F.; Lichtenberger, D. L. *J. Am. Chem. Soc.* **1994**, *116*, 5257. (b) Marzluff, E. M.; Campbell, S.; Rodgers, M. T.; Beauchamp, J. L. *J. Am. Chem. Soc.* **1994**, *116*, 7787.

9. Campbell, S.; Rodgers, M. T.; Marzluff, E. M.; Beauchamp, J. L. (submitted for publication).

10. Hyperchem Computational Software Package, Ver. 4.0 (Hypercube Inc., 1994). For a review of this computational package, see: Froimowitz, M. *Biotechniques* **1993**, *14*, 1010.

11.(a) Dewar, M. J. S..; Zoebisch, E. G.; Healy, E. F.; Stewart, J-J. P. *J. Am. Chem. Soc.* **1985**, *107*, 3902. (b) Dewar, M. J. S.; Dieter, K. M. *J. Am. Chem. Soc.* **1986**, *108*, 8075.

12. (a) Stewart, J-J. P. *Method J. Comput. Chem.* **1989**, *10*, 209. (b) Stewart, J-J. P. *Method J. Comput. Chem.* **1989**, *10*, 221.

13. Wu, Z.; Fenselau, C. *J. Am. Soc. Mass Spectrom.* **1992**, *3*, 863.

14. McDunn, J.; Campbell, S.; Beauchamp, J. L. (to be published).

15. Salvino, J. M.; Seoane, P. R.; Dolle, R. E. *J. Comput. Chem.* **1993**, *4*, 438.

16. Shida, N.; Barbara, P. F.; Almlof, J. *J. Chem. Phys.* **1991**, *94*, 3633.

17. Gross, D. S.; Williams, E. R. (submitted for publication).

18. Rashin, A. A.; Honig, B. *J. Mol. Biol.* **1984**, *173*, 515.